Towards Light Switchable Surfaces

By Paul Reader

Thesis presented in partial fulfilment of the requirements for the degree of Master of Science (Polymer Science) at the University of Stellenbosch

Supervisor: Prof Bert Klumperman

Co-supervisor: Dr Gareth Arnott

University of Stellenbosch – Faculty of Science

Department of Chemistry and Polymer Science

December 2011

Declaration

By submitting this thesis electronically, I declare the entirety of the work contained therein is my own, original work, that I am the owner of the copyright thereof (unless to the extent explicitly otherwise stated) and that I have not previously in its entirety or in part submitted it for obtaining any qualification.

Paul Reader December 2011

Abstract

Polymeric nanofibrous membranes that act as surfaces offer two compelling properties; they have extremely large surface areas that can be modified and they can offer multiple reactive sites depending on which polymer they were electrospun from. Combining nanofibrous surfaces such as these with photochromic dyes can give remarkable, light responsive materials.

In this study, a terpolymer was electrospun and crosslinked (to impart insolubility to the material) to produce a nanofibrous mat that contained surface secondary-hydroxyl units and benzyl chloride units, from which monomers could grow using surface-initiated atom transfer polymerization (SI-ATRP). The surface was further fluorinated though the secondary-hydroxyl moieties to produce a hydrophobic crosslinked nanofibrous surface.

n-Butyl acrylate and a photochromic spiropyran dye were copolymerized from the surface using SI-ATRP, in order to produce a surface that exhibited reversible adhesion towards a water droplet using ultraviolet and visible light as a stimulus to change between the two states. This in principle would allow the droplet to roll off and stick to the surface respectively. Although the surface displayed a colour change when switched, proving that the SI-ATRP had taken place, the droplet of water remained attached to the surface in both states.

Opsomming

Polimeriese nanovesel membrane wat dien as oppervlaktes bied twee aantreklike eienskappe; hulle het baie groot oppervlakareas wat gemodifiseer kan word en hulle bied veelvuldige reaktiewe punte, afhangende van die polimeer waarvan hulle ge-elektrospin is. Deur sulke nanovesel oppervlaktes met fotochromiese kleurstowwe te kombineer, kan uitstekende lig reagerende materiale verkry word.

In hierdie studie is ‘n terpolimeer ge-elektrospin en daarna gekruisbind (om die materiaal onoplosbaar te maak) om ‘n nanovesel web te kry wat oppervlak sekondêre-hidroksiel en benzielchloried eenhede bevat. Monomere kan dan vanaf hierdie eenhede groei deur middel van oppervlak-geïnisieerde atoom-oordrag polimerisasie (OI-AOPR). Die oppervlak was verder gefluorineer via die sekondêre-hidroksiel eenhede om ‘n hidrofobiese, gekruisbinde nanovesel oppervlak te vorm.

n-Butielakrilaat en ‘n fotochromiese spiropiraan kleurstof is gekopolimeriseer vanaf die oppervlak deur middel van OI-AORP om sodoende ‘n oppervlak te skep wat omkeerbare adhesie van ‘n water druppel gee as ultraviolet en sigbare lig as stimulus gebruik word om tussen die twee toestande te wissel. In beginsel sal die water druppel vanaf die oppervlak kan afrol én daaraan vassit, afhangende van die toestand van die oppervlak. Alhoewel die oppervlak van kleur verander het met die wisseling tussen die twee toestande, wat as bewys dien dat OI-AORP wel plaasgevind het, het die druppel water bly vassit aan die oppervlak in beide toestande.

Acknowledgements

Firstly, I would like to thank God for the opportunities I have received and the strength and wisdom He has given me. I would also like to thank God for the friends He has given me that have supported and prayed for me during this project, particularly near the end.

I would like to thank my supervisors, Prof. Bert Klumperman and Dr. Gareth Arnott, for their guidance, encouragement and friendship over the past few years.

I would like to thank all the staff at the Department of Chemistry and Polymer Science who have kept everything running smoothly and helped facilitate my project, in particular Calvin Maart, Jim Motshweni, Deon Koen, Erinda Cooper and Aneli Fourie. I would also like to thank Prof. Peter Mallon for his philosophical discussions about research and my project.

I would like to thank Elsa Malherbe for NMR analysis, Madelaine Frazenburg for SEM analysis and Gareth Harding for SEC analysis. Thanks to Eric Ward for all the creative glassware he has made for my project.

I would like to thank the National Research Foundation of South Africa for funding.

Special thanks to Eric van den Dungen for having shaped my lab technique, invaluable discussions we have had and a great friendship that has developed.

Thanks to all the free radical research members, past and present members: Jaco, Celeste, William, Khotso, Joris, Osama, Ahmed, Nathalie, Rueben, Ahson, Neli, Walid, Hamilton, Lizl, Sandile, Mpho, Barry, Wisdom, Reda, Njabu, Niels, Zaskia and Gwen. I really appreciate all the assistance, discussion and friendships we have made. A special thanks to Rueben for your synthetic knowledge and Osama for your electrospinning knowledge. I have learnt a great deal from you both and really value the discussions we had.

I would like to thank friends and family for motivation.

Finally, I would like to thank my fiancé, Tammy, for all the support and patience she has given me and her continual encouragement and blessing in my life.

Table of Contents

List of Figures

List of Schemes

Scheme 6-1: Proposed synthesis of a fluorinated diamine

List of Tables

List of Acronyms

4vbCl	4-vinylbenzyl chloride
ACE	Acetone
AIBN	2,2′-azobisisobutyronitrile
ARGET	Activators regenerated by electron transfer
AsAc	Ascorbic acid
ATR-FTIR	Attenuated total reflectance - Fourier transform infrared
ATRP	Atom transfer radical polymerization
BnCl	Benzyl chloride
Boc	*tert*-Butyloxycarbonyl
CRP	Controlled/Living radical polymerization
CyH	Cyclohexane
DCC	Dicyclohexyl carbodiimide
DCM	Dichloromethane
DIC	Diisopropyl carbodiimide
DMAP	Dimethylaminopyridine
DMF	Dimethylformamide
DMSO	Dimethylsulfoxide
EA	Ethyl acrylate
EBiB	Ethyl 2-bromoisobutyrate
E-DA	Ethylene diamine
EDTA	Ethylenediaminetetraacetic acid

EDX	Energy dispersive x-ray spectroscopy
FDA	Food and Drug Administration
FRP	Free radical polymerization
HEA	2-Hydroxy ethyl acrylate
HOBt	1-Hydroxybenzotrizole
HOSu	*N*-hydroxysuccinimide
iPrOH	Isopropanol
ISET	Inner sphere electron transfer
MaAh	Maleic anhydride
Me_6Tren	tris[2-(dimethylamino)ethyl]amine
NMP	Nitroxide mediated polymerization
NMR	Nuclear magnetic resonance
OH-DA	1,3-diamino-2-propanol
PEA	Poly(ethyl acrylate)
PFOC	pentadecafluorooctanoyl chloride
PMDETA	N,N,N′,N″,N″pentamethyldiethylenetriamine
PMMA	Poly(methyl methacrylate)
PRE	Persistent radical effect
PSMA	Poly(styrene-alt-maleic anhydride)
PSMA-Cl	Poly(styrene-co-4-vinylbenzyl chloride-co-maleic anhydride)
PSMI-Cl	Crosslinked nanofibrous mat - ring-closed malimide of PSMA-Cl
PSMI-Cl-F	Surface fluorinated PSMI-Cl

PSMI-F-G	PSMI-Cl-F-graft-poly(nBA-co-SpEA)
PStyEA	Poly(styrene-co-ethyl acrylate)
RAFT	Radical addition chain-transfer polymerization
SCA	Static contact angle
SEC	Size exclusion chromatography
SI-	Surface-initiated-
Sp	Spiropyran
SpAcid	1′-(2-carboxyethyl)-3′,3′-dimethyl-6-nitrospiro(indoline-2,2′[2*H*-1]benzopyran)
SpAmine	Amine-functionalized spiropyran
SpBuAmide	Butyl-functionalized spiropyran
Sp-EA	Spiropyran-based acrylate
Sty	Styrene
tBA	*tert*-Butyl acrylate
TBAF	Tetrabutylammonium fluoride
TBAI	tetrabutylammonium iodide
TCL	Triple-phase liquid/air/solid contact line
TEA	Triethylamine
THF	Tetrahydrofuran
TLC	Thin layer chromatography
TMS	Tetramethylsilane
TPMA	tris(2-pyridylmethyl)amine
UV	Ultraviolet

List of Symbols

Δ	Heat
λ	Wavelength
$[I]_0$	Initial initiator concentration
$[M]_0$	Initial monomer concentration
Đ	Dispersity
DP_n	Number average degree of polymerization
k_{act}	Activation rate coefficient
K_{ATRP}	Atom Transfer Radical Polymerization equilibrium rate coefficient
k_{deact}	Deactivation rate coefficient
k_p	Propagation rate coefficient
k_t	Termination rate coefficient
$M_{n,theo}$	Theoretical number-average molar mass
$MW_{initiator}$	Molecular weight of the initiator
$MW_{monomer}$	Molecular weight of the monomer

Chapter 1: Prologue

1.1 Introduction

Surface functionalization of polymeric materials has been studied for many years. Surface-selective chemistry allows the creation of novel surface properties through the incorporation of sophisticated organic molecules. The integration of photochromic dyes such as spiropyrans has allowed the production of light-responsive materials. This is because spiropyrans exist in two states, a hydrophobic spiropyran isomer in visible light and a hydrophilic merocyanine isomer in ultraviolet (UV) light. Surface functionalization has been achieved via a number of techniques that include doping thin-polymer films with active compounds,[1,2] graft-polymerization[3] and surface-specific chemistry.[4] Light-responsive surfaces can be responsible for many functions, such as reversible surface wettability,[5] reversible surface alignment in liquid crystals[6] and the transport of nano-objects along the surface.[7]

Polymeric nanofibrous mats produced by way of electrospinning have received a lot of attention in the last number of years due to their extremely high surface areas. In order for surface functionalization to be viable, the electrospun polymer has to contain suitable reactive groups. Copolymerization provides a pathway to synthesize polymers that contain multiple functionalities. This could allow several surface modifications to take place, such as surface-initiated polymerization from one functional group and crosslinking of the material from another.

1.2 Objectives

The aim of this project was to create a super-hydrophobic surface (static contact angle of water droplet $> 150\ ^{o}$) which was reversibly "sticky". This entailed that water droplets would stick to the tilted surface in one state, but would roll off the tilted surface in another state. UV and visible light would be used as the stimuli to switch between these states. The objectives of this study can be summarized as follows:

1. To synthesize an amine-functionalized spiropyran that could later be incorporated into a surface to provide reversibly switchable polarity.

2. To synthesize a crosslinked superhydrophobic nanofibrous mat (contact angle > 150 ^{o}) that contained atom transfer radical polymerization (ATRP) initiator sites, in order that surface-initiated polymerization could be conducted from this surface.
3. To polymerize a hydrophobic spiropyran-containing copolymer that could induce light-switchable polarity changes.
4. To copolymerize the two polymers in order to achieve a reversibly "sticky" surface

In summary, the reversibly "sticky" surface would remain superhydrophobic in both UV and visible light. The hydrophobic spiropyran-containing copolymer grafted from the surface would act, metaphorically speaking, as the anchor lines present on a hot air balloon, where the anchor lines represent the copolymer, the hot air balloon represents the water droplet and the ground represents the reversibly "sticky" surface. With visible light, the spiropyran units present in the copolymer would remain hydrophobic, repelling the droplet and allowing it to roll down the surface. This would be equivalent to the anchor lines on the hot air balloon being released, allowing the balloon to float away. In UV light however, the merocyanine units present in the copolymer would increase its hydrophilicity, causing the copolymer to adhere to the water droplet, preventing it from rolling down the surface.

1.3 Layout of the thesis

1.3.1 Chapter 1: Prologue

Surface chemistry is briefly introduced after which the studies objectives are clearly stated.

1.3.2 Chapter 2: Historical and theoretical background

Chapter 2 introduces historical and theoretical aspects that relate to the work within this study. Free radical polymerization (FRP) is discussed, with emphasis being put on atom transfer radical polymerization (ATRP) and its derivatives. The basics of the electrospinning process are described, including the optimization of fibre morphology. Photochromism is introduced with an emphasis being put on spiropyrans and finally light is shed on the intricacies of reversible adhesion.

1.3.3 Chapter 3: Spiropyran synthesis

This chapter describes the challenge of synthesizing an amine-functional spiropyran.

1.3.4 Chapter 4: Surface functionalization

The copolymerization of a suitable polymer for electrospinning, with multiple reactive groups, is discussed. The preparation of an electrospun crosslinked nanofibrous mat with surface hydroxyl and

benzyl chloride functionalities is described. Finally, the hydrophobicity of the hydroxyl-functional surface was increased by the introduction of fluorine groups, attached to the hydroxyl moieties present on the surface.

1.3.5 Chapter 5: Surface-initiated polymerization

This chapter discusses the difficulties of copolymerizing spiropyran with a suitable hydrophobic monomer, using activators regenerated by electron transfer (ARGET) ATRP. This information helped to develop the copolymerization of spiropyran and n-butyl acrylate using ATRP. The production of a reversibly "sticky" surface was assessed through surface-initiated ATRP of spiropyran and n-butyl acrylate, from the surface developed in chapter 4.

1.3.6 Chapter 6: Conclusions and outlook

Chapter 6 gives a short summary of the conclusions gathered from this study. It also describes the challenges encountered during this project and possible solutions.

1.4 References

(1) Wang, Y.; Zhao, J.; Si, J.; Ye, P.; Fu, X.; Qiu, L.; Shen, Y. *J. Chem. Phys.* **1995**, *103*, 5357-5361.

(2) Kausar, A.; Nagano, H.; Ogata, T.; Nonaka, T.; Kurihara, S. *Angew. Chem., Int. Ed.* **2009**, *48*, 2144-2147.

(3) Su, J.; Chen, J.; Zeng, F.; Chen, Q.; Wu, S.; Tong, Z. *Polym. Bull.* **2008**, *61*, 425-434.

(4) Katsonis, N.; Lubomska, M.; Pollard, M. M.; Feringa, B. L.; Rudolf, P. *Prog. Surf. Sci.* **2007**, *82*, 407-434.

(5) Xin, B.; Hao, J. *Chem. Soc. Rev.* **2010**, *39*, 769-782.

(6) Ichimura, K. *Chem. Rev.* **2000**, *100*, 1847-1873.

(7) Yang, D.; Piech, M.; Bell, N. S.; Gust, D.; Vail, S.; Garcia, A. A.; Schneider, J.; Park, C.-D.; Hayes, M. A.; Picraux, S. T. *Langmuir* **2007**, *23*, 10864-10872.

Chapter 2: Historical and Theoretical Background

2.1 Free Radical Polymerization

Natural polymers exist everywhere, for example, proteins in cellular systems and cellulose which can be found in plants. Synthetic polymers have been developed over the past few centuries to mimic some of the materials found in nature. Such synthetic polymers are applied in multiple different fields with a large fraction being produced industrially via free radical polymerization (FRP). FRP is a chain growth polymerization technique and is illustrated in scheme 2-1.

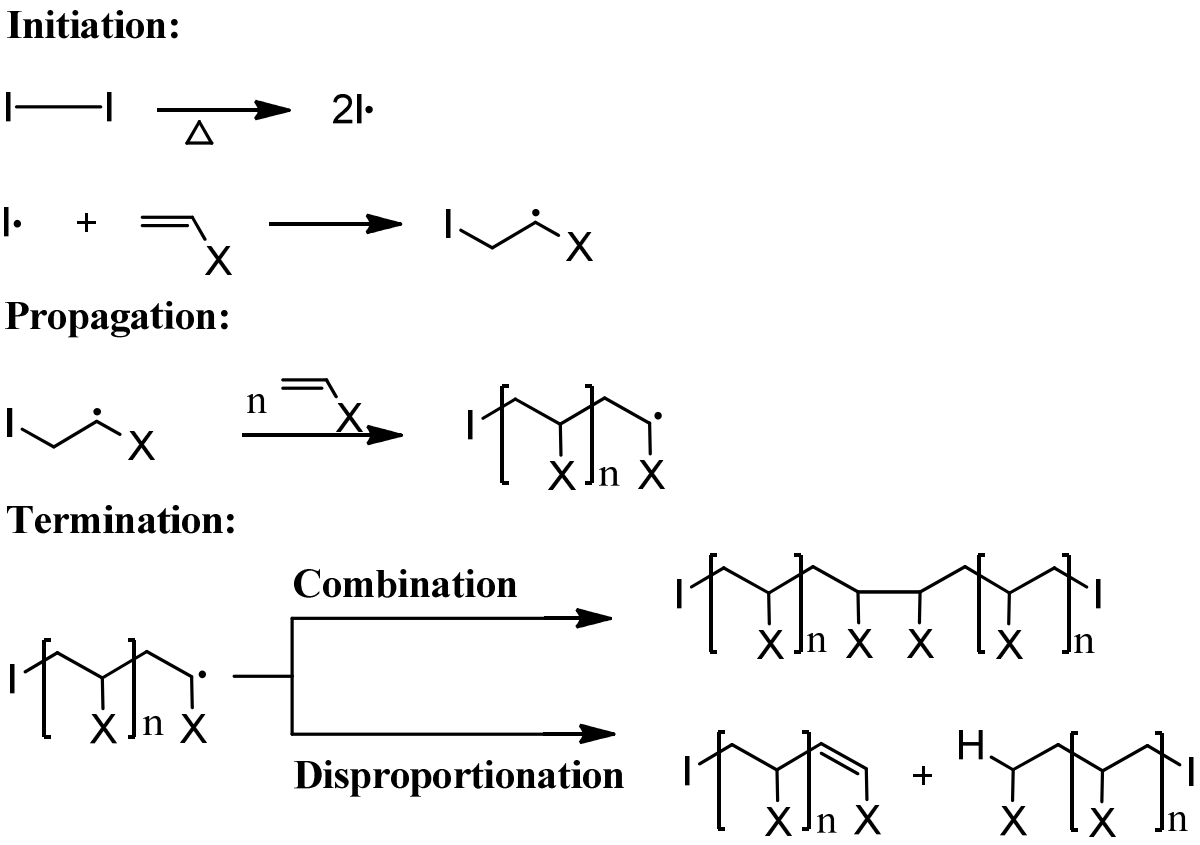

Scheme 2-1: General mechanism of FRP

During initiation, primary radicals can be generated in two ways, photochemically or thermally, both cases resulting in homolysis of the initiator. Initiators are often thermally labile compounds such as 2,2'-azobisisobutyronitrile (AIBN) or benzoyl peroxide. The primary radicals add to monomers, producing propagating radical species, shown in the second step of initiation, as depicted in scheme 2-1. Propagation occurs when monomer is added to the propagating radical in a chain growing reaction. Termination can occur in two ways, combination and disproportionation, with both termination reactions being bimolecular. Other side reactions can and do occur, such as chain transfer to solvent and monomer.

FRP is a very versatile polymerization technique that is often used in industry. It is tolerable to small amounts of oxygen and other trace materials. A large range of vinyl monomers and functionalities can be homo- or co-polymerized under many conditions. Although FRP has many advantages, its shortcomings become apparent in the lack of molar mass control. This is an outcome of initiation and termination occurring throughout the polymerization as a result of the highly reactive radicals. Under these conditions, termination cannot be eliminated. This results in a large dispersity ($Đ > 1.5$). These drawbacks become relevant when materials with specific properties are needed. Therefore, controlled/living radical polymerization has been developed to overcome the problems associated with conventional FRP.[1]

2.2 Controlled/Living Radical Polymerization (CRP)

Living polymerization was first documented by Szwarc[2] and essentially states that living polymerization is a direct result of a chain growth process where chain breaking reactions such as termination and chain transfer are absent. Szwarc discovered this concept while studying anionic polymerization of styrene and found that polymer chain growth continues until all monomer is consumed and starts again when more monomer is added. A block copolymer was thus formed when an appropriate second monomer was added to the system. The most well known CRP techniques are atom transfer radical polymerization (ATRP),[3] radical addition-fragmentation chain-transfer mediated polymerization (RAFT)[4] and nitroxide mediated polymerization (NMP).[5,6] NMP and RAFT will be briefly discussed, while more emphasis will be put on ATRP and its variations.

Generally CRP techniques try to suppress reactions that lead to irreversible termination in order that all chains grow simultaneously. This is achieved by establishing a dynamic equilibrium between a low concentration of propagating radicals versus a high concentration of dormant chains.[8] This results in chains getting sequentially longer over the polymerization compared to FRP where chains initiate, grow and terminate within a second. ATRP and NMP are both controlled via a reversible activation deactivation capping reaction which in turn is controlled via the persistent radical effect (PRE). RAFT, on the other hand, is controlled via degenerative transfer.[7] CRP is characterized by a linear increase of molar mass with conversion and a decreasing dispersity with conversion, tending towards unity. This is observed when the exchange reactions occur very quickly so that all chains grow equally. Initiation also needs to occur at low monomer conversion and be quantitative.

2.2.1 NMP

NMP makes use of persistent radicals (nitroxide radical) which reversibly deactivate propagating radicals by combination to dormant chains (alkoxyamine), as illustrated in scheme 2-2.

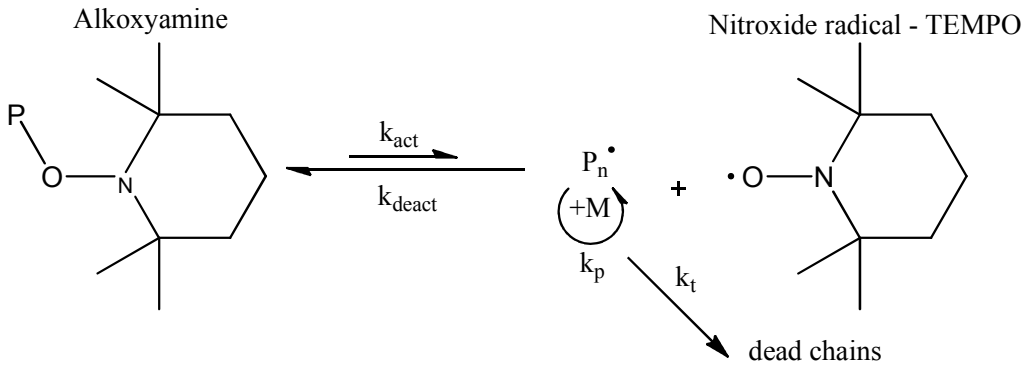

Scheme 2-2: General equilibrium mechanism of NMP

The dormant unstable species (alkoxyamine) is activated via thermal cleavage. The persistent radicals (nitroxide radical) are stable nitroxide compounds, which only react reversibly with propagating radicals, do not initiate other chains and do not self-terminate through combination. TEMPO, as illustrated in scheme 2-2, is one of the most widely used nitroxide radicals.[5,6]

2.2.2 RAFT

RAFT-mediated polymerization is controlled by a reversible addition-fragmentation mechanism which employs reversible deactivators known as RAFT agents illustrated in scheme 2-3.

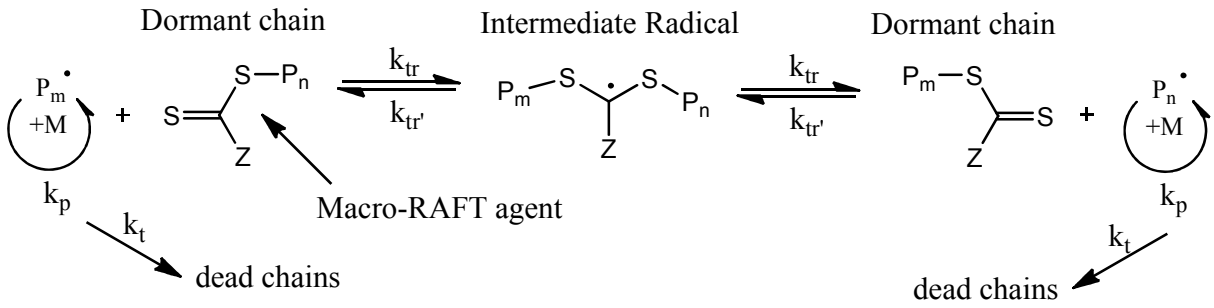

Scheme 2-3: General equilibrium mechanism for RAFT mediated polymerization

Control is achieved via a rapid equilibrium between the propagating radical species and the dormant polymeric RAFT agent (Macro-RAFT agent), where the rate of chain transfer is equal or larger than the rate of propagation.[4] Essentially, polymer chains spend more time in the dormant state (dormant chain) than they do in the active state (propagating radical), giving controlled molar masses with low dispersities.

2.2.3 ATRP

ATRP was first reported in the literature in 1995 by two different groups, Kato *et al.*[8] and Matyjaszewski and Wang.[9,10] Matyjaszewski and Wang reported copper catalyzed polymerizations, while Kato *et al.* recorded the use of ruthenium metal catalysts activated with aluminium complexes. Since ATRP was initially documented, many developments have been made, which have provided pathways to polymers with multiple topologies, compositions and functionalities.[11]

2.2.3.1 Mechanism of ATRP

ATRP is a transition metal complex catalysed system. The reaction is initiated with an alkyl halide and alkyl radicals ($P^{\bullet}$) are generated via a reversible redox process that is catalyzed by a transition metal complex (Mt^n/L), as illustrated in scheme 2-4. Homolytic cleavage of the alkyl halide occurs when it reacts with the transition metal complex (Mt^n/L), via an inner sphere electron transfer (ISET) process, resulting in a higher oxidation state metal halide complex ($X\text{-}Mt^{n+1}/L$) and a radical ($P^{\bullet}$).[12] This process is called activation and is defined by the activation rate coefficient (k_{act}).

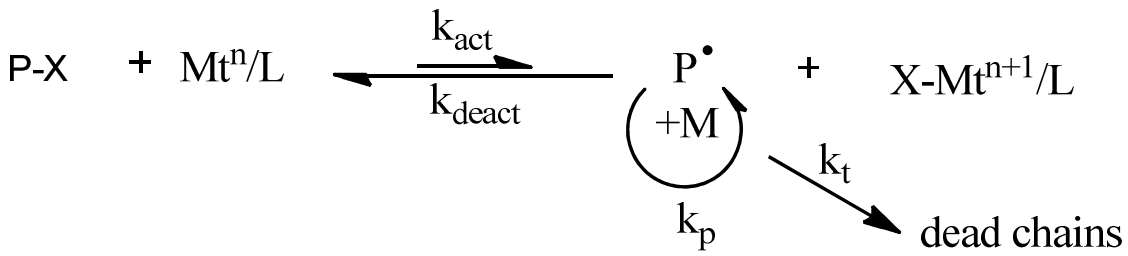

Scheme 2-4: General mechanism for ATRP

The radical propagates when it reacts with monomer and after a certain time abstracts a halide back from the higher oxidation state metal halide, thus reforming a dormant alkyl halide. This reversible process is known as deactivation and is defined via the deactivation rate coefficient (k_{deact}). The ratio of k_{act} to k_{deact} determines the equilibrium constant (K_{ATRP}), which in turn controls the rate of polymerization. The magnitude of K_{ATRP} is determined by the nature of the catalyst complex as well as by the relative stabilities of the alkyl halide and the corresponding radical.[13] A controlled system requires a small K_{ATRP} in order to maintain a low concentration of radicals, thus minimizing termination.

The oxidized metal complexes ($X\text{-}Mt^{n+1}/L$) behave as persistent radicals, reducing the concentration of growing radicals, thereby shifting the equilibrium to the dormant side (P-X). This greatly reduces the termination rate (by reducing the radical concentration) and is known as the persistent radical effect (PRE).[14,15] As a result, the molar mass increases linearly with time and the number average

degree of polymerization (DP_n) can be determined by the ratio of consumed monomer to initiator at a specific conversion as illustrated in equation 2-1.[16]

$$DP_n = \frac{[M]_0}{[I]_0} \times conversion \qquad 2\text{-}1$$

$[M]_0$ is the initial monomer concentration and $[I]_0$ is the initial initiator concentration. As previously discussed, ATRP relies on fast initiation and fast reversible deactivation. It also depends on factors such as the initiator, catalyst and ligands, monomer, solvent, temperature and additives, which are going to be discussed briefly.

2.2.3.2 Initiators

The initiator plays a large role in ATRP as it controls the number of chains that propagate, ultimately controlling the targeted molar mass. Initiation has to be fast and side reactions need to be kept to a minimum for an effective ATRP initiation to occur. ATRP initiators are most often found to be low molar mass alkyl halides (R-Br, Cl or I) with the activity of the initiator increasing with the increasing substitution of the halide ($1^o < 2^o < 3^o$).[17] It has been found that chlorine and bromine initiators are more efficient and achieve better molar mass control than iodine initiators.[18] The activity of the initiator decreases with increasing bond strength: R- I > R-Br > R-Cl, although alkyl iodide initiators need special precautions due to their instability.[9] The activity of the initiator also depends on the structure of the alkyl group and follows a generalized structural trend: phenyl ester > cyanide > ester > benzyl > amide.[19] Block or graft polymers can also be synthesized by attaching the initiator to a macromolecule.[20]

2.2.3.3 Catalyst and ligands

Transition metals from the d^n group most commonly serve as catalysts in ATRP. A few prerequisites need to be met in order for the transition metal to serve as a catalyst. The transition metal centre must be able to participate in an inner sphere one electron transfer and it must also be able to accommodate the halide transferred from R-X, through expansion of the coordination sphere. The metal centre also needs to be highly selective towards halogens to prevent side reactions.[21] This study employs the use of copper catalysts due to their versatility for a large range of monomers under diverse conditions.[10] Other types of catalysts have also been used such as iron,[22] ruthenium[8] and nickel.[23]

The selection of a suitable ligand is of utmost importance to conduct a controlled polymerization. The ligand determines the solubility of the catalyst complex but by doing so, also affects the redox potential of the metal centre. An appropriate ligand should affect the redox potential in such a way that the equilibrium between the propagating radicals and dormant species is shifted towards the

dormant species.[24] In practice, electron-withdrawing substituents on the ligand result in a higher concentration of Mt^n/L, while electron- donating groups favour Mt^{n+1}/L.[17] Ligand structure can also affect the activity of the catalyst complex by sterically obstructing the accommodation of the transferred halide, thus reducing the activity of the complex.[25] Nitrogen ligands have effectively been employed in copper mediated ATRP, where multidentate ligands promote a more controlled polymerization to monodentate ligands.[26] The activity of nitrogen based ligands in copper catalysed ATRP is related to the ligands structure and follows the following trend: tetradentate (cyclic-bridged) > tetradentate (branched) > tetradentate (cyclic) > tetradentate (linear) > tridentate > bidentate. The environment of the nitrogen atoms within the ligand are also key to the activity of the catalyst and also follow a trend: pyridine ≥ aliphatic amine > imine.[27] Examples of ligands successfully used in this study are N,N,N′,N″,N″pentamethyldiethylenetriamine (PMDETA), tris[2-(dimethylamino)ethyl]amine (Me_6Tren) and tris(2-pyridylmethyl)amine (TPMA) and are illustrated in figure 2-1.

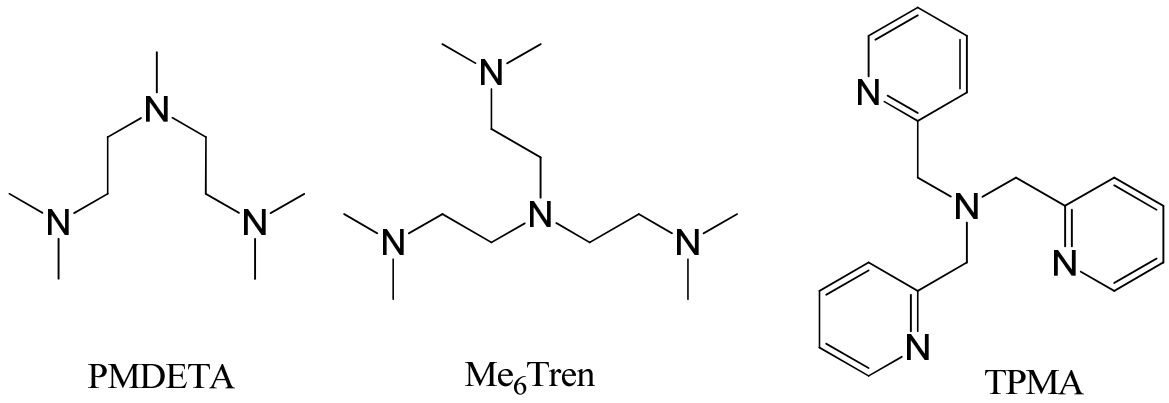

Figure 2-1: Examples of nitrogen based ligands used in copper mediated ATRP

2.2.3.4 Monomers, solvent, temperature and additives

Many different monomers have been successfully polymerized via ATRP. Monomers include styrene, acrylates, methacrylates, acrylamides, methacrylamides and others which can stabalize the propagating radical in polymerization.[21] ATRP can be performed in bulk but is more commonly found in solution.[28] Dilution allows higher conversions to be achieved but drastically decreases the reaction rate.[29] Most solvents are applicable with the exception of water, as long as the solvent does not negatively interact with the catalyst.[30] In additions, solvents are mostly non-polar such as toluene[31] and diphenylether,[32] although polar solvents such as alcohols[33] have also been used. The rate of polymerization increases with rising temperature because both the K_{ATRP} and k_p increase. This results in worse control due to a larger concentration of radicals and side reactions also become more pronounced.[31] Oxygen oxidizes transition metal catalysts in ATRP and thus needs to be

removed from the reaction prior to initiation. ATRP is however tolerant to a small amount of oxygen if a reducing agent is added.

2.2.3.5 Drawbacks of traditional ATRP

Although ATRP is one of the most efficient controlled radical techniques, relatively high concentrations of transition metal catalysts are needed. Apart from being an environmental concern, polymer properties such as thermal stability may also suffer from residual transition metal. Undesirable colour is also imparted on the synthesized polymer which needs to be removed.[34] Copper, for example, can be removed by passing the polymer solution through an alumina or silica column.[35] To overcome the high use of transition metal, an improved system has been developed to reduce the amount of copper catalyst required, by making use of redox reactions with organic or organometallic compounds. This system functions via an electron transfer mechanism and is known as "activators regenerated by electron transfer" (ARGET) ATRP.

2.2.3.6 ARGET ATRP

In conventional copper-mediated ATRP, the concentration of the catalyst to the initiator is generally 1:1. The concentration of the catalyst however, can be significantly reduced if an appropriate reducing agent is added in excess relative to the catalyst. The copper (II) that accumulates as a result of the PRE can be steadily regenerated to copper (I) by the reducing agent as illustrated in scheme 2-5.

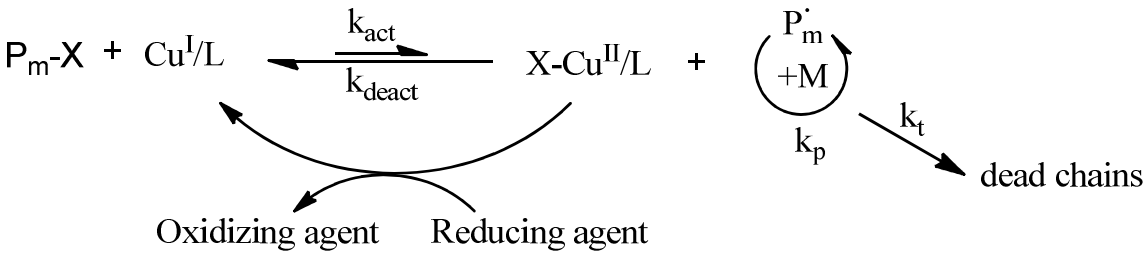

Scheme 2-5: General mechanism of ARGET ATRP

The catalyst concentration cannot be indefinitely reduced, but controlled polymerization has been reported using as low as 6.4 ppm copper catalyst for butyl acrylate.[36] Due to the reducing agent being present, a stable copper (II) species can be used as the catalyst. Various reducing agents have been reported including the Food and Drug Administration (FDA) approved tin(II) 2-ethylhexanoate and ascorbic acid.[37] Reducing agents also scavenge oxygen which allows polymerizations to be carried out in the presence of limited amounts of oxygen. An inhibition period is observed during which the oxygen is consumed, after which the polymerization commences.[38] ARGET ATRP removes the difficulties of grafting from surfaces in the presence of

oxygen.[39] The main drawback of ARGET ATRP is that ligand must be added to the metal up to many times molar excess (~ 10) to keep it solubilised and protect the catalyst from side reactions.[40]

2.3 Electrospinning

Electrospinning is a versatile technique used to produce continuous fibres from polymer solution or melt, with diameters in the nanometer to micrometer range. The typically produced nanofibrous mats have an extremely large surface area on which further surface modification can take place.

2.3.1 Basic electrospinning setup

An electrospinning setup comprises a syringe/syringe pump, a high voltage power supply, a spinneret (needle) and a collector (grounded or charged conductor) as illustrated in figure 2-2. The polymer solution runs through the needle in the case of a syringe or can be injected at a certain flow rate with the use of a syringe pump. A high voltage power source, usually direct current between 1 – 30 kV, induces charges that are spread evenly over the surface of the polymer droplet at the end of the needle. The polymer droplet experiences two electrostatic forces, the electrostatic repulsion of the surface charges and the Coulombic force exerted by the external electric field. As a result of these two forces, the drop is distorted into the Taylor cone. A liquid jet emerges from the cone once the electric field reaches a certain threshold and the electrostatic forces overcome the surface tension of the polymer solution. The liquid jet undergoes a whipping and stretching process, where the solvent evaporates, leading to the formation of a super thin fibre. The charged fibre is collected on the grounded/charged collector and is randomly orientated in a mat.[41,42]

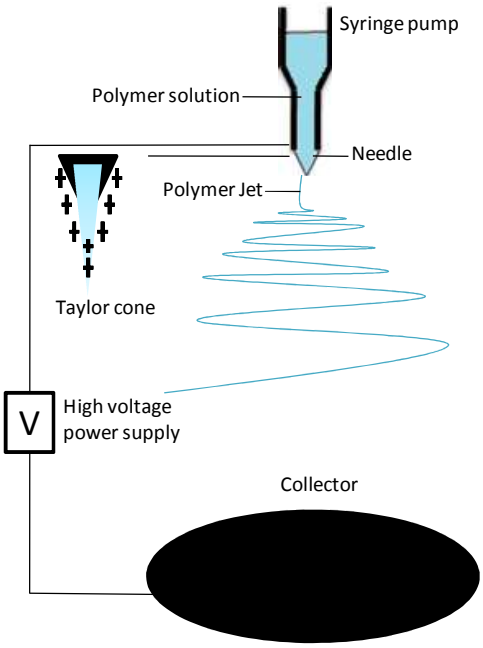

Figure 2-2: Basic setup for electrospinning

2.3.2 Controlling the morphology of the fibres

Several factors exist, which play a role on the morphology and diameter of the fibres which include the operation conditions of the electrospinning setup, the intrinsic properties of the solution and the environment. Operational conditions include the flow rate of the polymer solution, the distance between the spinneret and collector and the strength of the electric field. Intrinsic properties of the solution include viscosity, which can be affected by the solvent and polymer concentration, solvent, polarity, surface tension and electric conductivity. Environmental factors which can also have an impact include temperature and humidity.

One of the biggest problems in electrospinning is the formation of unwanted beads in the fibres, as illustrated in figure 2-3.[43] Beads form as a result of surface tension outweighing solution viscosity and net charge density.[43] Practically, beads can be suppressed by increasing the solution viscosity (higher polymer concentration), adding salts to increase the conductivity of the solution or using solvents with lower surface tensions.[44,45]

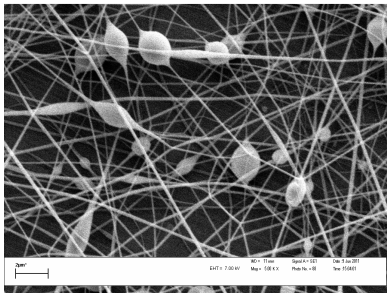

Figure 2-3: SEM image of beaded poly(sytrene-alt-maleic anhydride) nanofibres

2.4 Photochromism

Photochromic molecules are able to reversibly switch between two isomeric structures, A and B, as a result of the absorption of light of a specific wavelength (λ_1) as illustrated in scheme 2-6. These molecules are then able to return to their original state through the absorption of another wavelength of light (λ_2) or by a thermal process.

$$\mathbf{A} \underset{\lambda_2 \text{ or } \Delta}{\overset{\lambda_1}{\rightleftharpoons}} \mathbf{B}$$

Scheme 2-6: Basic scheme of photochromism

This phenomenon is known as photochromism and is accompanied by a colour change.[46] Molecules A and B each have their own absorption spectrum associated with a different visual colour.[47] Various different classes of photochromic molecules exist including spiropyrans,[48] azobenzenes,[49] diarylethenes[50] and many others. They are most commonly used to auto-colour photochromic sun(glasses) but have other applications such as the development of erasable memory, due to their

switching ability on a molecular level.[51] They have also been applied in reversible wettability as reviewed by Xin *et al*.[52] The diversity of the chemistry involved in the reverse switching processes is quite extensive due to the different classes of photochromic compounds. Spiropyrans are going to be discussed in more depth as they were the chosen molecule for this study

2.4.1 Photochemistry of spiropyrans

Spiropyrans (Sp) are defined as molecules which contain a pyran ring, containing two allylic hydrogens, and which are involved in a spiro-linkage (quaternary carbon) at their second carbon atom.[53] Spiropyran and its derivatives (ring-closed) are generally colourless and photoisomerize when irradiated with ultraviolet (UV) light to form the coloured merocyanine isomer (ring-open). This occurs via a ring opening reaction as a result of the photochemical cleavage of the C-O bond in the 2H-pyran ring.[54] Exposure of the merocyanine isomer to visible light converts it back to the spiropyran isomer as illustrated in scheme 2-7.[55] It can also be converted thermally back to the spiropyran isomer.[53]

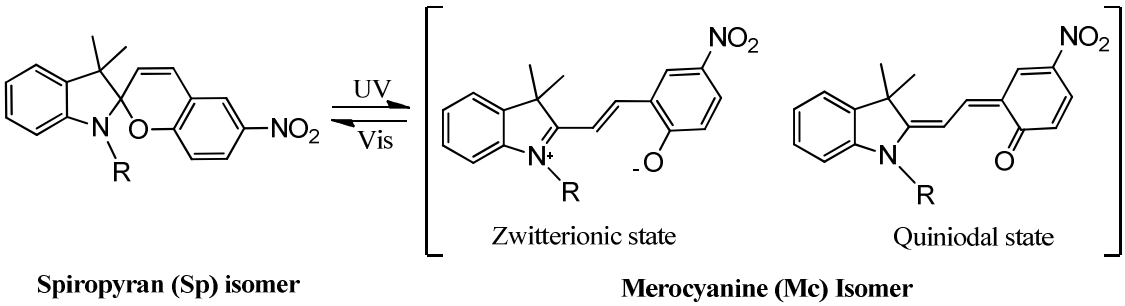

Scheme 2-7: Reversible photoisomerization of spiropyran to merocyanine

The merocyanine isomers can exist in two states, the zwitterionic and the quiniodal form. The zwitterionic state of the merocyanine isomer is favoured because there is no loss of aromaticity in the oxygen substituted-ring compared to the quiniodal state.[56] The merocyanine isomer is coloured because the increased conjugation causes the absorption band to be red-shifted towards the visible spectrum.[57] The ground state dipole moment of spiropyran is 5D while the ground state dipole moment of merocyanine is 20D. This change is a result of the conformational change which occurs during the photoisomerization. When these derivatives are functionalized on a surface, the surface tension will change in proportion to the dipole moments.[58] This allows these photochromic dyes to be used in light-activated smart surfaces.

2.4.2 Spiropyran Functionalized Surfaces

Photoresponsive materials have been studied for a long time and include surface-functionalized materials that have many different surface properties including controllable wettability and motion due to surface gradients.[56,59,60] Spiropyrans are ideal candidates for controlling the wettability of surfaces due to their hydrophilic zwitterionic merocyanine state while their spiropyran state is

hydrophobic. Many examples of spiropyran-functionalized surfaces have been reported in literature. Bletz *et al*. reported a photosensitive burst valve that controls the ion and water permeability through a membrane, by functionalizing an aluminium membrane with spiropyran.[59] Rosario *et al*. reported silicone nanowires grown off smooth silicone surfaces which were then functionalized covalently with spiropyran units and fluorinated hydrophobic units. This produced a photosensitive rough hydrophobic surface under visible light. Water droplet motion was induced using a light gradient as a result of the UV advancing contact angle being smaller than the visible receding contact angle.[61] It is our contention that electrospun nanofibrous mats will mimic the rough surface produced by the silicone nanowires.

2.5 Reversibly "sticky" surfaces

It is often necessary to be able to control the adhesion of surfaces. The idea of reversible adhesion, was devised while looking at the mechanism by which geckos are able to attach and detach their feet from surfaces. It was discovered that there were unique nano/microstructures on the gecko's feet which gave it this ability.[62] The example of the gecko relates to solid-solid adhesion but recently bio-inspired super-hydrophobic (contact angle (CA) > 150 ^{o}) surfaces with liquid-solid adhesion properties have come to light. These materials are important for biotechnology, microfluidic systems and further applications in material science.[63,64]

2.5.1 Liquid-solid adhesion

Two types of liquid-solid adhesion exist, high adhesion to water and low adhesion to water. High adhesion-to-water super-hydrophobic surfaces are bio-inspired by a rose petal where although the CA is larger than 150 ^{o}, the water droplet sticks to the petal. The water droplet remains in the same position even if the petal is tilted or hung upside down.[65] Low adhesion-to-water super-hydrophobic surfaces are bio-inspired by a lotus leaf. Water droplets roll of a tilted lotus leaf, removing dust particles as they go.[61] These two examples can be explained using Wenzel's and Cassie's theories as well as the triple-phase liquid/air/solid contact line (TCL).[66]

Wenzel's model[67] describes the liquid droplet completely filling the grooves of the rough surface and the TCL is continous, causing the droplet to stick. Cassie's model[68] describes the droplet sitting on air pockets thereby decreasing the liquid-solid interface (TCL discontinuous) allowing the droplet to roll off the surface (figure 2-4).[69] Most cases are however known as a metastable state where a droplet partially wets a surface. These states are controlled by the surface morphology as well as the chemical composition on the surface.[70.71] Switching between the Wenzel and Cassie

states will allow the formation of a reversibly "sticky" surface. Practically this can be performed by changing the chemical composition or morphology of the surface by external stimuli such as temperature, photoelectric and magnetic fields.[69]

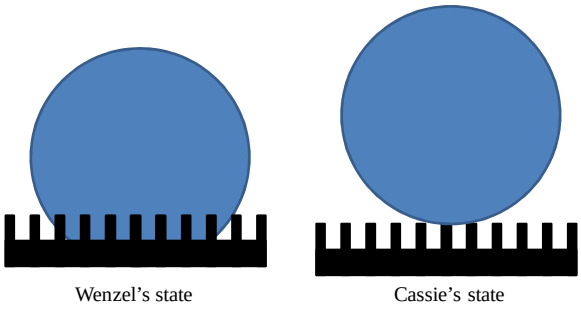

Figure 2-4: Difference between Wenzel's and Cassie's states

2.5.2 Reversibly "sticky" surfaces through spiropyran

As previously described, spiropyran has been used to create reversible wettability, using light as the stimulus. In a similar fashion, spiropyran could also be used to create a reversibly "sticky" surface, provided the surface is sufficiently hydrophobic. The spiropyran used in this study had a carboxylic acid functionality. In order to covalently bond it to the surface, an amine functionality was needed. Chapter 3 introduces amide coupling chemistry, in order that an amine-functionalized spiropyran could be produced as illustrated in scheme 2-8.

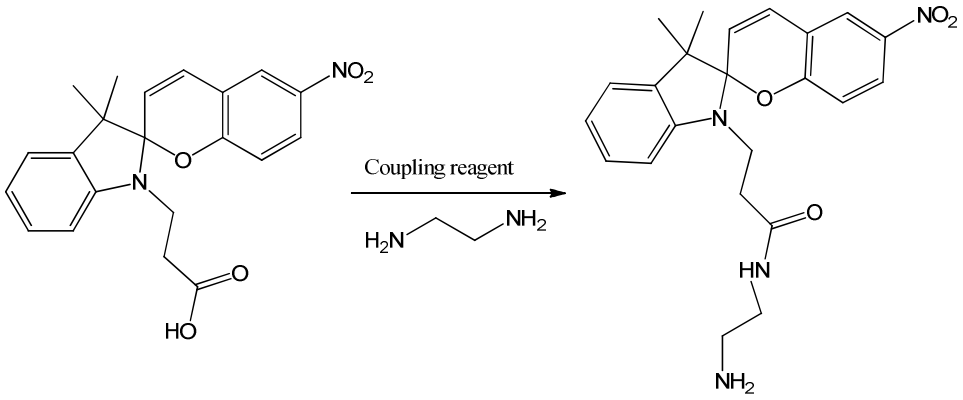

Scheme 2-8: Proposed synthesis of amine-functionalized spiropyran

2.6 References

(1) Matyjaszewski, K. In *Controlled/Living Radical Polymerization*; American Chemical Society: **2000**; Vol. 768, p 2-26.

(2) Szwarc, M. *Nature* **1956**, *178*, 1168-1169.

(3) Ayres, N. *Polym. Rev.* **2011**, *51*, 138-162.

(4) Moad, G.; Solomon, D. H. *The chemistry of radical polymerization*; Elsevier, **2006**.

(5) Grubbs, R. B. *Polym. Rev.* **2011**, *51*, 104-137.

(6) Tebben, L.; Studer, A. *Angew. Chem., Int. Ed.* **2011**, *50*, 5034-5068.

(7) Braunecker, W. A.; Matyjaszewski, K. *Prog. Polym. Sci.* **2007**, *32*, 93-146.

(8) Kato, M.; Kamigaito, M.; Sawamoto, M.; Higashimura, T. *Macromolecules* **1995**, *28*, 1721-1723.

(9) Wang, J.-S.; Matyjaszewski, K. *J. Am. Chem. Soc.* **1995**, *117*, 5614-5615.

(10) Wang, J.-S.; Matyjaszewski, K. *Macromolecules* **1995**, *28*, 7901-7910.

(11) Braunecker, W. A.; Matyjaszewski, K. *J. Mol. Catal. A: Chem.* **2006**, *254*, 155-164.

(12) Lin, C. Y.; Coote, M. L.; Gennaro, A.; Matyjaszewski, K. *J. Am. Chem. Soc.* **2008**, *130*, 12762-12774.

(13) Braunecker, W. A.; Tsarevsky, N. V.; Gennaro, A.; Matyjaszewski, K. *Macromolecules* **2009**, *42*, 6348-6360.

(14) Fischer, H. *J. Polym. Sci., Part A: Polym. Chem.* **1999**, *37*, 1885-1901.

(15) Fischer, H. *Chem. Rev.* **2001**, *101*, 3581-3610.

(16) Matyjaszewski, K.; Davis, T. P. *Handbook of Radical Polymerization*; John Wiley & Sons, Hoboken **2003**.

(17) Tang, W.; Kwak, Y.; Braunecker, W.; Tsarevsky, N. V.; Coote, M. L.; Matyjaszewski, K. *J. Am. Chem. Soc.* **2008**, *130*, 10702-10713.

(18) Gillies, M. B.; Matyjaszewski, K.; Norrby, P.-O.; Pintauer, T.; Poli, R.; Richard, P. *Macromolecules* **2003**, *36*, 8551-8559.

(19) Tang, W.; Matyjaszewski, K. *Macromolecules* **2007**, *40*, 1858-1863.

(20) Klaikherd, A.; Nagamani, C.; Thayumanavan, S. *J. Am. Chem. Soc.* **2009**, *131*, 4830-4838.

(21) Matyjaszewski, K.; Xia, J. *Chem. Rev.* **2001**, *101*, 2921-2990.

(22) Teodorescu, M.; Gaynor, S. G.; Matyjaszewski, K. *Macromolecules* **2000**, *33*, 2335-2339.

(23) Uegaki, H.; Kotani, Y.; Kamigaito, M.; Sawamoto, M. *Macromolecules* **1997**, *30*, 2249-2253.

(24) Matyjaszewski, K.; Göbelt, B.; Paik, H.-j.; Horwitz, C. P. *Macromolecules* **2001**, *34*, 430-440.

(25) Xia, J.; Zhang, X.; Matyjaszewski, K. In *Transition Metal Catalysis in Macromolecular Design*; American Chemical Society: **2000**; Vol. 760, p 207-223.

(26) Tang, H.; Arulsamy, N.; Radosz, M.; Shen, Y.; Tsarevsky, N. V.; Braunecker, W. A.; Tang, W.; Matyjaszewski, K. *J. Am. Chem. Soc.* **2006**, *128*, 16277-16285.

(27) Tang, W.; Matyjaszewski, K. *Macromolecules* **2006**, *39*, 4953-4959.

(28) Matyjaszewski, K. In *Solvent-Free Polymerizations and Processes*; American Chemical Society: **1999**; Vol. 713, p 96-112.

(29) Davis, K. A.; Paik, H.-J.; Matyjaszewski, K. *Macromolecules* **1999**, *32*, 1767-1776.

(30) Matyjaszewski, K.; Davis, K.; Patten, T. E.; Wei, M. *Tetrahedron* **1997**, *53*, 15321-15329.

(31) Haddleton, D. M.; Crossman, M. C.; Dana, B. H.; Duncalf, D. J.; Heming, A. M.; Kukulj, D.; Shooter, A. J. *Macromolecules* **1999**, *32*, 2110-2119.

(32) Coessens, V.; Pintauer, T.; Matyjaszewski, K. *Prog. Polym. Sci.* **2001**, *26*, 337-377.

(33) Robinson, K. L.; Khan, M. A.; de Paz Banez, M. V.; Wang, X. S.; Armes, S. P. *Macromolecules* **2001**, *34*, 3155-3158.

(34) Tsarevsky, N. V.; Matyjaszewski, K. *Chem. Rev.* **2007**, *107*, 2270-2299.

(35) Ma, I. Y.; Lobb, E. J.; Billingham, N. C.; Armes, S. P.; Lewis, A. L.; Lloyd, A. W.; Salvage, J. *Macromolecules* **2002**, *35*, 9306-9314.

(36) Chan, N.; Cunningham, M. F.; Hutchinson, R. A. *Macromol. Chem. Phys.* **2008**, *209*, 1797-1805.

(37) Min, K.; Gao, H.; Matyjaszewski, K. *Macromolecules* **2007**, *40*, 1789-1791.

(38) Matyjaszewski, K.; Dong, H.; Jakubowski, W.; Pietrasik, J.; Kusumo, A. *Langmuir* **2007**, *23*, 4528-4531.

(39) Hansson, S.; Östmark, E.; Carlmark, A.; Malmström, E. *ACS Appl. Mater. Interfaces* **2009**, *1*, 2651-2659.

(40) Matyjaszewski, K.; Jakubowski, W.; Min, K.; Tang, W.; Huang, J.; Braunecker, W. A.; Tsarevsky, N. V. *Proc. Natl. Acad. Sci.* **2006**, *103*, 15309-15314.

(41) Doshi, J.; Reneker, D. H. *J. Electrostatics* **1995**, *35*, 151-160.

(42) Li, D.; Xia, Y. *Adv. Mater.* **2004**, *16*, 1151-1170.

(43) Fong, H.; Chun, I.; Reneker, D. H. *Polymer* **1999**, *40*, 4585-4592.

(44) Lee, K. H.; Kim, H. Y.; Bang, H. J.; Jung, Y. H.; Lee, S. G. *Polymer* **2003**, *44*, 4029-4034.

(45) Greiner, A.; Wendorff, J. H. *Angew. Chem., Int. Ed.* **2007**, *46*, 5670-5703.

(46) Schnabel, W. *Polymers and Light: Fundamentals and Technical Applications*; 1st ed.; WILEY-VCH: Weinham, **2007**.

(47) Bouas-Laurent, H.; Dürr, H. *Pure Appl. Chem.* **2001**, *73*, 639–665.

(48) Lukyanov, B.; Lukyanova, M. *Chem. Heterocycl. Compd. (N. Y., NY, U. S.)* **2005**, *41*, 281-311.

(49) Hamon, F.; Djedaini-Pilard, F.; Barbot, F.; Len, C. *Tetrahedron* **2009**, *65*, 10105-10123.

(50) Irie, M.; Kobatake, S.; Horichi, M. *Science* **2001**, *291*, 1769-1772.

(51) Irie, M. *Chem. Rev.* **2000**, *100*, 1683-1684.

(52) Xin, B.; Hao, J. *Chem. Soc. Rev.* **2010**, *39*, 769-782.

(53) Shibaev, V.; Bobrovsky, A.; Boiko, N. *Prog. Polym. Sci.* **2003**, *28*, 729-836.

(54) Emsting, N. P.; Arthen-Engeland, T. *J. Phys. Chem.* **1991**, *95*, 5502-5509.

(55) Chibisov, A. K.; Gorner, H. *J. Photochem. Photobio., A* **1997**, *105*, 261-267.

(56) Rosario, R.; Gust, D.; Hayes, M.; Springer, J.; Garcia, A. A. *Langmuir* **2003**, *19*, 8801-8806.

(57) Maafi, M. *Molecules* **2008**, *13*, 2260-2302.

(58) Bletz, M.; Pfeifer-Fukumura, U.; Kolb, U.; Baumann, W. *J. Phys. Chem. A* **2002**, *106*, 2232-2236.

(59) Vlassiouk, I.; Park, C.-D.; Vail, S. A.; Gust, D.; Smirnov, S. *Nano Lett.* **2006**, *6*, 1013-1017.

(60) Rosario, R.; Gust, D.; Hayes, M.; Jahnke, F.; Springer, J.; Garcia, A. A. *Langmuir* **2002**, *18*, 8062-8069.

(61) Rosario, R.; Gust, D.; Garcia, A. A.; Hayes, M.; Taraci, J. L.; Clement, T.; Dailey, J. W.; Picraux, S. T. *J. Phys. Chem. B* **2004**, *108*, 12640-12642.

(62) Autumn, K.; Liang, Y. A.; Hsieh, S. T.; Zesch, W.; Chan, W. P.; Kenny, T. W.; Fearing, R.; Full, R. J. *Nature* **2000**, *405*, 681-685.

(63) Wu, D.; Wu, S.-Z.; Chen, Q.-D.; Zhang, Y.-L.; Yao, J.; Yao, X.; Niu, L.-G.; Wang, J.-N.; Jiang, L.; Sun, H.-B. *Adv. Mater.* **2010**, *23*, 545-549.

(64) Wang, D.; Wang, X.; Liu, X.; Zhou, F. *J. Phys. Chem. C* **2010**, *114*, 9938-9944.

(65) Feng, L.; Zhang, Y.; Xi, J.; Zhu, Y.; Wang, N.; Xia, F.; Jiang, L. *Langmuir* **2008**, *24*, 4114-4119.

(66) Yoshimitsu, Z.; Nakajima, A.; Watanabe, T.; Hashimoto, K. *Langmuir* **2002**, *18*, 5818-5822.

(67) Wenzel, R. N. *Ind. Eng. Chem.* **1936**, 28, 988-994

(68) Cassie, A. B. D.; Baxter, S. *Trans. Faraday Soc.* **1944**, 40, 546-551

(69) Liu, M.; Jiang, L. *Adv. Funct. Mater.* **2010**, *20*, 3753-3764.

(70) Kusumaatmaja, H.; Yeomans, J. M. *Langmuir* **2007**, *23*, 6019-6032.

(71) Johnson, R. E.; Dettre, R. H. *J. Phys. Chem.* **1964**, *68*, 1744-1750.

Chapter 3: Spiropyran synthesis

3.1 General Amide Chemistry

The synthesis of amides is a vast research topic due to its importance in the synthesis of proteins. Montalbetti et. al.[1] has written a comprehensive review on the various synthetic routes that lead to amide coupling. There are two important steps in the synthesis of amides: activation of the carboxylic acid and nucleophilic attack of the amine group in question (scheme 3-1). It is necessary to activate the acid with a suitable leaving group to prevent the amine from deprotonating it, thus deactivating the acid.

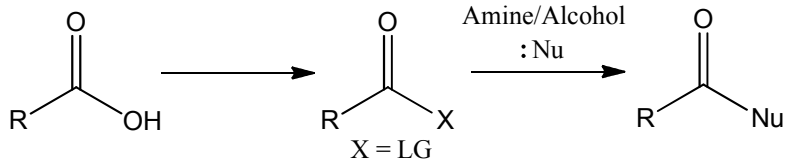

Scheme 3-1: Ester/Amide formation

3.1.1 Amide Coupling Techniques

There are many ways of activating the carboxylic acid to make it more susceptible to nucleophilic attack. All of these techniques involve the formation of an activated intermediate that has a better leaving group than the parent carboxylic acid -OH. A classic example is the activation of a carboxylic acid, with for example thionyl chloride, to produce a highly reactive acid chloride. This group can be attacked by a nucleophilic amine giving an amide functional group.[2]

More elaborate activation of carboxylic acids is also common and can be achieved by making use of various carbodiimides including dicyclohexyl carbodiimide (DCC) and diisopropyl carbodiimide (DIC).[3] An *O*-acylisourea is the activated species formed when a carbodiimide reacts with a carboxylic acid (Scheme 3-2). This activated species is however susceptible to rearrangement with the formation of an inactive *N*-acylurea species.[4] This can be prevented by the addition of a secondary nucleophile which reacts with the *O*-acylisourea before the undesired rearrangement can take place. The secondary nucleophile, however, must still be a good leaving group so that the amine can attack with formation of an amide. These nucleophiles also prevent racemization of the carboxylic acid where stereochemistry is important (eg. peptide chemisty). Examples of these secondary nucleophiles are 1-hydroxybenzotriazole (HOBt), dimethylaminopyridine (DMAP) and N-hydroxysuccimide (HoSu).[5]

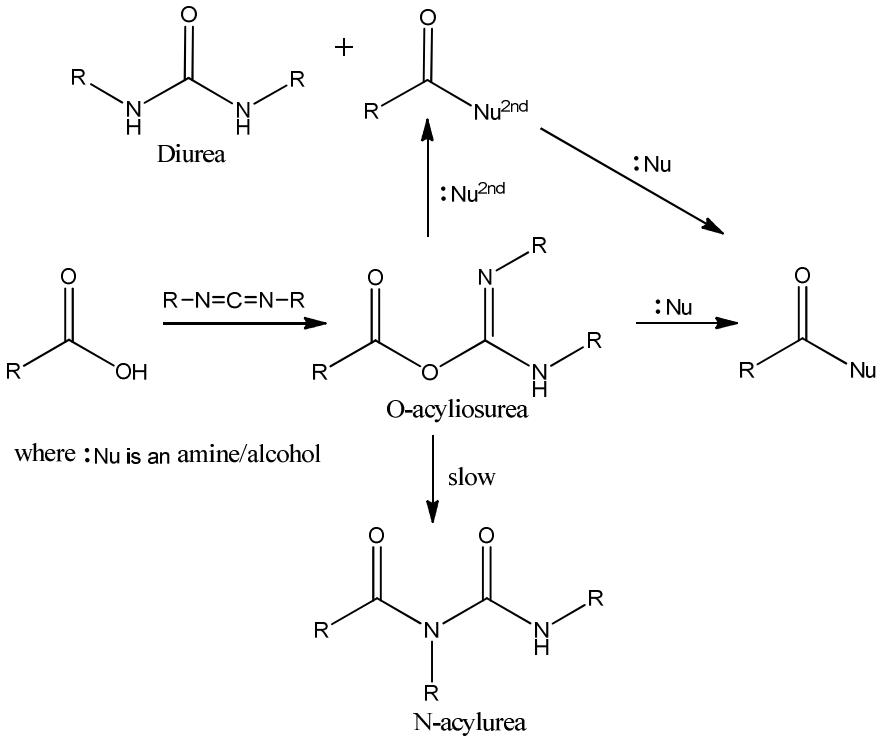

Scheme 3-2: Carbodiimide coupling

Activation can also be accomplished in a two pot synthesis via the formation of an activated ester. This activated ester readily reacts with an amine nucleophile producing an amide. The activated ester can be formed with an alcohol for example HOBt of HOSu, or via a mixed anhydride such as that formed when a carboxylic acid reacts with pivaloyl chloride.[6,7,8] In the mixed anhydride case the amine nucleophile is forced to attack the alpha carbon due to the steric hindrance of the *tert*-butyl group on the β-carbon (Scheme 3-3).

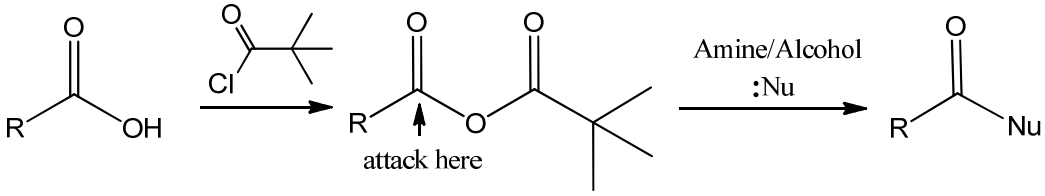

Scheme 3-3: Pivaloyl chloride-assisted coupling

As has been mentioned, there are many ways to create amides; the decision as to which one to use is based on many factors as different systems have different optimal coupling conditions. Each of these amide coupling techniques described are useful in their own right, depending on the system and molecules involved. Spiropyrans (Sp), as described in the literature chapter, are photochromic compounds that are able to switch between two states using light as the stimulus (Scheme 3-4). They exist in the ring-closed spiropyran state in visible light and when irradiated with ultraviolet

light, isomerise to the ring-open merocyanine state.[9] These ring-opening factors have to be considered when trying to couple amines to spiropyrans.

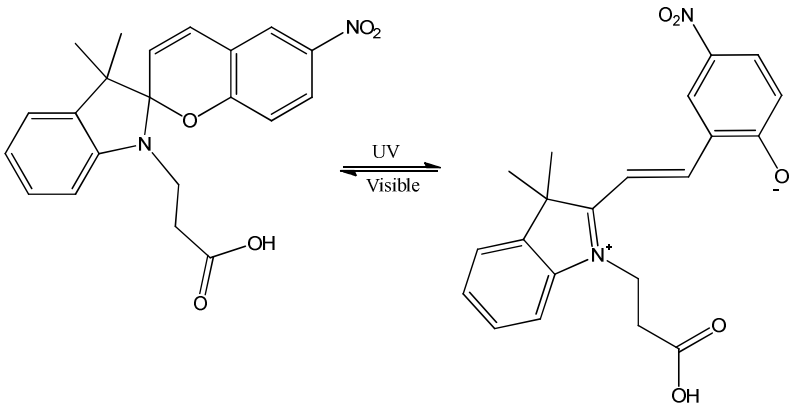

Scheme 3-4: Photochromic spiropyran

3.2 Results and Discussion

The aim of this section of the study was to produce a spiropyran dye with an amine-functionality. The strategy involved the coupling of a carboxylic acid-functionalized spiropyran to a diamino-compound using general amide coupling techniques. The diamino compound in question was ethylenediamine, which was chosen to give a certain degree of flexibility between the dye and whichever surface it may have been reacted with in later stages. This flexibility would allow the dye to have movement space in which it would be able to ring-open and –close. The reaction seemed simple in theory but proved to be far more complicated experimentally.

3.2.1 SpAcid Synthesis

1′-(2-Carboxyethyl)-3′,3′-dimethyl-6-nitrospiro(indoline-2,2′[2*H*-1]benzopyran) (SpAcid) was prepared using a procedure derived from literature, which involved a two part synthesis.[10] The first step involved the synthesis of 1′-(2-carboxyethyl)-2,3,3-trimethylindoline iodide which was an off-yellow salt. Trimethylindolenine and 3-iodopropanoic acid were refluxed in methyl ethyl ketone at 100 ^{o}C for 3 hours affording the product in 83% yield. The target SpAcid was then formed by condensing this salt with 5-nitrosalicylaldehyde, catalysed by piperidine, yielding a green powder (scheme 3-5). This was accomplished by refluxing at 100 ^{o}C for three hours in methyl ethyl ketone with a 62% yield. The successful formation of SpAcid was confirmed using ^{1}H and ^{13}C NMR spectroscopy.

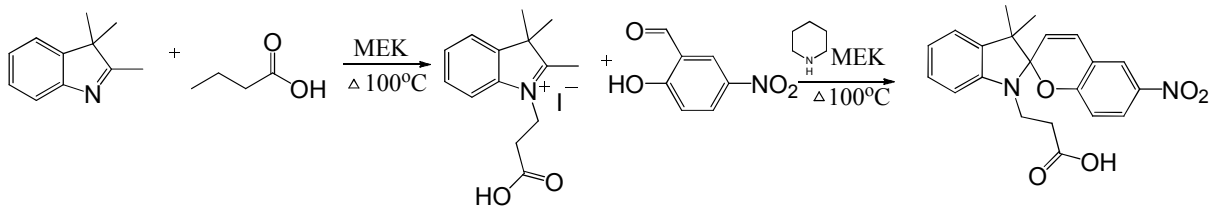

Scheme 3-5: SpAcid synthesis

The suggested mechanism for the formation of the SpAcid is shown in scheme 3-6. The piperidine base initiates the reaction through abstraction of a proton from the terminal methyl group. The electron-rich enamine is then able to attack the aldehyde carbon on 5-nitrosalicylaldehyde in an aldol reaction. The importance of a good organic base is shown in the mechanism. SpAcid is formed with the release of water as a byproduct.

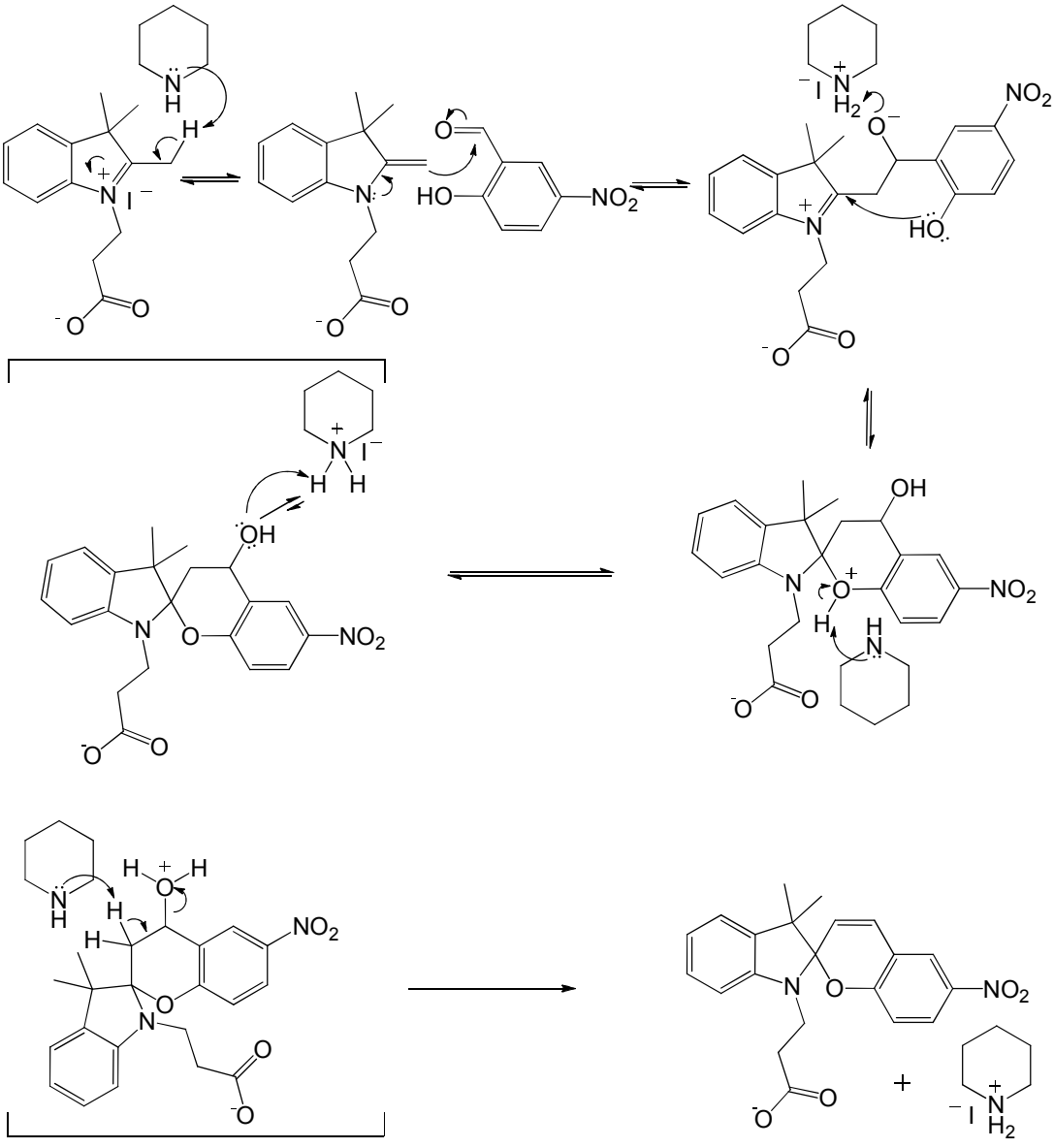

Scheme 3-6: SpAcid formation mechanism

3.2.2 Attempted synthesis of amine-terminated SpAcid

Two important factors were considered when choosing the experimental conditions for the coupling of ethylenediamine to SpAcid (Scheme 3-7). The first important consideration was the choice of the coupling reagents to be used. The carbodiimide coupling method was chosen because it is one of the most widely used methods for amide synthesis in the literature. DCC was selected as the carbodiimide of choice and it was used with a catalytic amount of DMAP to prevent the formation of the inactive N-acrylurea species. The second concern was the unwanted formation of a bi-functionalised amine. This was addressed by adding a statistical excess of ethylenediamine (10 times) to ensure that the mono-functionalised dye was produced. All experiments were run in amberised glassware to ensure that the SpAcid remained in the ring-closed isomer. Even though all of these considerations were implemented experimentally, the synthesis of the amine-functional spiropyran (SpAmine) was unsuccessful under these conditions. It was concluded that the SpAcid had to be activated with a better leaving group in order to form SpAmine.

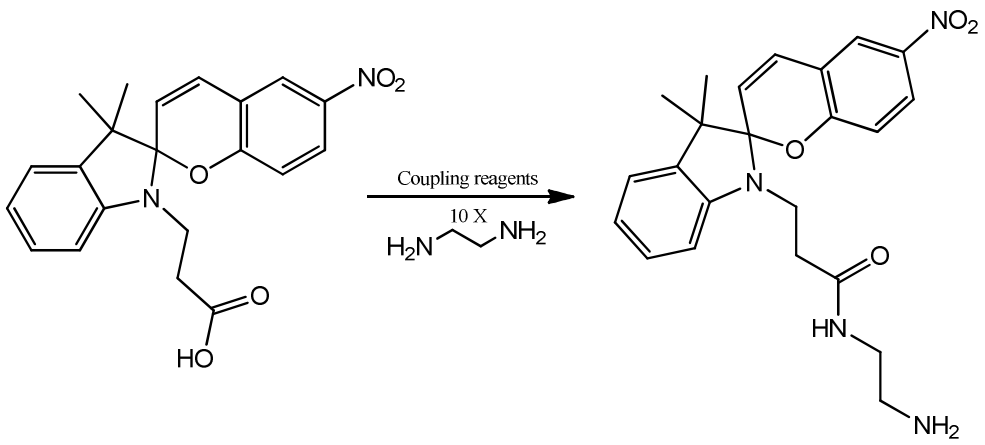

Scheme 3-7: SpAmine formation

3.2.3 Model study of SpAcid

It was suggested that a mono-functional amine should be used to determine the optimum coupling conditions for ethylenediamine to SpAcid. *n*-Butylamine was chosen for the model study because it was available in the laboratory. The product formed would be a spiropyran with an amide bond and a butyl chain (SpBuAmide) (Scheme 3-8).

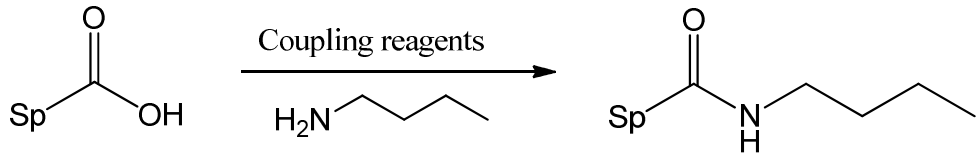

Scheme 3-8: SpBuAmide formation

Five different coupling conditions were applied to the system. An equimolar amount of SpAcid to *n*-butylamine was always used. The main coupling reagent was always used in 20% excess to SpAcid. The secondary coupling reagent was used in 1:2 ratio relative to SpAcid. Tetrahydrofuran was used as a solvent for the entire model study. All reactions were performed with 0.25 M SpAcid and all reactions were completed in two steps. The first step involved the addition of SpAcid, the primary and secondary coupling reagent and solvent to an amberised three-necked flask. This was stirred on ice (0 ^{o}C) for an hour after which n-butylamine in a small amount of solvent was added dropwise over a further hour. The reaction was thus slowly warmed to room temperature and allowed to stir for 24 hours.

The first four coupling conditions involved use of the carbodiimide species. Both DCC and DIC were used in combination with HOBt and HOSu. This led to four separate reactions, DCC/HOSu, DCC/HOBt, DIC/HOSu and DIC/HOBt, which have been summarized in table 3-1. These reactions were all tracked using thin layer chromatography (TLC) and after 24 hours, no further change was observed. The four reactions were thus worked up in the same way. First the solutions were filtered to remove the urea and then they were purified using silica flash chromatography (ethyl acetate: pentane – 1:1). The filtration step removed the by-product from carbodiimide coupling, dicyclohexylurea in the case of DCC and diisopropylurea in the case of DIC. That which was not removed via filtration was removed in the silica flash chromatography. Interesting results were obtained when comparing DCC to DIC coupling in the model study. In the case of DCC, the undesired N-acylurea species was formed when using HOSu and HOBt as a secondary nucleophile. This was observed, while tracking the reaction using TLC, as a spot just above the main product. The unwanted rearrangement was also characterised using ^{1}H NMR spectroscopy (figure 3-1). The *N*-acylurea species was not seen when using DIC as a primary coupling reagent in both cases of secondary coupling reagents.

Table 3-1: SpBuAmide coupling conditions

Primary coupling agent	Secondary coupling agent	Yield (%)	N-acylurea
DCC	HOSu	70	Yes
DCC	HOBt	75	Yes
DIC	HOSu	95	No
DIC	HOBt	98	No

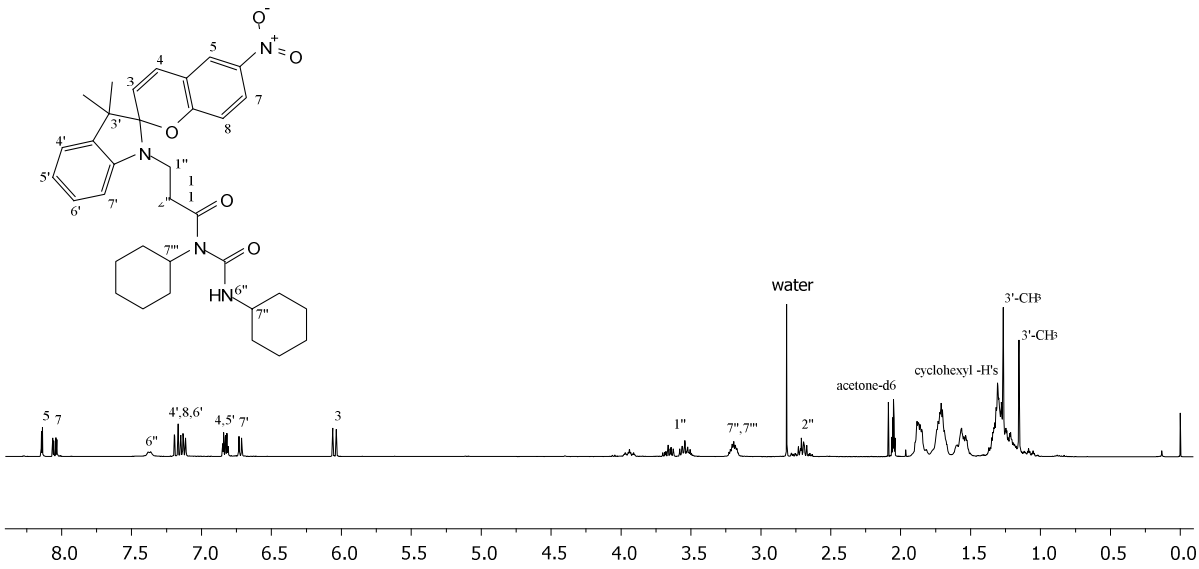

Figure 3-1: ^{1}H NMR spectroscopy of N-acylurea by-product

DCC coupling gave a lower SpBuAmide percentage yield compared to DIC coupling due to the formation of the *N*-acylurea side-product. DCC with HOSu gave a 70% yield while DCC with HOBt gave a 75% yield. DIC couplings with both secondary coupling reagents gave a higher percentage yield due to the absence of *N*-acylurea. Pleasingly, DIC with HOBt gave a 98% product yield while DIC with HOSu yielded 95% product.

SpAcid was also converted to SpBuAmide using pivaloyl chloride. This coupling reagent was added to the model study to confirm whether mixed anhydride chemistry was a viable alternative to carbodiimide chemistry. There was no secondary coupling reagent as with the prior four model conditions. Pyridine was used in a two-to-one molar excess to SpAcid to trap the released chloride after activation via pivaloyl chloride. *N*-butylamine was added to a cooled reaction flask (0 ^{o}C) dropwise following the previous test conditions. The reaction was tracked with TLC (ethyl acetate: pentane – 1:1) and showed the formation of one new spot. Characterisation via ^{1}H NMR spectroscopy revealed that the product was formed in a 85% yield.

The model study of *n*-butylamine with SpAcid revealed that DIC/HOBt was the best combination of coupling reagents to form the amide. These optimum model conditions were used to couple SpAcid to ethylenediamine. The result was similar to the previous attempt when DCC/DMAP was used as a coupling combination, with separation being very complicated and no sign of SpAmine being observed.

3.2.4 Alternative synthetic pathways for the synthesis of SpAmine

SpAcid **2** was also activated using pivaloyl chloride under similar conditions to the model study (scheme 3-9). Unfortunately, SpAmine was not formed after the addition of excess ethylenediamine. The resulting solution was ultra-violet (UV) inactive. This led to the conclusion that the aromatic structure of the spiropyran had been changed. It was not possible to separate the products using flash column chromatography due to overlapping of products. Later in the study, the loss in the aromatic system was linked to the effect that the free-amine had on the spiropyran ring system.

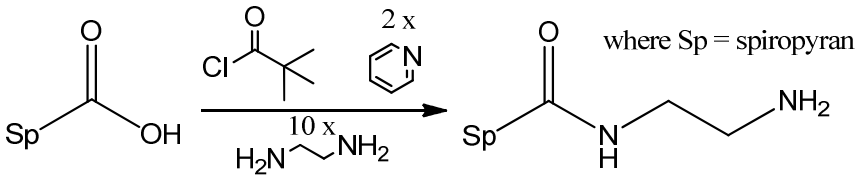

Scheme 3-9: SpAmine via pivaloyl chloride coupling method

Fissi *et al*. reported how SpAcid was activated using N-hydroxysuccinimide with standard DCC/DMAP coupling conditions.[10] SpAcid was then coupled to an amine-functional polymer [Poly($_L$-lysine)]. A similar approach was attempted with the successful formation of the activated ester spiropyran, which was then reacted with an excess of ethylenediamine in an attempt to form SpAmine (scheme 3-10). The expected product was not formed, with multiple spots present on the TLC, which could not be separated via flash chromatography. The complexity of the system became more and more apparent as further pathways were attempted.

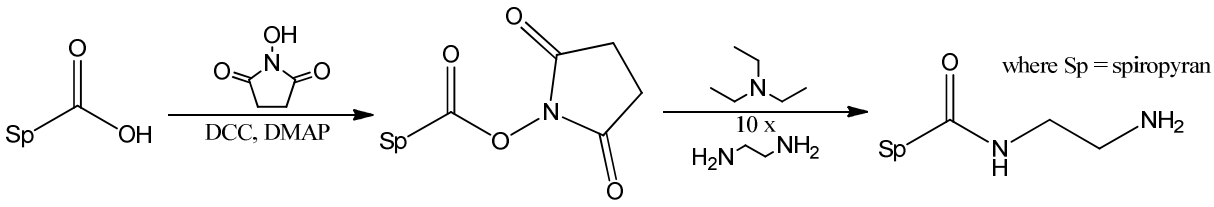

Scheme 3-10: SpAmine via N-hydroxysuccinimide activation

A final attempt was made to form SpAmine by initially protecting aminoethanol. Often, functional groups are protected prior to further synthesis to prevent side reactions occurring. Amines can be readily protected using *tert*-butyloxycarbonyl (Boc).[11] Boc can be removed in a gentle manner by refluxing in tetrabutylammonium fluoride (TBAF). This is important for molecules which have acid and base sensitive functional groups such as esters.[12]

Aminoethanol was therefore protected with Boc and was then esterified to SpAcid. The reaction took place at 0 ^{o}C and proceeded in high yield (90%). The BOC-protected amine was subsequently deprotected using TBAF, in order to maintain the labile ester bond (scheme 3-11). The final solution was unfortunately UV inactive similar to the result obtained when using pivaloyl chloride as a coupling medium. The products were purified using flash column chromatography (dichloromethane:methanol 25:1) but products overlapped during the separation. The deprotection of the spiropyran Boc-protected amine led to the conclusion that the free terminal amine had some effect on the structure of the spiropyran ring. It was also speculated that a possible irreversible ring-opening reaction had occurred leading to unexpected results.

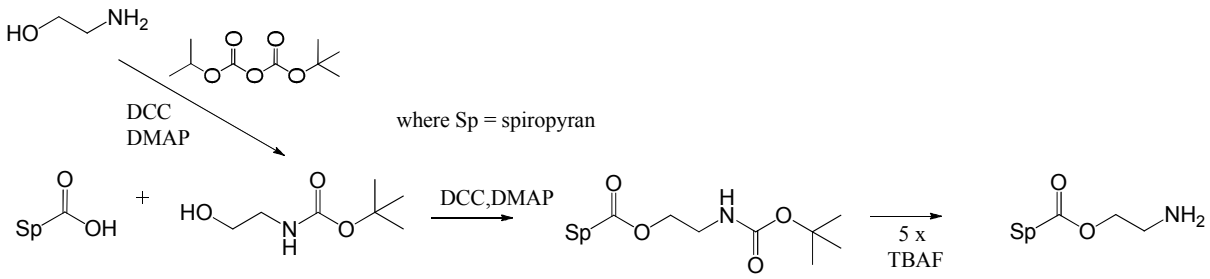

Scheme 3-11: Boc protected SpAmine pathway

3.2.5 Negative presence of the diamine

The difficulty in synthesising SpAmine was attributed to the effect that ethylenediamine had on SpAcid. To fully understand this, SpAcid was stirred in a large excess of ethylenediamine overnight after which all the excess ethylenediamine was removed under vacuum. ^{1}H NMR spectroscopy next revealed a dirty spectrum and the clean aromatic part of the spectrum as seen earlier in figure 3-3 had multiple new peaks. This suggested that the problem encountered synthesizing SpAmine was due to the negative interaction of the free amine and the ring. It also suggested that the free amine interfered with the aromatic ring-structure.

It was postulated that after SpAcid was activated, ethylenediamine would react, forming an amide bond. The pendant free amine would be available to interfere with the labile hemi-aminal oxygen in the ring structure of SpAcid. Scheme 3-13 shows the proposed theoretical scheme more clearly.

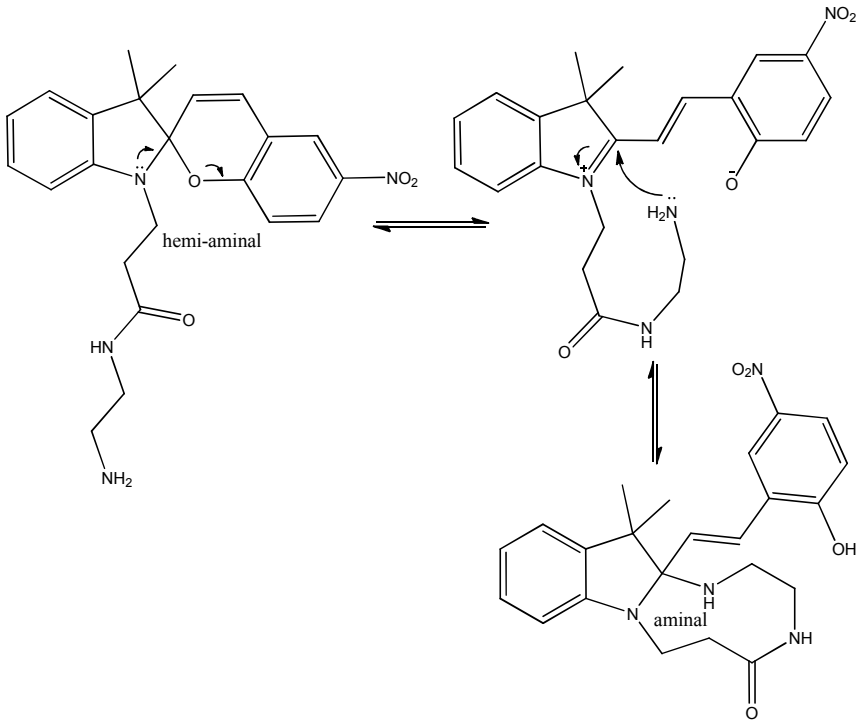

Scheme 3-13: Hemi-aminal to aminal rearrangement

3.2.6 SpAcid Salt

The literature stated that SpAcid was a yellow powder and soluble in dichloromethane (DCM).[13] The SpAcid that was synthesised in the study was a green powder and only partially soluble in DCM. This did call into question the purity of the SpAcid; however the ^{1}H NMR and ^{13}C NMR spectra both matched the literature values, and mass spectrometry (MS) revealed an expected M + H peak at 381 dalton.[10,13] All of this characterisation suggested that the SpAcid was indeed pure.

One possibility was that SpAcid was a salt and that the central nitrogen atom was protonated and positively charged. If this was the case, it would be possible to deprotonate the nitrogen using a base such as sodium bicarbonate ($NaHCO_3$). SpAcid was therefore stirred in a 0.80 M solution of $NaHCO_3$ for an hour after which the SpAcid (**b**) was extracted using DCM. The vacuum dried DCM-soluble SpAcid (**b**) was a purple crystalline solid. The extracted DCM-soluble SpAcid (**b**) was characterised with ^{13}C NMR spectroscopy and found to be identical to the partially soluble SpAcid (figure 3-2). ^{1}H NMR spectroscopy revealed similar observations except that the DCM-soluble SpAcid (**b**) had lost its acid –O<u>H</u> proton at 12.3 ppm (figure 3-3). This suggests that a salt had been formed. MS, however, confirmed that their mass peaks were identical.

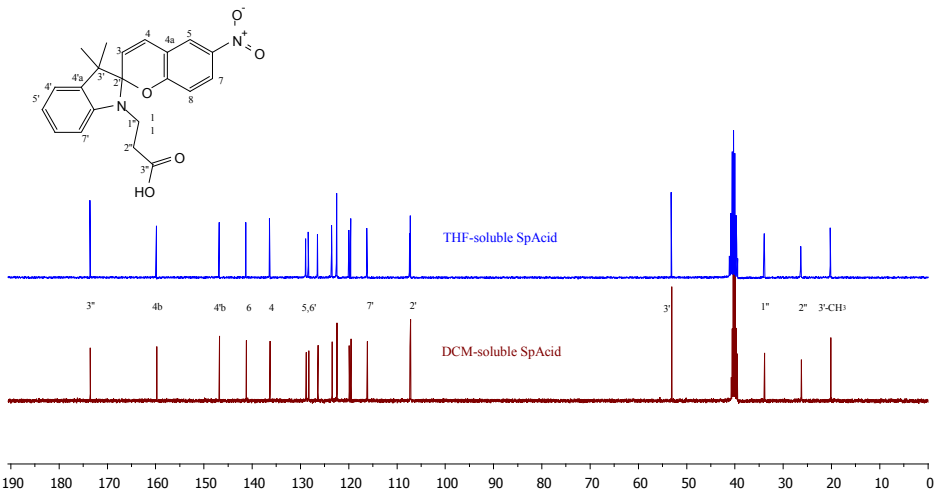

Figure 3-2: ^{13}C NMR spectroscopy of THF-soluble SpAcid vs. DCM-soluble SpAcid

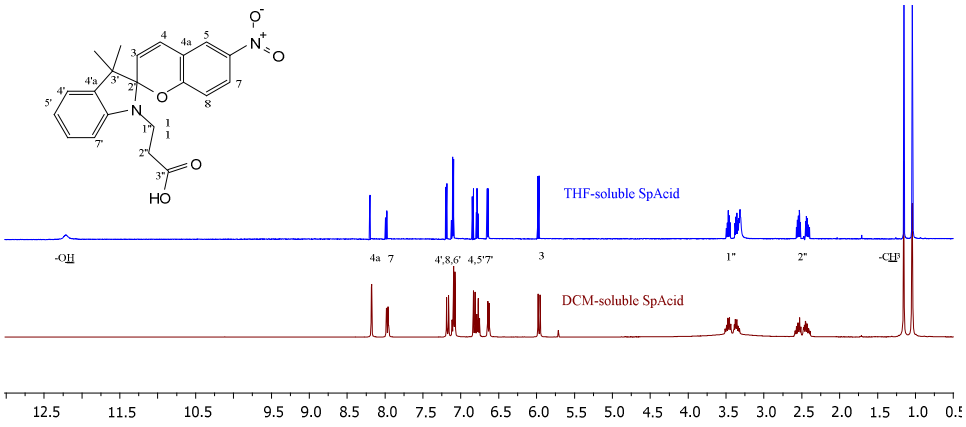

Figure 3-3: ^{1}H NMR spectroscopy of THF-soluble SpAcid vs. DCM-soluble SpAcid

To substantiate on the possible presence of a salt, SpAcid was refluxed in DCM for 3 hours. The solution was then filtered to remove the remaining undissolved SpAcid. The DCM was removed under vacuum to yield a yellow powder (**c**) (50%). ^{1}H and ^{13}C NMR spectroscopy both revealed similar spectra compared to those of SpAcid and compound **b**.

Figure 3-4: Colour of different spiropyran dyes

In solution [dimethylsulfoxide (DMSO)], SpAcid and compound **c** were clear in visible light (inside) and purple in UV light (365 nm) as illustrated in figure 3-5. This is analogous to the SpAcid synthesised in literature. The refluxed DCM-soluble SpAcid (**b**) however, was light purple in visible light and pink/purple in UV light (365 nm). UV light at 365 nm was used because

spiropyrans absorb at that wavelength. UV spectroscopy was thus used to further understand this phenomenon.

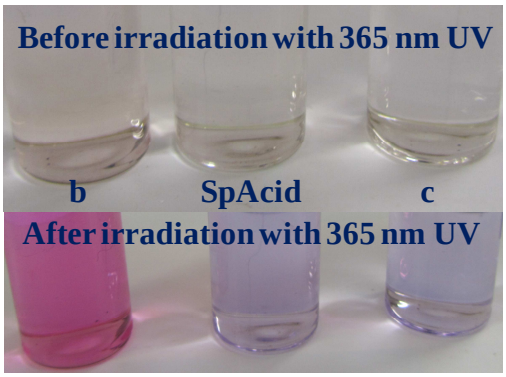

Figure 3-5: Spiropyran dyes before and after irradiation with 365 nm UV light

UV spectroscopy, in DMSO, was performed on all three samples and they all had similar spectra (figure 3-5). The graph on top is that of the ring-closed spiropyran form for all three samples and below is that of the ring-open merocyanine form. The slight difference in absorbances is due to differing concentrations as a result of not knowing the absolute molar mass. The absorption at 575 cm^{-1} on the bottom graph is due to the ring-open merocyanine form. This result is what would be expected for those samples that were exposed to UV light.

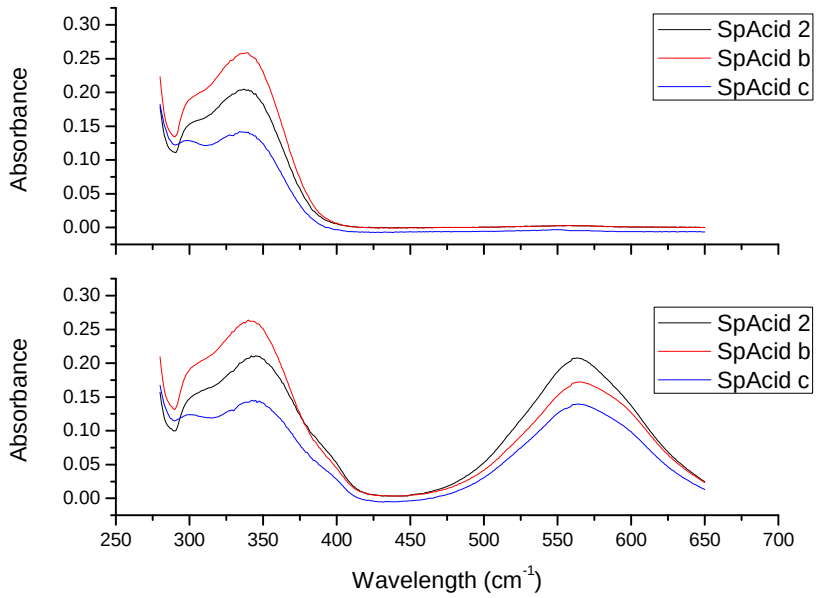

Figure 3-6: UV spectroscopy of SpAcid varieties

Achilleos *et al*. describe reverse photochromism occurring when the polarity of the environment stabilises the ring-open merocyanine form.[14] A similar mechanism could be occurring with compound **b**. The reason it was observed as purple in visible light could be due to some sort of stabilisation occurring. This would suggest that it was the sodium salt of the literature SpAcid and it

would also suggest that the SpAcid that was synthesised was in fact pure and identical to the compound that has been reported in literature. The polar ionic bond of the sodium salt would help to stabilize the ring-open merocyanine form giving rise to the purple solution.

3.2.6.1 SpAcid salts investigated

During the investigation into the purity of SpAcid, it was found that the sodium salt SpAcid (**b**) was a different shade of purple to SpAcid in UV light. Questions arose whether different salts would affect SpAcid in different ways and whether or not it was possible to tune the properties of the dye using different salts. A model study was performed using $NaHCO_3$, K_2CO_3, $CaCO_3$ and tetrabutylammoniumiodide (TBAI) as an organic salt, as illustrated in scheme 3-12.

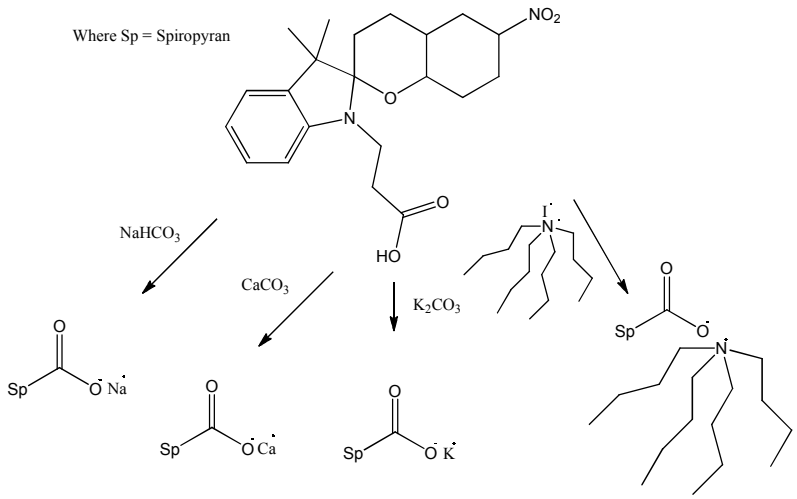

Scheme 3-12: Synthesis of SpAcid salts

SpAcid **2** was stirred in a 0.80 M solution of each salt for 3 hours after which the spiropyran salts were extracted in DCM, as reported for the sodium salt. The calcium and potassium spiropyran salt showed similar characteristics to the sodium salt in DMSO. The TBAI spiropyran salt on the other hand had a much lighter shade of pink in UV light. UV spectroscopy was next used to resolve this colour change under UV irradiation. Unfortunately, no shift in absorption was observed for the merocyanine absorption band region. In order to determine whether a shift occurred, a multi-beam UV spectrometer would be required which could continually irradiate the sample with UV light (365 nm) while the spectrum was being taken. This was unfortunately not available in our labs or those at other universities we contacted.

3.3 Conclusion

Despite the use of many different coupling techniques available, it turned out that the synthesis of an amine-functional spiropyran-derivative (SpAmine) was not possible under these conditions. This meant that another technique would have to be found in order to couple the spiropyran to a surface.

It was found that the origin of the problem appeared to lie in the pendant free amino group which interfered with the integrity of the ring-structure in SpAcid.

The plan thus far had been to incorporate SpAmine into a surface, by making use of its amine functionality. Due to its unsuccessful synthesis, the study focussed on providing a surface which could accommodate the spiropyran. Towards the end of this project, a paper was released describing the synthesis of SpAmine. It had been synthesised by activating the SpAcid with pentafluorophenyl trifluoroacetate as illustrated in scheme 3-14.[15] At the stage that this was found, an alternative strategy had been implemented for attaching the SpAcid to the polymer surface, so it was not utilized.

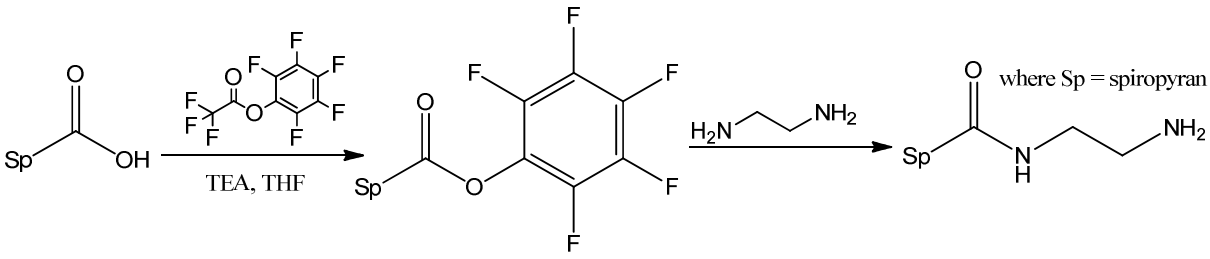

Scheme 3-14: Successful synthesis of SpAmine[10]

3.4 Experimental

3.4.1 Materials

The following chemicals were utilized in this part of the project: 2,2,3-trimethylindolenine (Aldrich, 99%), 3-iodopropanoic acid (Aldrich, 95%), 5-nitrosalicylaldehyde (Aldrich, 95%), piperidine (Sigma Aldrich, 99%), *N*,*N*-diisopropylcarbodimide (Fluka, 99%), 1-hydroxybenzotrizole hydrate (Aldrich, 95%), n-butylamine (Aldrich, 99%), dimethylsulphoxide-D_6 (Merck, 99.9%) and chloroform-D_1 (Merck, 99.8%) were used without further purification. Tetrahydrofuran (Aldrich, 98%) was distilled over lithium with benzophenone as an indicator. Chloroform, ethyl acetate, pentane, methyl ethyl ketone, and methanol (KIMIX, CP-grade, 99.5%) were used without further purification.

3.4.2 Experimental procedures

3.4.2.1 Preparation of 1′-(2-carboxyethyl)-2,3,3-trimethylindoline iodide (1)

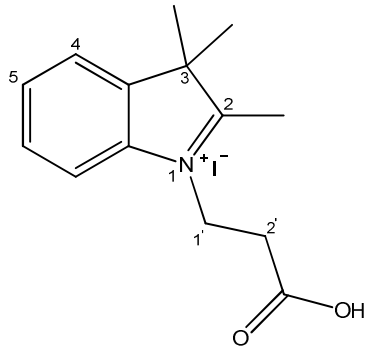

2,2,3-Trimethylindolenine (6.37 g, 40.0 mmol) and 3-iodopropanoic acid (7.99 g, 40.0 mmol) were dissolved in methyl ethyl ketone (9 mL) and heated at 100 ^{o}C under nitrogen for three hours. The solid material formed was dissolved in water after which the solution was washed with chloroform. The water was evaporated under vacuum yielding a pale yellow product. The product was dried under vacuum overnight at 60 ^{o}C leaving an off-yellow solid. (11.95 g, 83%). ^{1}H NMR (400 MHz, DMSO-d_6) δ 8.02 – 7.96 (m, 1H, H_{Ar}), 7.87 – 7.81 (m, 1H, H_{Ar}), 7.67 – 7.58 (m, 2H, H_{Ar}), 4.66 (t, J = 7.0 Hz, 2H, H-1′), 2.99 (t, J = 7.0 Hz, 2H, H-2′), 2.87 (s, 3H, -CCH_3), 1.54 (s, 6H, 2 -CH_3).

3.4.3.2 Preparation of 1′-(2-carboxyethyl)-3′,3′-dimethyl-6-nitrospiro(indoline-2,2′[2*H*-1]benzopyran) (2)

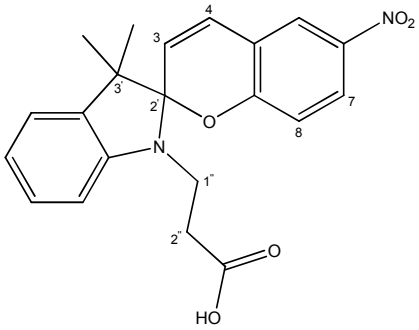

Compound **1** (10.00 g, 28.0 mmol), 5-nitrosalicylaldehyde (4.56 g, 28.0 mmol) and piperidine (2.37 g, 28.0 mmol) were dissolved in methyl ethyl ketone (20 mL). The solution was then refluxed at 100 ^{o}C for three hours. The product precipitated during refluxing as a green/yellow powder. The product was filtered and washed with cold methanol leaving a green powder. (6.60 g, 62%). ^{1}H NMR (400 MHz, DMSO-d_6) δ 12.01 (s, 1H, -OH), 8.21 (d, *J* = 2.8 Hz, 1H, H-5), 7.99 (dd, *J* =8.2, 1.8 Hz, 1H, H-7), 7.15 (m, 3H, H-4′,6′,8), 6.89 - 6.77 (m, 2H, H-4,5′), 6.64 (t, *J* = 10.9 Hz, 1H, 7′), 5.98 (t, *J* = 11.4 Hz, 1H, H-3), 3.44 (m, 2H, H-1′′), 2.50 (s, 2H, H-2′′), 1.18 (s, 3H, -CH_3), 1.07 (s, 3H, -CH_3)

3.4.3.3 1′-(3-(butylamino)-3-oxopropyl)-3′,3′-dimethyl-6-nitrospiro(indoline-2,2′[2*H*-1]benzopyran) (3)

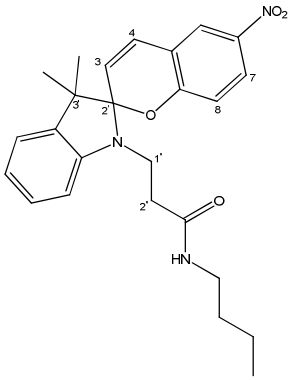

Compound **2** (0.500 g. 1.31 mmol) was dissolved in tetrahydrofuran (5 mL) in an ambered 3-neck flask. The solution was cooled to 0 ^{o}C with ice. *N*,*N*-diisopropylcarbodimide (0.200 g, 1.58 mmol) and 1-hydroxybenzotrizole hydrate (0.10 g, 0.67 mmol) were added to the solution and allowed to stir for 1 hour. *n*-butylamine (0.10 g, 1.3 mmol) in tetrahydrofuran (1 ml) was added dropwise over 1 hour. The solution was kept on ice for a further hour after which it was warmed to room temperature and left stirring for 24 hours. The product was purified by flash column chromatography (ethyl acetate : pentane 1 : 1) yielding off-yellow crystals (0.53 g, 92%). MP 127 –

128 °C. ^{1}H NMR (400 MHz, $CDCl_3$) δ 8.07 – 7.92 (m, 2H, H-5,7), 7.22 – 7.04 (m, 2H, H-4′,6′), 6.95 – 6.85 (m, 2H, H-8,4), 6.67 (dd, *J* = 8.1, 1.2 Hz, 2H, H-5′,7′), 5.84 (d, *J* = 10.4 Hz, 1H, H-3), 5.45 (s, 1H, -NH) 3.78 – 3.65 (m, 1H, H-1″), 3.51 – 3.40 (m, 1H, H-1″), 3.25 – 3.05 (m, 2H, 5″), 2.56 – 2.30 (m, 2H, H-2″), 1.42 – 1.20 (m, 7H, 6″,7″, -CH_3), 1.13 (s, 3H, -CH_3), 0.86 (t, *J* = 7.3 Hz, 3H, H-8″).

3.4.4 Characterization techniques

3.4.4.1 NMR spectroscopy

^{1}H NMR and ^{13}C NMR spectra were obtained in DMSO-d_6 (unless stated otherwise) with a Varian VXR-Unity (400 MHz) spectrometer. Chemical shifts were reported in parts per million (ppm) and tetramethylsilane (TMS) was used as internal reference.

3.4.4.2 UV-Vis spectroscopy

UV-Vis spectra were measured using a Perkin Elmer photodiode array spectrophotometer. The model of the spectrophotometer was a Lambda 20 which comprised a holographic monochromator, pre-aligned deuterium and halogen lamps and a photodiode array detector. Samples were measured in a 2mmm by 2mm cuvette at 25 °C. UV Winlab (version 2.0) software was used for data acquisition and processing.

3.5 References

(1) Montalbetti, C. A. G. N.; Falque, V. *Tetrahedron* **2005**, *61*, 10827-10852.

(2) Brown, H. C. *J. Am. Chem. Soc.* **1938**, *60*, 1325-1328.

(3) Kurzer, F.; Douraghi-Zadeh, K. *Chem. Rev.* **1967**, *67*, 107-152.

(4) Balcom, B. J.; Petersen, N. O. *J. Org. Chem.* **1989**, *54*, 1922-1927.

(5) Han, S.-Y.; Kim, Y.-A. *Tetrahedron* **2004**, *60*, 2447-2467.

(6) Anderson, G. W.; Zimmerman, J. E.; Callahan, F. M. *J. Am. Chem. Soc.* **1963**, *85*, 3039-3039.

(7) König, W.; Geiger, R. *Chem. Ber.* **1973**, *106*, 3626-3635.

(8) Wittenberger, S. J.; McLaughlin, M. A. *Tetrahedron Lett.* **1999**, *40*, 7175-7178.

(9) Chibisov, A. K.; Gorner, H. *J. Photochem. Photobio., A* **1997**, *105*, 261-267.

(10) Fissi, A.; Pieroni, O.; Ruggeri, G.; Ciardelli, F. *Macromolecules* **1995**, *28*, 302-309.

(11) Anderson, G. W.; McGregor, A. C. *J. Am. Chem. Soc.* **1957**, *79*, 6180-6183.

(12) Routier, S.; Saugé, L.; Ayerbe, N.; Coudert, G.; Mérour, J.-Y. *Tetrahedron Lett.* **2002**, *43*, 589-591.

(13) Su, J.; Chen, J.; Zeng, F.; Chen, Q.; Wu, S.; Tong, Z. *Polym. Bull.* **2008**, *61*, 425-434.

(14) Achilleos, D. S.; Vamvakaki, M. *Macromolecules* **2010**, *43*, 7073-7081.

(15) Kessler, D.; Jochum, F. D.; Choi, J.; Char, K.; Theato, P. *ACS Appl. Mater. Interfaces* **2011**, *3*, 124-128.

Chapter 4: Surface functionalization

4.1 Introduction

Electrospinning offers a simple, but versatile process to produce fibres with submicron diameters. Nanofibrous surfaces offer extremely high surface-areas as a result of their three-dimensional nano-structured surface topologies. This makes electrospinning the perfect tool to create functional surfaces because of the high area in which surface-specific chemistry can occur. In order to functionalize a surface, reactive groups are required and for this reason poly(styrene-alt-maleic anhydride) (PSMA) derivatives were chosen for this study (scheme 4-1).

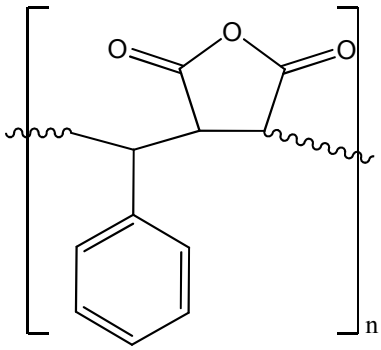

Scheme 4-1: Poly(styrene-alt-maleic anhydride)

4.1.1 Poly(styrene-alt-maleic anhydride)

Maleic anhydride (MaAh) is very reactive towards primary amines and undergoes a nucleophilic ring opening reaction as illustrated in scheme 4-2. The ring-opened MaAh can be ring-closed under high temperatures to produce the maleimide.[1,2] Unfortunately, MaAh cannot be homopolymerized under normal conditions. However, it is well known that styrene (Sty) copolymerized with MaAh in equimolar ratios via free radical polymerization produces an alternating copolymer.[3,4] As a result, PSMA is the perfect polymer for electrospinning because the resulting nanofibrous mat is highly reactive towards primary amines.

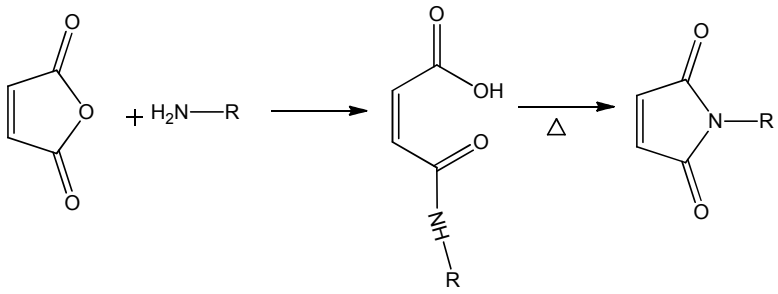

Scheme 4-2: Nucleophillic reaction of an amine with maleic anhyride

4.1.2 Electrospinning PSMA

Electrospun PSMA has been well reported in literature and it has been found that nanofibres are readily produced with dimethylformamide (DMF) solvent combinations.[5,6] Cécile *et al*. reported that adding a non-solvent such as cyclohexane (CyH) in small amounts (< 10%) led to a large decrease in fibre diameter, allowing PSMA nanofibres to be collected in the 200 – 300 nm range.[7] Generally, fibres are electrospun onto a conductive surface such as aluminium foil but sometimes it is convenient to electrospin fibres directly onto a liquid surface for post-spinning workup.[8,9] The liquid needs to be electrically conductive, unreactive towards the polymer and must be a non-solvent for the polymer, in order that the fibres remain intact on contact.

4.1.3 Hydrophobic surfaces

Nanofibrous surfaces are inherently hydrophobic due to their "rough" surface topology.[10] However, other factors also influence the surface hydrophobicity such as chemical structure, for example the abundance of hydrophilic polar functional groups such as hydroxyl (~OH). For this reason, surface modification with fluorinated groups such as pentadecafluorooctanoyl chloride (PFOC) is needed in order to produce superhydrophobic surfaces (contact angle > 150 ^{o}).[11]

4.2 Results and Discussion

The aim of this section of the study was to produce a crosslinked hydrophobic nanofibrous mat which had inherently reactive functional groups present of the surface. Furthermore, the implementation of atom transfer radical polymerization (ATRP) surface-initiators, where surface-initiated ATRP could later occur, was investigated.

4.2.1 PSMA derivatives

As previously discussed, PSMA can provide smooth nanofibres which have reactive anhydride moieties. This would make PSMA an ideal candidate for this study. However, due to the complexity of this project, multiple surface modifications were envisioned including graft polymerization from the surface. For this reason, PSMA was insufficient as it only had one functional group, MaAh. Huang and Wirth first reported surface-initiated ATRP (SI-ATRP) graft polymerization in 1997 and they successfully grafted poly(acrylamide) brushes from benzyl chloride-derivatized silica particles.[12] A polymerizable benzyl chloride derivative, 4-vinylbenzyl chloride (4vbCl), has since been used to initiate polymerizations from a polymer backbone. 4vbCl has a similar reactivity ratio to styrene and was used to polymerize poly(Sty-co-4vbCl-co-MaAh) (PSMA-Cl), a statistical terpolymer of the three monomers.

4.2.2 Polymerization of PSMA-Cl

PSMA-Cl was prepared via free radical polymerization using azobisisobutronitrile (AIBN) as an initiator. The three monomers, MaAh, Sty and 4vbCl were added in a 5:4:1 molar ratio. A three-neck round-bottom flask was charged with all three monomers, solvent (1,4-dioxane) and 0.1 mol% AIBN relative to the monomers. The polymerization was initiated by immersing the round-bottom in a 60 ^{o}C oil bath and allowed to polymerize for 8 hours under an argon atmosphere, as illustrated in scheme 4-3. The resulting turbid solution was precipitated dropwise into isopropanol (iPrOH), redissolved in tetrahydrofuran (THF) and then reprecipiated into iPrOH, yielding a white powder with a 89.6% yield. The structure was confirmed using ^{1}H and ^{13}C NMR spectroscopy.

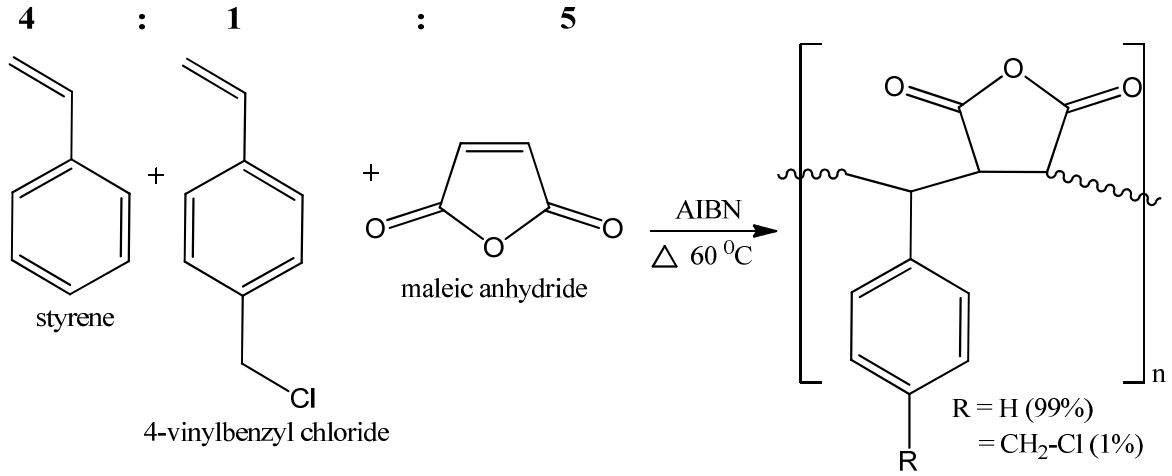

Scheme 4-3: Polymerization of PSMA-Cl

4.2.3 Characterization of PSMA-Cl

^{1}H NMR spectroscopy was used to characterize PSMA-Cl as illustrated in figure 4-1. The broad peak between 6.1 and 7.7 ppm is a consequence of the aromatic protons from the styrene and benzyl rings respectively. The methine and methylene protons from the polymer backbone are found as broad peaks between 1.4 to 3.8 ppm. The isolated broad peak at 4.6 ppm is due to the methylene protons (–C$\underline{H}_2$-Cl) from the benzyl ring. Some solvent peaks were also present that were not removed while drying the polymer in vacuum. Thus, the ^{1}H NMR spectroscopy shows clear evidence that PSMA-Cl was successfully synthesized. ^{13}C-NMR spectroscopy confirms these results and it is possible to see the methylene protons (–C$\underline{H}_2$-Cl) at 47.49 ppm.

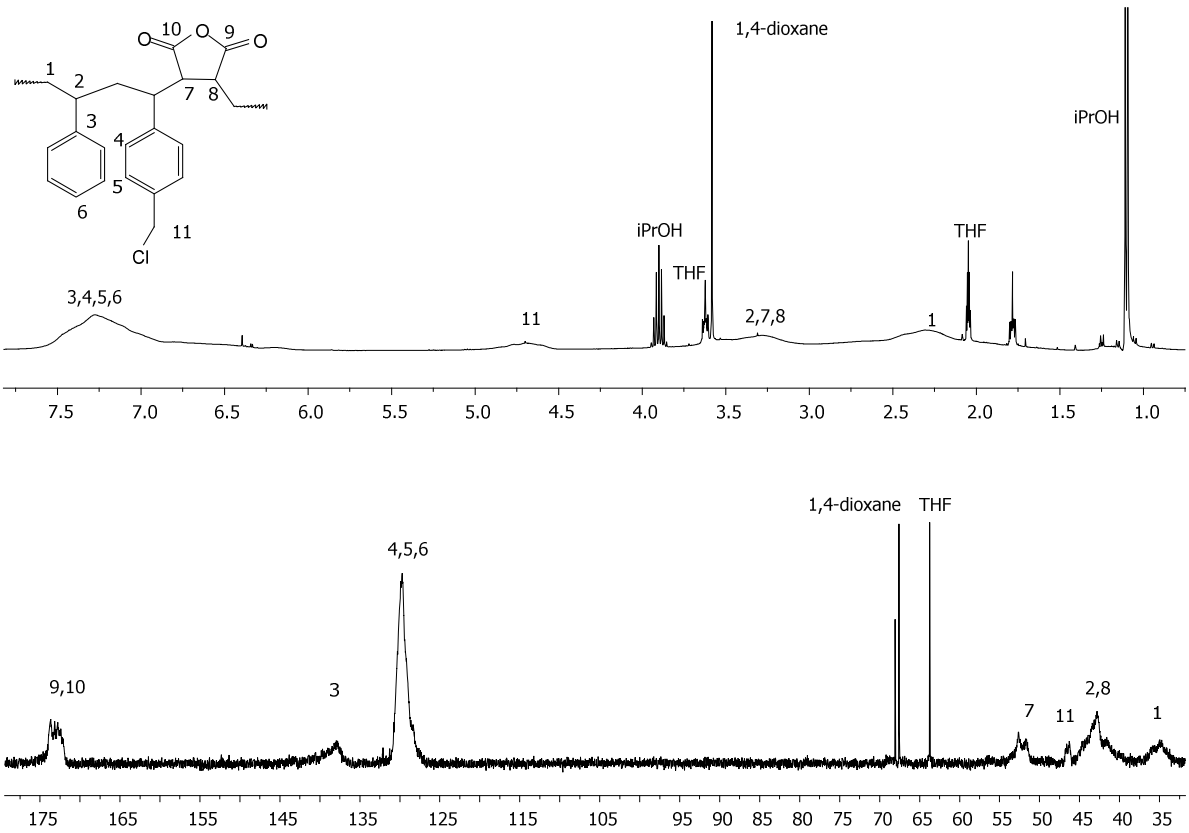

Figure 4-1: ^{1}H and ^{13}C NMR Spectroscopy of PSMA-Cl

Although, ^{1}H-NMR spectroscopy clearly shows that PSMA-Cl structure is intact, it cannot give the ratios that the three monomers were incorporated into the backbone. It is assumed that MaAh accounts for 50% of the backbone because it is statistically more likely that a styrene/4vbCl unit will cross-propagate with a MaAh unit than homo-propagate. It is important to know the ratio of Sty to 4vbCl, in order to know how many SI-ATRP initiator sites there are. This information is not possible to derive from the ^{1}H-NMR spectroscopy because the aromatic protons of Sty and 4vbCl are found under the same broad peak (6.1 – 7.7 ppm) and there is only one distinguishable methylene proton (4vbCl). Due to this complication, elemental analysis of the PSMA-Cl was performed using energy dispersive X-ray spectroscopy (EDX).

EDX data is only quantitative if an internal standard is used to setup a calibration curve. This would require the correct standards, which were not available for this project. This meant that all data received were only qualitative. However, EDX would still give a good idea of the ratio of the various elements present in PSMA-Cl which could then be used to determine the relative ratios of monomer incorporation. Three different samples of PSMA-Cl were analyzed and ten EDX

spectrums were recorded for each sample. The average mol percentages of carbon-to-oxygen-to-chlorine are presented in table 4-1.

Table 4-1: WDS data for PSMA-Cl

	Carbon	Oxygen	Chlorine
% incorporation	72.34	27.15	0.51
Moles		0.5656	0.01437
Ratio		39	1

To analyze the data, each weight percentage was made to be its equivalent value in grams. It was then possible to determine the relative molar quantity of oxygen and chlorine. The 3 oxygen atoms in MaAh were responsible for 27.15% of the composition. This meant that 9.05% of the sample was one of these three oxygen atoms. Only one chlorine atom was present in 4vbCl and was responsible for 0.51% of the total composition. Determining the molar ratio of these two elements gave a ratio of 39 : 1 (oxygen : chlorine). Each oxygen atom was responsible for one MaAh unit and each chlorine atom was respectively responsible for one 4vbCl unit. Assuming that MaAh made up 50% of PSMA-Cl, the styrene units would have to make up the rest giving the ratio 38:1:39 (Sty : 4vbCl : MaAh). Therefore, according to the assumption that MaAh forms 50% of the terpolymer, 48.7% belongs to Sty while the remaining 1.3% belongs to 4vbCl.

Attenuated total reflectance - fourier transform infrared (ATR-FTIR) was performed for additional quantification of structure but will be discussed in later sections of this chapter. Size exclusion chromatography was also performed to determine the number average molar mass (M_n) and dispersity. It was found that PSMA-Cl had a M_n of 177991 $g.mol^{-1}$ and a dispersity of 1.75. FRP was used for the very reason that electrospinning requires high molar mass polymers which is what PSMA-Cl was classified under.

4.2.3 Electrospinning of PSMA-Cl

Electrospun PSMA-Cl would provide a nanofibrous surface for subsequent reactions so it was necessary to determine the best conditions in order to spin a bead-free surface. A basic electrospinning setup was used and is described in more detail in the experimental section. Initially, all conditioning studies were performed using aluminium foil as the conductive collecting surface. As explained in the literature chapter, many parameters affect the stability of the electrospinning

polymer jet. These include the solvent system, viscosity of the polymer solution, flow rate, voltage and others. The variables affect each other, which means careful control of each is needed to electrospin smooth bead-free fibres. The same polymer batch was used for all electrospinning studies to ensure that the results were consistent. Fibre diameter and structure were examined using a scanning electron microscopy (SEM).

The start of any electrospinning experiment begins with the choice of a solvent system. Initially, acetone (ACE):dimethylformamide (DMF) (2:1) was chosen because previous work in our group and literature studies showed that PSMA spun well from this system.[11] ACE was used in combination with DMF because acetone is far more volatile, in comparison to DMF. Acetone alone would cause the Taylor cone (cone at the needle tip from which the polymer jet emerges) to gel and needle blocking would occur, stopping the electrospinning process. The correct combination of these solvents allowed optimal volatility and thus sufficient fibre draw.

The distance between the needle tip and the conductive collector was adjusted to 15 cm for all samples. A negative voltage of -2.5 kV was always applied to the conductive collector while the positive voltage on the needle was changed between 10 – 15 kV. This was optimized by ensuring the Taylor cone remained stable. Due to the basic setup, it was not possible to control the laboratory's humidity; however, the temperature was kept constant at 25 ^{o}C

The second parameter that was explored was solution viscosity. Viscosity plays a large role in the morphology of the fibres. Beaded fibres are less likely to form as the solution viscosity is increased, up to a threshold, after which spinning stops. As the viscosity increases, the distance between beads becomes less until the beads become elongated and eventually disappear.[13] It was found that at 20 weight%, no bead formation occurred. Figure 4-2 illustrates how the fibre morphology changes from electrospray droplets (< 8 wt%), to beads-on-a-string (10 wt%), to beaded fibres (15 wt%) and finally smooth bead-free fibres (20 wt%).

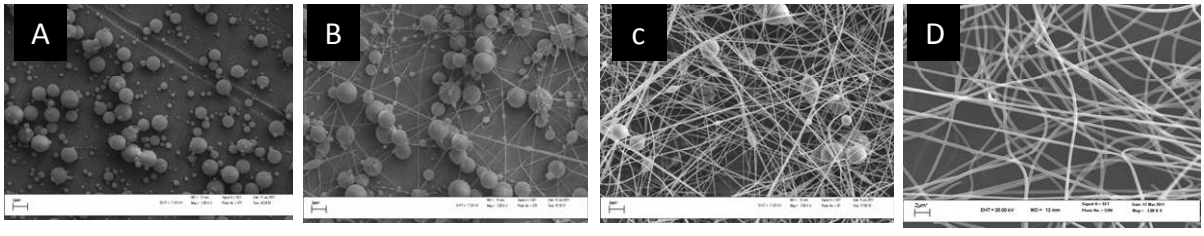

Figure 4-2: SEM images of electrospun PSMA-Cl in ACE:DMF (2:1) - (A) < 8 wt%, (B) 10 wt%, (C) 15 wt%, (D) 20 wt%

Not only does solution viscosity play a role in bead formation but also in fibre diameter. It was found that as the viscosity of the PSMA-Cl solution increased, the fibre diameter increased respectively, as illustrated in figure 4-3.

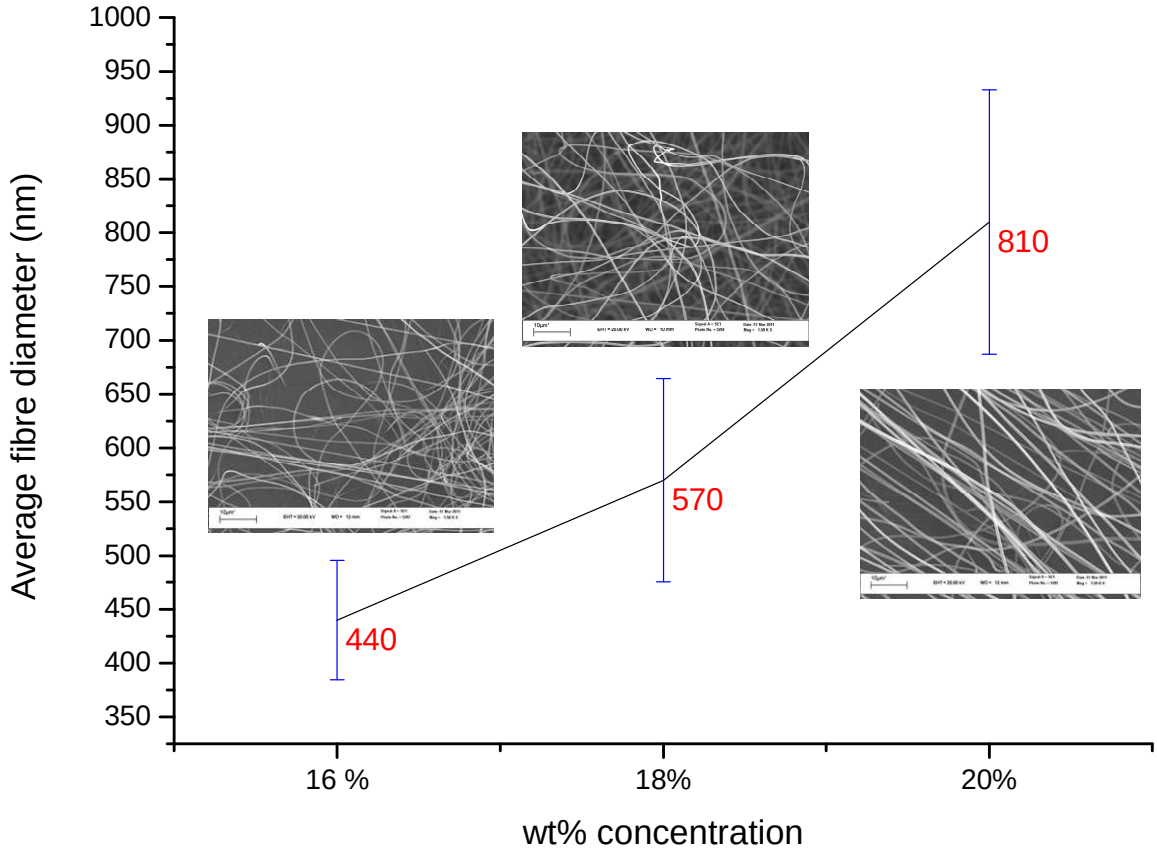

Figure 4-3: Average fibre diameter (nm) vs. wt% concentration of PSMA-Cl solutions spun from an ACE:DMF (2:1) solvent ratio

Although smooth PSMA-Cl nanofibres were obtained using an ACE:DMF (2:1) solvent system, a second solvent system was explored. Cécile and Hsieh reported ultrafine fibre diameters for PSMA by combining a good solvent such as DMF and a small percentage of non-solvent, such as CyH.[7] A DMF:CyH (47:3) solvent system was applied to PSMA-Cl and optimized. It was found that beadless fibres were obtained using 20 wt% PSMA-Cl solution, 11 kV potential on the needle, -2.5 kV on the conductive surface, a 15 cm spinning distance and a 0.01 ml/min flow rate. Figure 4-4 illustrates how smaller fibres (270 ± 60 nm) with a lower standard deviation were obtained using the DMF:CyH solvent system. For this reason, these conditions were used for further nanofibrous mat production.

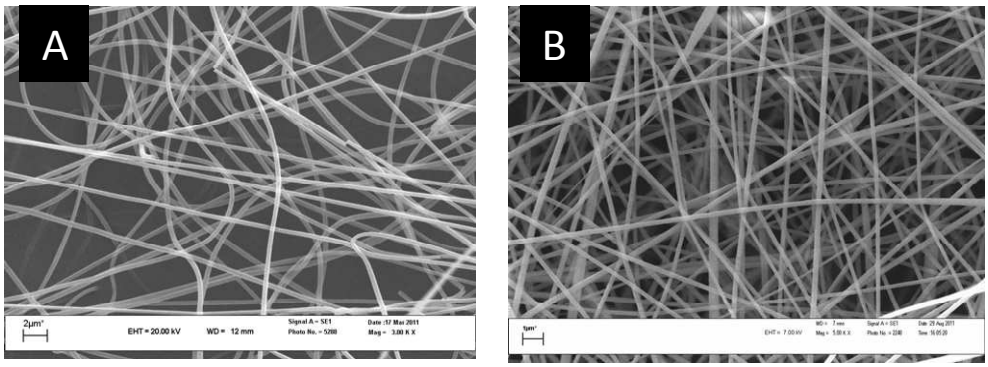

Figure 4-4: SEM images of the electrospun fibres: (A) DMF:ACE 440 ± 120 nm (B) DMF:CyH 270 ± 60 nm

4.2.5 Crosslinking PSMA-Cl

Although the conditions had been fine tuned for the electrospinning of PSMA-Cl, the resulting nanofibrous membrane was still susceptible to organic solvents. One of the best ways to change this dilemma was via crosslinking, rendering the nanofibres insoluble in all media. This would allow future surface modifications to take place in organic solvents.

Earlier in the chapter, it was mentioned that primary amines are very reactive towards MaAh and it was assumed PSMA-Cl is made up of about 50% MaAh. Previously in our group, diamine compounds, such as ethylenediamine (E-DA), have been used to crosslink PSMA. Every MaAh unit, that comes in contact E-DA will react at each side of a diamine, causing the polymer chains to become one large insoluble molecule. This was accomplished by electrospinning PSMA onto a liquid bath, containing E-DA dissolved into a non-solvent for PSMA, such as iPrOH. As soon as the PSMA nanofibres touched the surface, the MaAh units in the backbone reacted with E-DA, producing a crosslinked nanofibrous membrane.

While a fully crosslinked membrane was achieved, no MaAh units remained for further surface modification. In PSMA-Cl, benzyl chloride groups would still remain on the surface, but an additional functionality was needed to attach the acid chloride fluoro-compound, PFOC. Thus, the approach was modified for PSMA-Cl by using 1,3-diamino-2-propanol (OH-DA) as illustrated in figure 4-5. Amines are far more reactive than hydroxyl groups, thus allowing OH-DA to be used in the crosslinking mechanism of PSMA-Cl. This would result in one new surface hydroxyl for every two MaAh groups. The hydroxyl functionality could then be used to attach PFOC to increase the surface hydrophobicity.

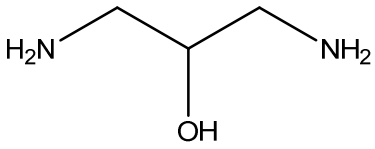

Figure 4-5: OH-DA used for crosslinking reaction for PSMA-Cl nanofibres

4.2.5.1 Electrospinning PSMA-Cl onto liquid bath

Optimal electrospinning conditions had already been obtained for PSMA-Cl, electrospun onto an aluminium foil conductive surface. These conditions were used to test how well fibre formation occurred when electrospun onto a liquid bath. This setup is described in the experimental section of this chapter. iPrOH was used as the non-solvent because it conducts electricity well, allowing a negative voltage of -2.5 kV to be applied evenly through it. A 20% DMF:CyH (47:3) PSMA-Cl solution was used as previously optimized and a 15 cm distance between the needle tip and the liquid bath. OH-DA was used in a molar ratio of 1:2 (OH-DA:anhydride), which was an excess as only the surface reacts. If 2 mL of a 20% solution was electrospun, 0.40 g of polymer was present and thus 0.20 g of MaAh units (2.0 mmol) available for funtionalization. The OH-DA was dissolved in 150 mL iPrOH (6 mmol) in an aluminium cooking tray and 11 kV was applied to the needle. The iPrOH was allowed to evaporate overnight in a fumehood after which the fibres were dried in a vacuum oven at 130 ^{o}C for 3 hours. It was found that if nanofibrous mats were still wet, bubbles were formed on the surface when a vacuum was applied. This crosslinking reaction is illustrated in scheme 4-4.

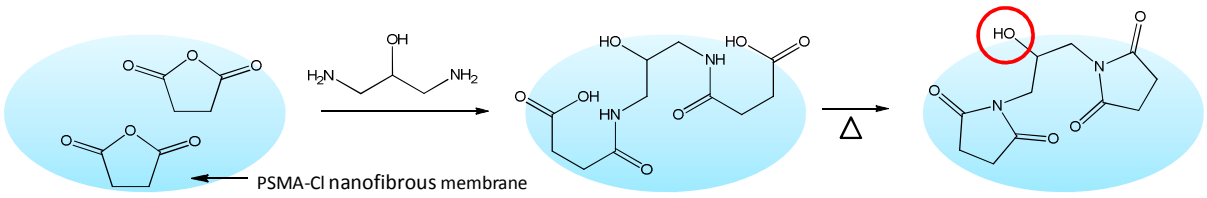

Scheme 4-4: Schematic description of PSMA-Cl nanofibrous membrane crosslinking reaction

4.2.5.2 Crosslinked nanofibrous mat characterization

SEM confirmed that nanofibres were obtained using similar conditions as those used for the aluminium foil collection process, as illustrated in figure 4-6. However, SEM also revealed that fibre diameter broadening occurred when spun onto a liquid bath, 390 ± 60 nm as opposed to 270 ± 60 nm, when spun onto a surface.

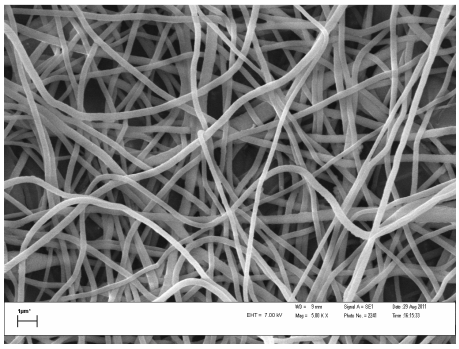

Figure 4-6: SEM image of crosslinked PSMA-Cl fibres (390 ± 60 nm)

ATR-FTIR was used to characterize the nanofibrous crosslinked surface structure. NMR spectroscopy was not possible due to the fact that the crosslinked surfaces were insoluble in all solvents and solid-state NMR spectroscopy was not investigated. Figure 4-7 illustrates the difference between a PSMA-Cl nanofibrous mat and a crosslinked ring-closed maleimide (PSMI-Cl) nanofibrous mat. It is easy to distinguish between the PSMA-Cl and PSMI-Cl nanofibres by observing the intense symmetric and weak asymmetric stretch of the carbonyls. The stretches occur at 1770cm^{-1} and 1850 cm^{-1} for PSMA-Cl while at 1695 cm^{-1} and 1770 cm^{-1} for PSMI-Cl. The PSMI-Cl carbonyl peak is due to the imide versus the anhydride carbonyl group from PSMA-Cl. PSMI-Cl also shows an unique broad hydroxyl stretch around 3300 cm^{-1}. This information confirms that PSMA-Cl was successfully crosslinked and has surface hydroxyl groups present.

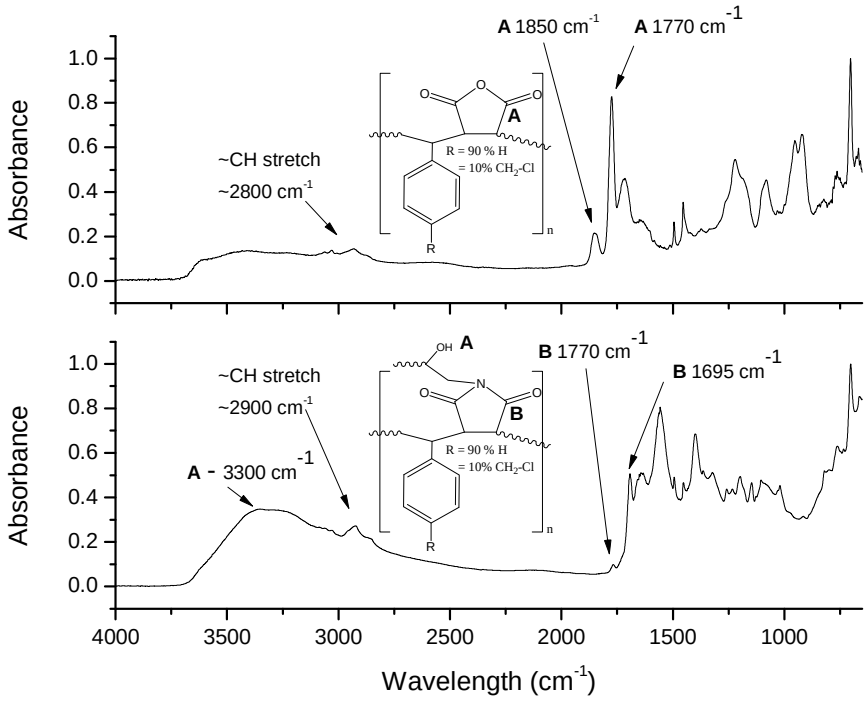

Figure 4-7: ATR-FTIR spectroscopy comparison of PSMA-Cl to PSMI-Cl nanofibres

The PSMI-Cl nanofibrous membrane was also insoluble and maintained its fibrous structure in DMF, THF and ACE, all good solvents for the polymer. Figure 4-8 illustrates the preserved nanofibrous structure after solubility studies in the various solvents. In comparison, non-crosslinked PSMA-Cl nanofibres dissolved immediately after coming into contact with any three of the solvents. Thus, SEM, ATR-FTIR and a visual solubility study all confirmed that PSMA-Cl was successfully crosslinked after electrospinning onto a non-solvent liquid bath containing OH-DA. They also confirmed this crosslinked nanofibrous mat had surface hydroxyl functionalities present.

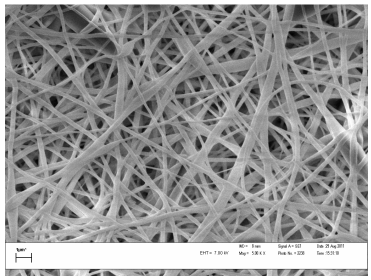

Figure 4-8: SEM image of crosslinked PSMI-Cl structure retention after solubility tests

4.2.6 Increasing the hydrophobicty of the PSMI-Cl nanofibrous mat

The objective of this part of the study was to increase the hydrophobicity of the nanofibrous mat. Similar to lotus leaves, nanofibrous mats are inherently hydrophobic due to their three-dimensional nano-surface structure.[14] However, due to the polar surface hydroxyl functionality on PSMI-Cl, the nanofibrous mat was completely hydrophilic. This meant that when a water droplet was placed on

the surface, it was absorbed immediately. In order to improve the hydrophobicity of the mat, it was decided to fluorinate the surface using an acid chloride functionalized fluoro-compound, PFOC, to produce PSMI-Cl-F as illustrated in scheme 4-5.

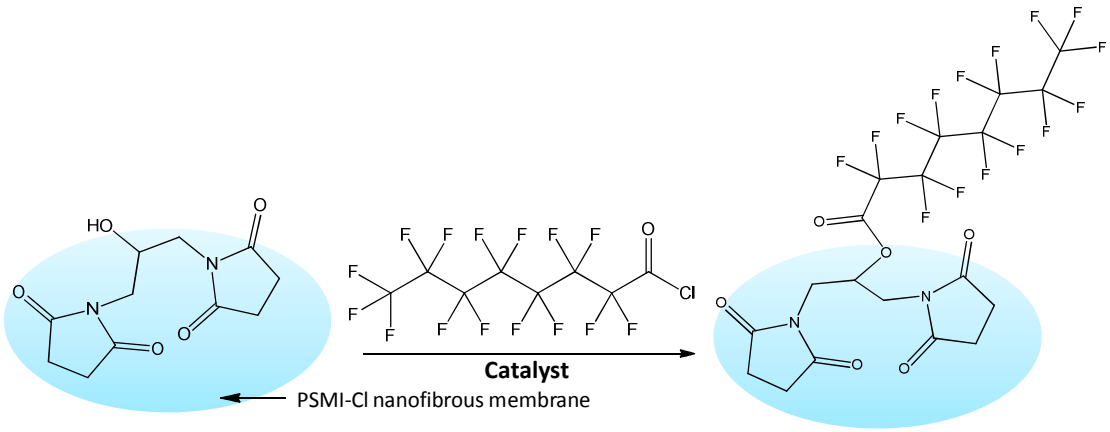

Scheme 4-5: Proposed fluorination of PSMI-Cl nanofibrous membrane

4.2.6.1 PFOC fluorination of the PSMI-Cl nanofibrous mat

PFOC was chosen because acid chlorides are highly reactive towards hydroxyl groups. Even though the PSMI-Cl surface contained secondary hydroxyl groups, the hopes were still high that the reactivity of an acid chloride would overcome the steric enviroment of a 2^{o} alcohol. All reactions were run in THF. Two main techniques were used to confirm surface functionalization, ATR-FTIR and contact angle. Contact angle was used first as a visual test, to observe whether or not the droplet of water was spherical on the surface or if it had been absorbed by the surface. Secondly, EDX was used to verify if fluorine was present on the surface.

Initially, no catalyst was used and the nanofibrous mat was placed into the reactor and cooled to 0 ^{o}C. A 10 × excess of PFOC was then added dropwise. The reaction was allowed to run for 3 hours, after which the surface was washed with THF to remove all unreacted PFOC and dried in the vacuum oven at 25 ^{o}C. A droplet of water (5 µL) was placed on the surface and it was immediately absorbed. Thus static contact angle measurements were not possible. ATR-FTIR confirmed that no surface change had occurred. It was suggested that the hydroxyl groups may have been sterically hard to reach and thus unreactive. It was decided that a mild base may help the hydroxyl groups to react.

Triethyl amine (TEA) was added to neutralize the HCl produced by the reaction. The mat was reacted with a 10 × excess TEA for 10 hours at 25 ^{o}C, after which the reaction was cooled to 0 ^{o}C and 10 × exess PFOC was added dropwise. The surface was washed with THF to remove all unreacted excess PFOC and TEA and dried in the vacuum oven at 25 ^{o}C. Once again, the surface was still completely hydrophilic and the ATR-FTIR spectrum remained unchanged. It was possible that the 2^{o} alcohol was both unreactive and hidden, making the required procedure difficult. TEA is a fairly weak organic base and a stronger base was thought likely to assist in this reaction.

Sodium hydride (NaH) was therefore chosen since it is an irreversible base and is strong enough to deprotonate OH groups. It was added in a 10 × excess to the hydroxyl groups present on the surface and allowed to react for ten hours at 25 ^{o}C. The reaction was cooled to 0 ^{o}C and 10 × excess PFOC was added dropwise. The surface was washed with THF to remove all unreacted PFOC, NaH and NaCl and dried in the vacuum oven at 25 ^{o}C. A droplet of water (5 µL) was placed on the surface and it was visibly hydrophobic as illustrated in figure 4-9. The same procedure was repeated to test whether refluxing the solution in NaH at 80 ^{o}C would increase the hydrophobicity but no difference was found between the two surfaces after they had been characterized.

Figure 4-9: Coloured water droplets (5 µL) on the PSMI-Cl fluorinated nanofibrous surface

FTIR was used to confirm that the surface fluorination had occurred as illustrated in figure 4-10. The PSMI-Cl nanofibrous mat was compared to the PSMI-Cl-F mat and PFOC. The C-F stretch present at ~1200 cm^{-1} in the PSMI-CL-F mat confirmed the presence of PFOC incorporated into the surface. This is the same C-F stretch that was found in PFOC. The acid chloride stretch found at 1795 cm^{-1} in PFOC is masked by the carbonyl imide unsymmetric stretch found in the same region in PSMI-Cl-F. It is interesting to observe that the ~OH stretch is still present in the PSMI-Cl-F mat. This is due to the fact that only the surface was fluorinated and ATR-FTIR detects up to 100 nm into the surface, where hydroxyl groups are still present. It was obvious due to these results that the surface had been successfully fluorinated. The next step was to inspect the nanofibres using SEM to ensure that fibre structure had been preserved, despite the harsh conditions from using a strong base such as NaH.

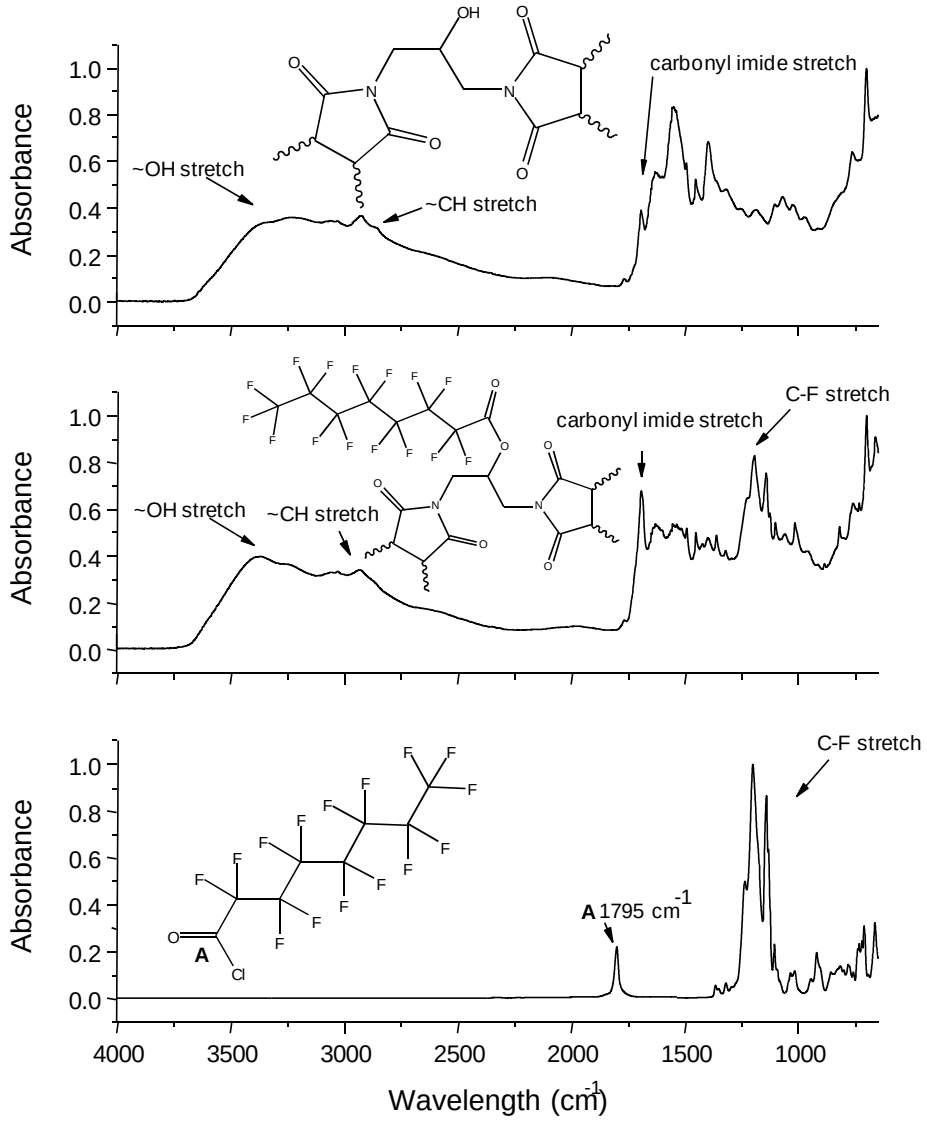

Figure 4-10: ATR-FTIR spectrum confirming fluorination

Figure 4-11 shows that fibre morphology was maintained but that there was a slight increase in fibre diameter for PSMI-Cl fibres (390 ± 60 nm) compared to the PSMI-Cl-F fibres (420 ± 71 nm). The increase in fibre diameter is due the additional steric bulkiness derived from the PFOC functionalized on the fibre surface.

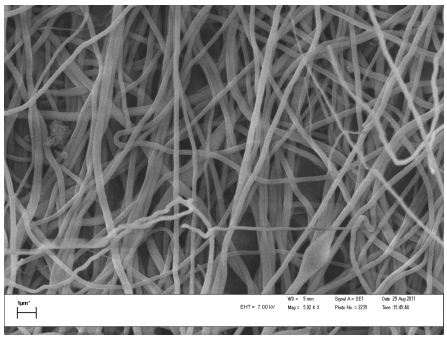

Figure 4-11: SEM image of PSMI-Cl-F nanofibrous mat (420 ± 71 nm)

EDX was also used to qualitatively determine whether fluorine was present on the surface. It was found that that there was a small amount of fluorine present on the PSMI-CL-F surface where none was present on the PSMI-Cl surface as illustrated in table 4-2. Although this result should only be interpreted qualitatively, it provides additional evidence that fluorine was present on the surface.

Table 4- 2: EDX data of PSMI-Cl versus PSMI-Cl-F nanofibres

	C (%)	N (%)	O (%)	Cl (%)	F (%)
PSMI-Cl	78.325	10.134	7.634	3.904	0
PSMI-Cl-F	77.853	10.152	7.652	3.52	0.391

The static contact angle was used to determine the extent of the surface hydrophobicity. It was found that the PSMI-Cl-F nanofibrous mat had a contact angle of 93.4 ± 3 ^{o}. This was lower than expected for a fluorinated surface. In literature, fluorinated surfaces usually had contact angles greater than 150 ^{o} and were classified as super hydrophobic.[10,15] It was mentioned earlier that ATR-FTIR showed the presence of hydroxyl functional groups present on the surface. These groups were assumed to be present under the surface of the fibres but some could still be present on the surface, giving rise to a reduced contact angle. It was also found that a droplet of water stuck to a tilted surface and did not roll off and illustrated in figure 4-12. The droplets may have adhered to the surface because the lower static contact angle induced a larger area of the droplet to be in contact with the nanofibrous surface and thus increased adhesion with the possible unreacted surface hydroxyl groups. A second reason could be attributed to a metastable-state where the water droplet partially wets the surface increasing the adhesion between the droplet and surface, causing it to stick.

Figure 4-12: Coloured water droplets on tilted PSMI-Cl-F nanofibrous surface

4.3 Conclusion

A terpolymer, PSMA-Cl, was successfully polymerized, which contained reactive MaAh units and 1% SI-ATRP initiator sites. Crosslinked PSMI-CL was formed by electrospinning SPMA-Cl onto a solution of OH-DA dissolved in isopropanol. Ring-closing occurred at high temperature in a vacuum oven and fibre structure was maintained. Fluorination of the crosslinked surface was achieved using a strong base, NaH, in addition with PFOC. The contact angle on the surface was lower than expected due to possible surface hydroxyl groups and a metastable state.

The final section of the study involves growing light-sensitive spiropyran-containing polymers from the PSMI-Cl-F nanofibrous surfaces to achieve light switchable “sticky surfaces”. Although superhydrophobicity was not possible with fluorination, it is expected that the hydrophobic spiropyran polymer in combination with the already fluorinated surface will increase the hydrophobicity of the surface in the ring-closed spiropyran state. This should allow a droplet of water to roll off the surface in the hydrophobic ring-closed spiropyran state but stick to the surface in the polar ring-opened merocyanine state.

4.4 Experimental Section

4.4.1 Materials

The following chemicals were utilized in this part of the project: Styrene (Sigma Aldrich, 99%) was washed three times with aqueous 0.3 M KOH solution to remove the inhibitor after which the styrene was subsequently distilled under reduced pressure and stored on molecular sieves (4 Å pore size) . Azobisisobutronitrile (AIBN, Riedel de Haën) was recyrstallized from methanol and dried under vacuum at 25 ^{o}C. Tetrahydrofuran (Aldrich, 98%) was distilled over lithium with benzophenone as an indicator. Maleic anhydride (Acros Organics, 99%), 4-vinylbenzylchloride (Sigma Aldrich, 99%), 1,4-dioxane (Saarchem uniLab, 99%), isopropanol (Kimix, 98%), *N*,*N*-dimethylformamide (Sigma Alrich, 98%), cyclohexane (Sigma Aldrich, 98%), sodium hydride (Sigma Aldich, 60% dispersion in mineral oil), 1,3-Diamino-2-propanol (Sigma Aldrich, 95%), pentadecaflurooctanoyl chloride (Sigma Aldrich, 97%) and dimethylsulphoxide-D6 (DMSO-d6, Merck, 99.9%).

4.4.2 Polymerization of poly(styrene-co-4-vinylbenzyl chloride-co-maleic anhydride) (PSMA-Cl)

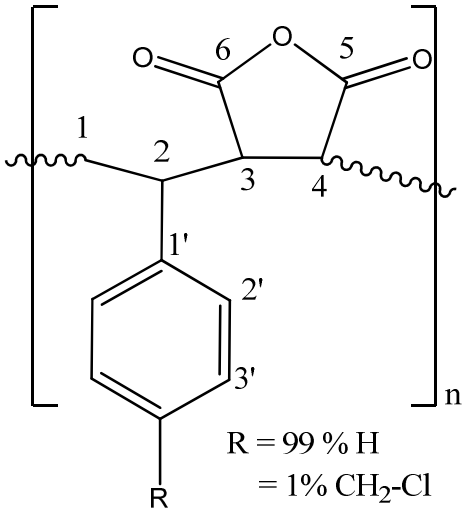

Styrene (8.50 g, 81.6 mmol), 4-vinylbenzyl chloride (3.11g, 20.1 mmol), maleic anhydride (11.84 g, 101 mmol) and AIBN (0.0394 g, 0.240 mmol) were added to 1,4-dioxane (300 mL). The solution was heated at 60 ^{o}C for 8 hours under an argon atmosphere. The turbid solution was then precipitated dropwise into isopropanol (900 mL) over 6 hours, yielding an off-white powder. This was redissolved into tetrahydrofuran (200 mL) and reprecipitated into iPrOH (900 mL) yielding a white drop-sized powder (21.0 g, 89.6%). ^{1}H-NMR spectroscopy was analyzed in the discussion section of this chapter.

4.4.3 Electrospinning setup and general procedure

The custom build electrospinning setup that was used for the nanofibre production is illustrated in figure 4-13. It comprises a high-voltage power source, syringe pump, syringe with capillary tubing to a 26-gauge needle (Hamilton) and a conductive collection surface on a height adjustable jack. The collection surface was an aluminium dish that was either filled with a non-solvent or left empty.

A 20% solution of PSMA-Cl was used for all electrospinning experiments. This was made up in bulk by dissolving PSMA-Cl (15.0 g) in DMF:CyH (47:3, v/v, 75 mL). PSMA-Cl nanofibres were obtained by electrospinning a 20% PSMA-Cl DMF:CyH (47:3) solution through a 26 gauge needle at a flow rate of 0.01 mL/min, a spinning distance of 15 cm, a positive voltage of 11 kV and a negative voltage of -2.5 kV. The nanofibres were collected on an empty aluminium dish.

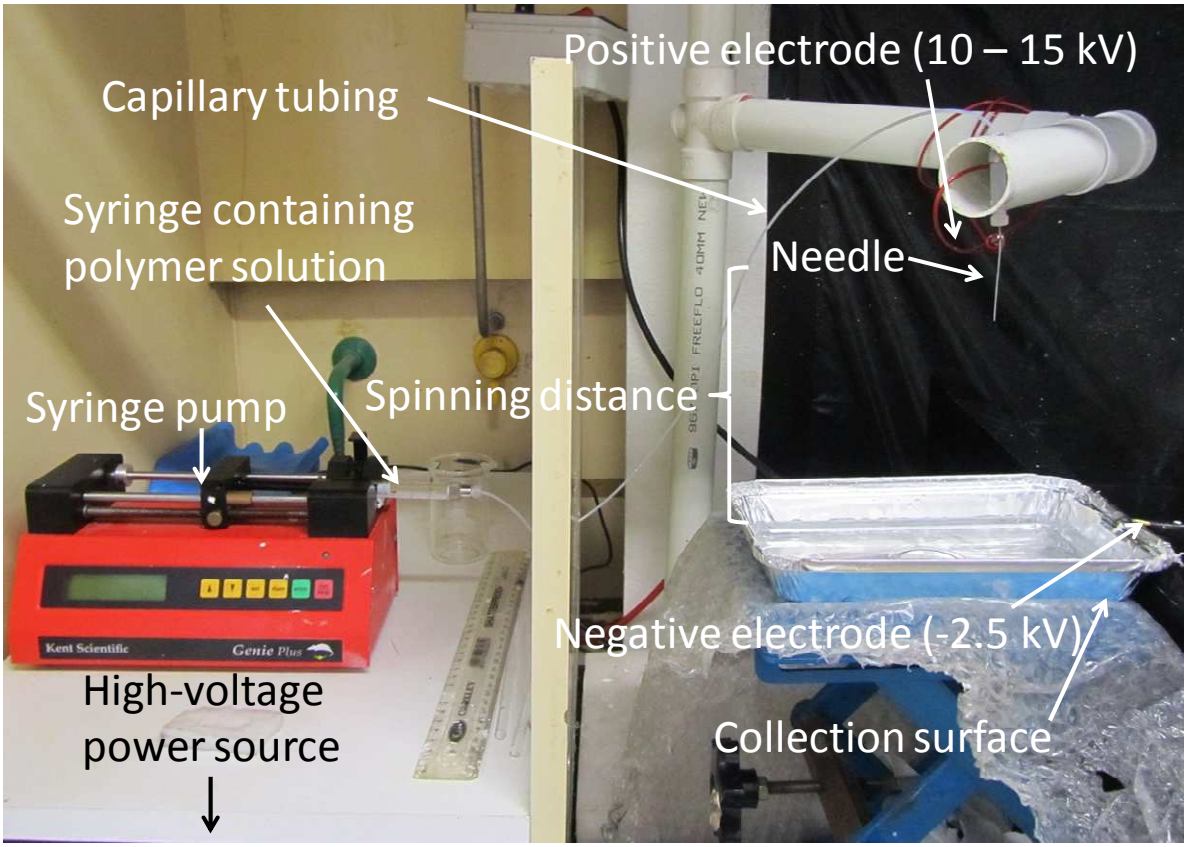

Figure 4-13: Custom build electrospinning setup

4.4.4 PSMA-Cl crosslinking procedure

PSMI-Cl crosslinked nanofibres were obtained using the electrospinning setup previously described. A 20% PSMA-Cl DMF:CyH (47:3) was injected through a 26 gauge needle at a flow rate of 0.01 mL/min, a spinning distance of 15 cm, a positive voltage of 11 kVand a negative

voltage of -2.5 kV. The nanofibres were collected on an aluminium dish containing a solution of OH-DA in iPrOH. The OH-DA solution was made up by dissolving OH-DA (0.09 g, 1.0 mmol) in iPrOH (150 mL) to give a concentration of 6 mM. After electrospinning was completed, the iPrOH was allowed to evaporate overnight in a fumehood after which the surface was dried for 3 hours in a vacuum oven at 130 ^{o}C.

4.4.5 Fluorination of PSMI-Cl nanofibrous mat

A custom reactor was built to prevent the stirring bar from hitting the nanofibrous surface and allow the surface to be inserted and removed easily as illustrated in figure 4-14. A PSMI-Cl nanofibrous mat (10 mg), 10 × excess NaH (5.8 mg, 0.25 mmol) and THF (10 mL) was placed in the custom built reactor and allowed to stir at 25 ^{o}C for 10 hours. The reaction was then cooled to 0 ^{o}C and 10 × excess PFOC (108 mg, 0.25 mmol) was added dropwise to the reaction. The PSMI-Cl-F mat was washed thoroughly with THF to remove excess NaH and PFOC after which it was dried in a vacuum oven for 3 hours at 25 ^{o}C.

Figure 4-14: Custom built reactor for nanofibrous surface reactions

4.4.6 Characterization techniques

4.4.6.1 NMR Spectroscopy

^{1}H NMR and ^{13}C NMR spectra were obtained in DMSO-d_6 with a Varian VXR-Unity (400 MHz) spectrometer. Chemical shifts were reported in parts per million (ppm) and tetramethylsilane (TMS) was used as internal reference.

4.4.6.2 SEC

Molar mass and dispersity were obtained using SEC. The SEC instrument comprised a Waters Alliance apparatus fitted with a 50 × 8 mm guard column in series with three 300 × 8 mm, 10 µm

particle size, GRAM columns (2 × 3000 Å and 100 Å), a Shimadzu LC-10AT isocratic pump, a Waters 717+ autosampler, a refractive index detector and a Waters2487 dual wavelength UV detector. The flow rate was set at 1 mL/min,and the injection volume was 100 µL. Dimethylacetamide (DMAc) HPLC grade was used for the solvent, with 0.05% (w/v) 2,6-di-*tert*-butyl-4-methylphenol (BHT) and 0.03% (w/v) lithium chloride (LiCl). The calculated molar masses were relative to a calibration curve for poly(methyl methacrylate) (PMMA) standards (molar mass range of 8.50×10^2 to 3.5×10^5 g/mol) of low dispersity from Polymer Laboratories. Data acquisition and processing were performed using Millemium[32] (version 4) software.

4.4.6.3 ATR-FTIR

Infrared spectra were recorded using a Thermo-Nicoletter iS10 FTIR spectrometer with a ZnSe ATR and LC-transform attachment. No sample preparation was necessary and samples could either be in the liquid or solid state. Omnic software (version 8.1) was used for data acquisition and processing.

4.4.6.4 SEM and EDX

Sections of nanofibrous mats were cut out and fixed to SEM stubs. The samples were sputter-coated with gold for 2.5 minutes. Images were obtained using a Leo® 1430VP scanning electron microscope equipped with an Oxford Instruments® 133KeV detector using Oxford INCA software. Elemental analysis was possible with an energy dispersive x-ray spectrometer attachment. The average fibre diameters were obtained using Carl Zeiss AxioVision LE software. Three images were taken at various places on each sample and approximately 100 measurements were taken on each image.

4.4.6.5 Contact angle

The hydrophobicity of surfaces was measured using static contact angle. Magnification was achieved using a Zeiss microscope unit. A 1 µL drop of distilled water was placed onto the sample mat and the magnified image was captured using a Nikon SMZ-2T (Japan). Static contact angles were measured using Carl Zeiss AxioVision LE software. Figure 4-15 illustrates the captured image of a water droplet with the marked parameters that were needed to calculate the contact angle. Equation 4-1 was used to determine the static contact angle.

$$\theta = 2 \times tan^{-1}\left(\frac{H}{R}\right) \qquad 4\text{-}1$$

The average of 10 droplets was used in order to determine the static contact angle.

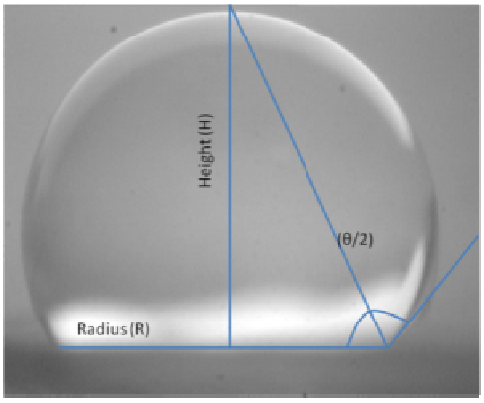

Figure 4-15: Static contact angle parameters needed for determination of the contact angle

4.5 References

(1) Coleman, L.; Bork, J.; Dunn, H. *J. Org. Chem.* **1959**, *24*, 135-136.

(2) Schmidt, U.; Zschoche, S.; Werner, C. *J. Appl. Polym. Sci.* **2003**, *87*, 1255-1266.

(3) Zeng, W.; Shirota, Y. *Macromolecules* **1989**, *22*, 4204-4208.

(4) Barron, P. F.; Hill, D. J. T.; O'Donnell, J. H.; O'Sullivan, P. W. *Macromolecules* **1984**, *17*, 1967-1972.

(5) Tang, C.; Ye, S.; Liu, H. *Polymer* **2007**, *48*, 4482-4491.

(6) Ignatova, M.; Stoilova, O.; Manolova, N.; Mita, D. G.; Diano, N.; Nicolucci, C.; Rashkov, I. *Eur. Polym. J.* **2009**, *45*, 2494-2504.

(7) Cécile, C.; Hsieh, Y. L. *J. Appl. Polym. Sci.* **2009**, *113*, 2709-2718.

(8) Kim, C.-W.; Kim, D.-S.; Kang, S.-Y.; Marquez, M.; Joo, Y. L. *Polymer* **2006**, *47*, 5097-5107.

(9) Srinivasan, G.; Reneker, D. H. *Polym. Int.* **1995**, *36*, 195-201.

(10) Yoshimitsu, Z.; Nakajima, A.; Watanabe, T.; Hashimoto, K. *Langmuir* **2002**, *18*, 5818-5822.

(11) Nystrom, D.; Lindqvist, J.; Ostmark, E.; Hult, A.; Malmstrom, E. *Chem. Commun. (Cambridge, U. K.)* **2006**, 3594-3596.

(12) Huang, X.; Wirth, M. J. *Anal. Chem.* **1997**, *69*, 4577-4580.

(13) Fong, H.; Chun, I.; Reneker, D. H. *Polymer* **1999**, *40*, 4585-4592.

(14) Rosario, R.; Gust, D.; Garcia, A. A.; Hayes, M.; Taraci, J. L.; Clement, T.; Dailey, J. W.; Picraux, S. T. *J. Phys. Chem. B* **2004**, *108*, 12640-12642.

(15) Wang, M.; Vail, S. A.; Keirstead, A. E.; Marquez, M.; Gust, D.; Garcia, A. A. *Polymer* **2009**, *50*, 3974-3980.

Chapter 5: Surface-Initiated Polymerization

5.1 Introduction

Recently, properties such as adhesion, wettability and biocompatibility, have been introduced to surfaces by employing polymer brushes.[1,2] They have an advantage over other surface modifications because they can be controlled on a molecular level and they allow the introduction of functional groups, such as in this study, spiropyran. Polymer brushes have been applied using surface-initiated controlled/living radical polymerization, which allows control over many variables, including branch thickness, graft density and composition.[3] Surface-initiated atom transfer radical polymerization (SI-ATRP) is one of these techniques and is used in many applications such as the production of anti-fouling surfaces.[2,4]

5.1.2 SI-ATRP

SI-ATRP is classified under the "grafting-from" approach where the initiators are immobilized on the surface and polymer chains are grown from the surface via SI-ATRP as illustrated in figure 5-1.

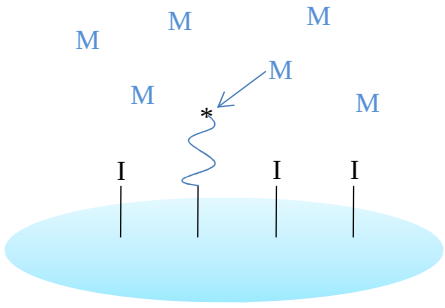

Figure 5-1: "Grafting from" approach where, M = monomer and I = initiator

Sacrificial initiators are used in order to characterize the molar mass and dispersity of the tethered chains. It is assumed that the sacrificial initiators concentration is far greater than the surface-attached initiators. As explained in the literature chapter, a large amount of copper is needed to facilitate controlled polymerization, and propagating radicals are also easily trapped by oxygen. For this reason, activators regenerated by electron transfer (ARGET) ATRP is a more suitable technique for surface-initiated polymerization.

5.1.3 ARGET ATRP

Matyjaszewski *et al*. published a paper in 2007 entitled: "Grafting from Surfaces for "Everyone": ARGET ATRP in the Presence of Air" which detailed how it was possible to perform graft polymerization in the presence of a limited amount of air, with small amounts of a copper catalyst

and a suitable reducing agent.[5] The authors emphasized that this eliminated the necessity of de-oxygenation protocols like freeze-pump-thaw cycles and did not require any special equipment. In this manner, ARGET ATRP allows the copolymerization of various monomers such as styrene and acrylonitrile as reported by Pietrasik *et al*.[6] In our study, it was important that a non-polar monomer could be copolymerized with a spiropyran-containing monomer in a 9:1 ratio, in order that the copolymer remained as hydrophobic as possible. This would ensure that only the spiropyran units, incorporated within the copolymer, would play a role in the adhesion towards water.

5.1.4 Spiropyran-containing copolymers

Spiropyrans, as explained in the literature chapter, exist in a hydrophobic ring-closed state in visible light but when irradiated with UV light, isomerize to their ring-open hydrophilic state. Stimuli-responsive polymers can be synthesized by copolymerizing a spiropyran-derived monomer with a suitable comonomer. Samanta and Locklin reported SI ring-opening polymerization of spiropyran from oxide surfaces.[7] Achilleos and Vamvakaki, on the other hand, reported ATRP copolymerization of a spiropyran methacrylate monomer with 2-(dimethylamino)ethyl methacrylate, in the bid to make multistimuli responsive polymers.[8]

5.2 Results and Discusion

The aim of the final section of this study was to polymerize a hydrophobic spiropyran-containing copolymer from the crosslinked fluorinated surface (PSMI-Cl-F) described in chapter 4. The ultimate aim of this project was to develop a hydrophobic reversibly “sticky surface” as illustrated in figure 5-2. In one state a droplet of water would adhere to the surface, but after irradiating the surface with ultra-violet (UV) light, the droplet would roll off.

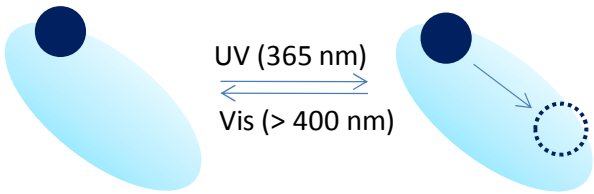

Figure 5-2: Reversibly "sticky" surface

In order to accomplish this, a hydrophobic stimuli-responsive spiropyran-containing copolymer would need to be grown from the PSMI-Cl-F surface. The previously synthesized PSMI-Cl-F surface gave water droplets a static contact angle of 94 ^{o} due to the surface fluorination. Hydrophobic spiropyran-containing copolymer chains grown from the surface would repel the water droplet in their hydrophobic ring-closed spiropyran state. However, the hydrophilic ring-open

merocyanine state would adhere and hold the droplet, as illustrated in figure 5-3. In order to achieve this result, ARGET ATRP was investigated to graft chains from the surface.

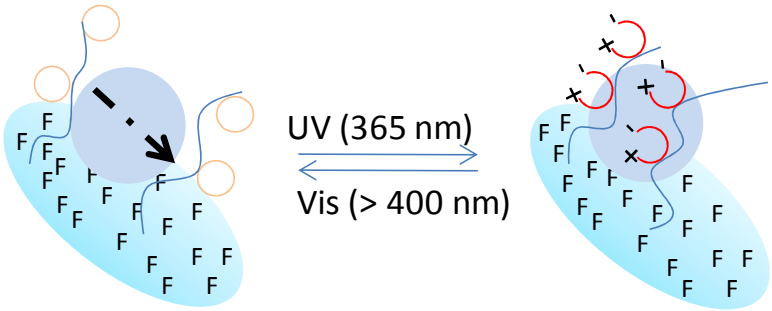

Figure 5-3: Reversibly "sticky" surface visualized

5.2.1 ARGET ATRP model system

Sty was chosen to represent the hydrophobic monomer and ethyl acrylate (EA) was chosen to model spiropyran, as discussed in the introduction, in order to polymerize poly(Sty-co-EA). After the model studies had been completed, hydroxy ethyl acrylate (HEA) could be coupled to the carboxylic acid-functionalized spiropyran (SpAcid) using standard coupling methods, in order to form a spiropyran-based acrylate (SpEA). SpEA would replace EA to produce a Sty-SpEA copolymer as illustrated in scheme 5-1.

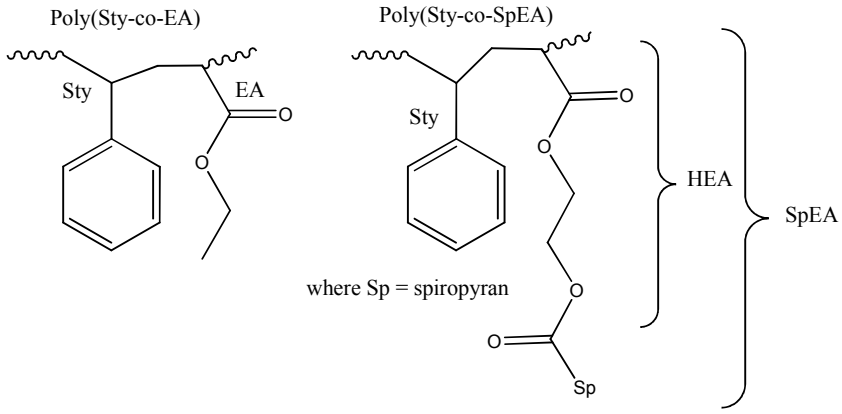

Scheme 5-1: Poly(Sty-co-EA) model system vs poly(Sty-co-SpEA) real system

5.2.1.1 ARGET ATRP model conditions

It was imperative that the correct ligands were chosen to ensure that the low concentration of copper was kept in solution. Three ligands were investigated, namely *N,N,N′,N″,N″*pentamethyldiethylenetriamine (PMDETA), Tris[2-(dimethylamino)ethyl]amine (Me_6Tren) and tris(2-pyridylmethyl)amine (TPMA). Matyjaszewski *et al*. suggested that during ARGET ATRP, Me_6Tren and TPMA showed better control over molar mass and dispersity when compared to PMDETA.[9] Ethyl 2-bromosiobutyrate (EBiB) was used as the initiator and copper (II)

bromide ($CuBr_2$) was used as the transition metal salt. In addition, the ligand was always used in a 10 × excess to $CuBr_2$.

Two reducing agents were investigated, tin(II)-2-ethylhexanoate [$Sn(EH)_2$] and ascorbic acid (AsAc). AsAc has a much higher activity relative to $Sn(EH)_2$ and for that reason has to be used in a poor solvent such as anisole, in which its limited solubility controls its reducing capability.[10] As a result, AsAc can be added in a large excess without jeopardizing the regeneration rate of Cu^I, which would result in poor control. $Sn(EH)_2$ on the other hand is a poor reducing agent and thus an excess is needed to obtain high conversions. Practically, it was found that $Sn(EH)_2$ was far easier to work with because it is present as a liquid at room temperature whereas AsAc is a solid. More consistent results were obtained using $Sn(EH)_2$ as the reducing agent and for this reason, only the $Sn(EH)_2$ results will be mentioned. Anisole was used as the solvent for all ARGET ATRP polymerizations.

All polymerizations were carried out in a 20 mL pear-shaped Schlenk flask which was heated in an oil bath. Even though ARGET ATRP is able to occur in the presence of a limited amount of air, solutions were degassed to obtain optimal results with no inhibition period. Degassed reducing agent was injected to initiate the polymerization. A more detailed description is available in the experimental section.

5.2.1.2 ARGET ATRP of EA

In order to find the appropriate reaction conditions for the Sty-EA copolymer, suitable conditions were first found for each monomer respectively. Scheme 5-2 illustrates the homopolymerization reaction of EA.

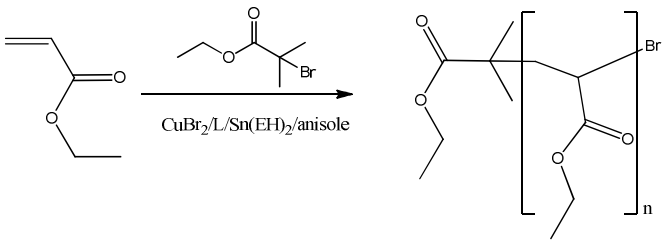

Scheme 5-2: Homopolymerization of EA using ARGET ATRP

A literature study showed that controlled polymerizations were achieved using an average of 50 ppm copper relative to monomer and 10 × reducing agent relative to copper.[11] All polymerizations were carried out in 50% solutions of monomer (volume) at 60 ^oC and run for 24 hours. Table 5-1

shows the conditions used for the polymerization of poly(ethyl acrylate) (PEA). It was found that Me_6Tren gave superior control compared to PMDETA and ^{1}H NMR spectroscopy confirmed the PEA structure.

Table 5-1: Conditions and properties for ARGET ATRP of EA

Ligand	EA/EBiB/$CuBr_2$/L/Sn(EH)$_2$	Conv.[a](%)	$M_{n,theo}$[b]	$M_{n,SEC}$	Đ
PMDETA	100/1/0.005/0.05/0.05	98	9928	11799	1.43
Me_6Tren	100/1/0.005/0.05/0.05	95	9627	9189	1.11

[a] Monomer conversion calculated from ^{1}H NMR. [b] $M_{n,theo} = DP \times MW_{monomer} \times conv. + MW_{initiator}$

5.2.1.3 ARGET ATRP of Sty

A similar model homopolymerization was performed using Sty as illustrated in scheme 5-3.

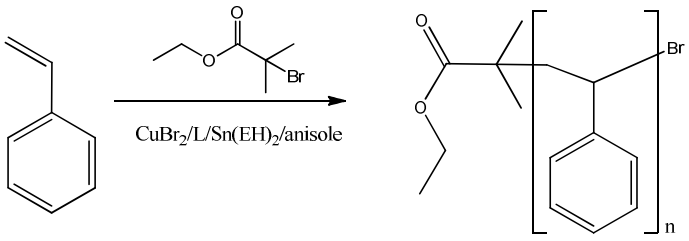

Scheme 5-3: Homopolymerization of Sty using ARGET ATRP

Similarly to EA, literature suggested that controlled polymerizations could be attained using copper concentrations of 50 ppm relative to styrene and using 10 × reducing agent relative to copper.[9] All polymerizations carried out in 50% solutions of monomer (volume) and were run at 100 ^oC for 24 hours. Table 5-2 shows the homopolymerization conditions for Sty. Similarly to EA, the Sty homopolymerization also favoured Me_6Tren and ^{1}H NMR spectroscopy confirmed the structure.

Table 5-2: Experimental conditions and properties for ARGET ATRP of Sty

Ligand	EA/EBiB/$CuBr_2$/L/Sn(EH)$_2$	Conv.[a](%)	$M_{n,theo}$[b]	$M_{n,SEC}$	Đ
PMDETA	100/1/0.005/0.05/0.05	45	4798	5965	1.63
Me_6Tren	100/1/0.005/0.05/0.05	52	5531	5856	1.26

[a] Monomer conversion calculated from ^{1}H NMR. [b] $M_{n,theo} = DP \times MW_{monomer} \times conv. + MW_{initiator}$

5.2.1.3 ARGET ATRP copolymerization of Sty and EA

Well-controlled homopolymerization conditions had been found for EA and Sty respectively. Me_6Tren was found to show the best control of molar mass and dispersity in both

homopolymerizations, however three ligands were used to test the copolymerization conditions, PMDETA, Me_6Tren and TPMA. Scheme 5-4 illustrates the copolymerization of EA and Sty.

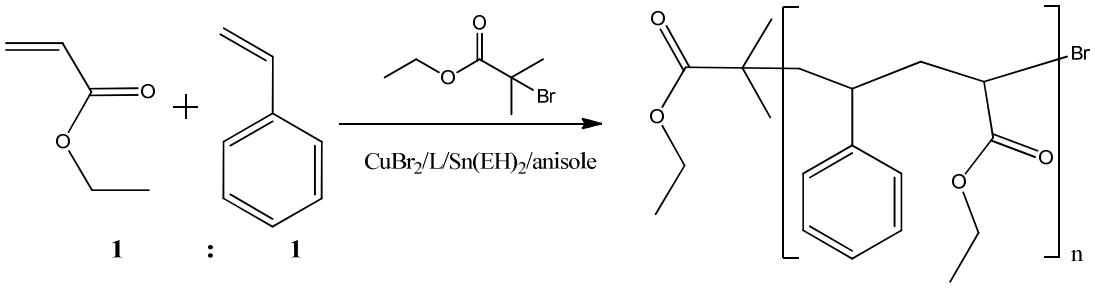

Scheme 5-4: Copolymerization of Sty and EA using ARGET ATRP

Copolymerizations carried out in 50% solutions of monomer (volume), 1:1 ratios (EA:Sty), were run at 100 ^{o}C for 24 hours and are summed up in table 5-3.

Table 5-3: Experimental conditions and results of ARGET ATRP copolymerization of Sty and EA

Ligand	EA/Sty/EBiB/$CuBr_2$/L/$Sn(EH)_2$	Conv.[a](%)	$M_{n,theo}$[b]	$M_{n,SEC}$	Đ
PMDETA	100/100/1/0.01/0.1/0.1	50	10331	15153	3.43
Me_6Tren	100/100/1/0.01/0.1/0.1	10	2171	4970	4.50
TPMA	100/100/1/0.01/0.1/0.1	85	17471	20402	2.15

[a] Monomer conversion calculated from ^{1}H NMR. [b] $M_{n,theo} = DP \times MW_{monomer} \times conv. + MW_{initiator}$

The best control of molar mass was exhibited using TPMA as a ligand. Me_6Tren, which gave low homopolymerization dispersities, showed poor control for the copolymerization. This is more clearly illustrated by looking at the SEC chromatograms of the three copolymers shown in figure 5-4. Both copolymerizations conducted using PMDETA and Me_6Tren showed multimodal curves while that conducted with TPMA showed a monomodal curve with tailing in the lower molar mass region.

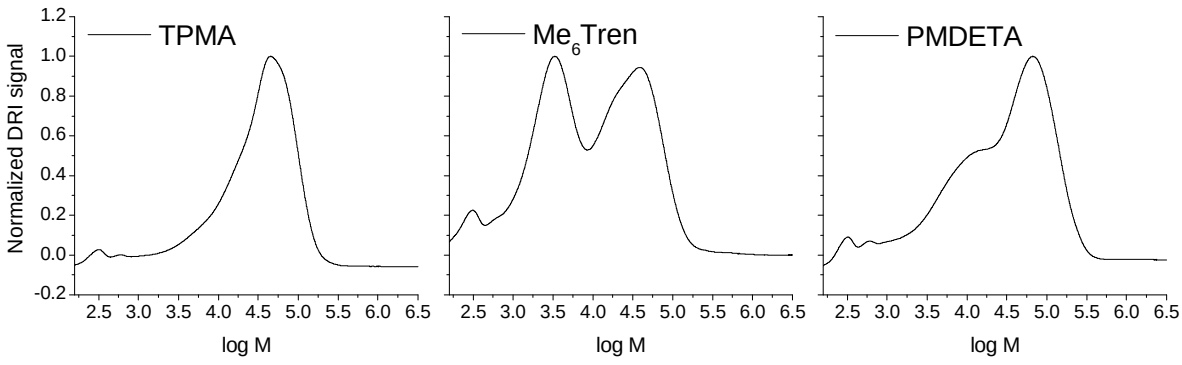

Figure 5-4: SEC chromatograms of PStyEA, each polymerized with different ligands

^{1}H NMR spectroscopy confirmed that poly(styrene-co-ethyl acrylate) (PStyEA) was structurally intact and it also confirmed that there was a one-to-one ratio of Sty to EA as illustrated in figure 5-5. This was calculated by comparing the integration of protons A from Sty to B from EA.

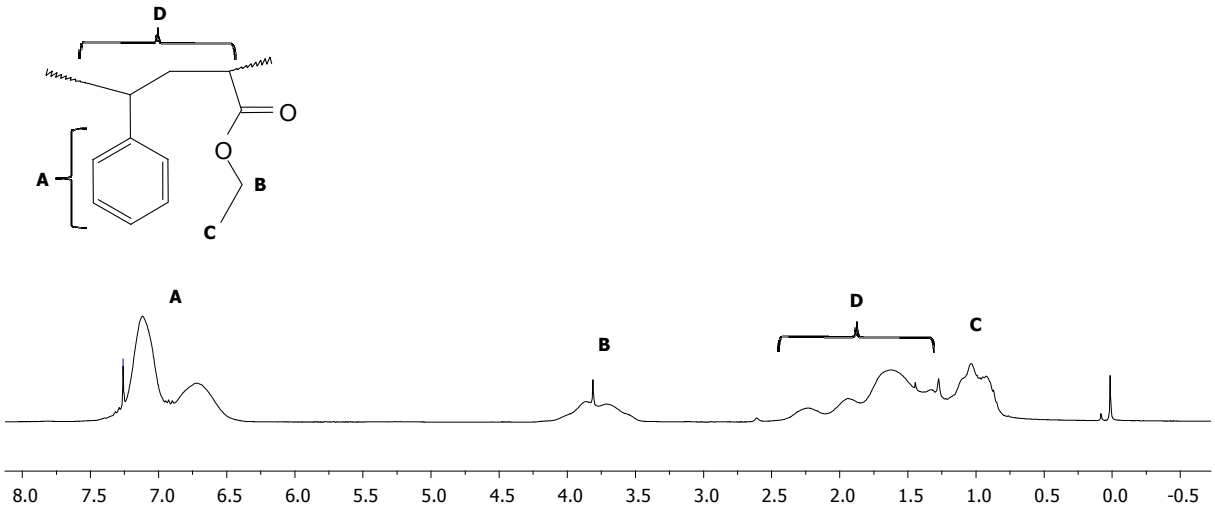

Figure 5-5: ^{1}H NMR spectroscopy of PStyEA using Me_6Tren: 100/100/1/0.01/0.1/0.1

Although the TPMA copper catalysed copolymerization did not exhibit low dispersities (Đ < 1.5), the conditions were used to test the copolymerization with SpEA, instead of EA, with Sty.

5.2.1.4 Synthesis of SpEA

Scheme 5-5 illustrates the synthesis of SpEA.

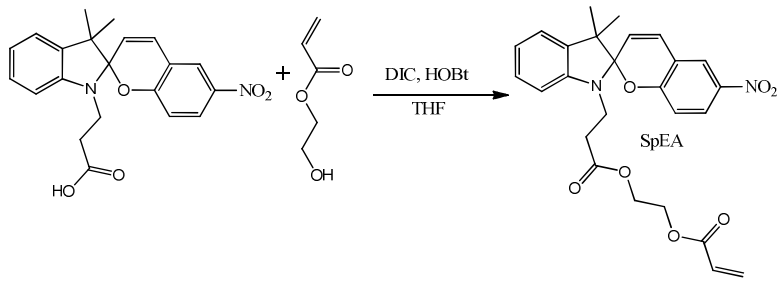

Scheme 5-5: Synthesis of SpEA

SpAcid was coupled to HEA using DIC in a 20% excess, relative to SpAcid. HOBt (50% to SpAcid) was used as the secondary coupling reagent. The reaction was performed in two steps. First, SpAcid, DIC, HOBt dissolved in THF were stirred for an hour at 0 ^{o}C in an amberized three-neck flask. After an hour had past, an equimolar ratio of HEA to SpAcid was added dropwise over an hour after which the reaction was warmed to room temperature and allowed to stir for 24 hours.

The product was purified by filtering the solution to remove the diurea, followed by flash column chromatography (diethyl ether : pentane, 1 : 1). The filtrate containing the compound was recovered via rotary evaporation at room temperature to ensure that the monomer did not polymerize and the yellow powder was then recrystallized from diethyl ethyer: pentane (1:1) yielding yellow crystals with a 60% yield. ^{1}H NMR spectroscopy confirmed that SpEA had been synthesized with the olefinic protons from the monomer appearing at 5.7 and 6.5 ppm, as illustrated in figure 5-5.

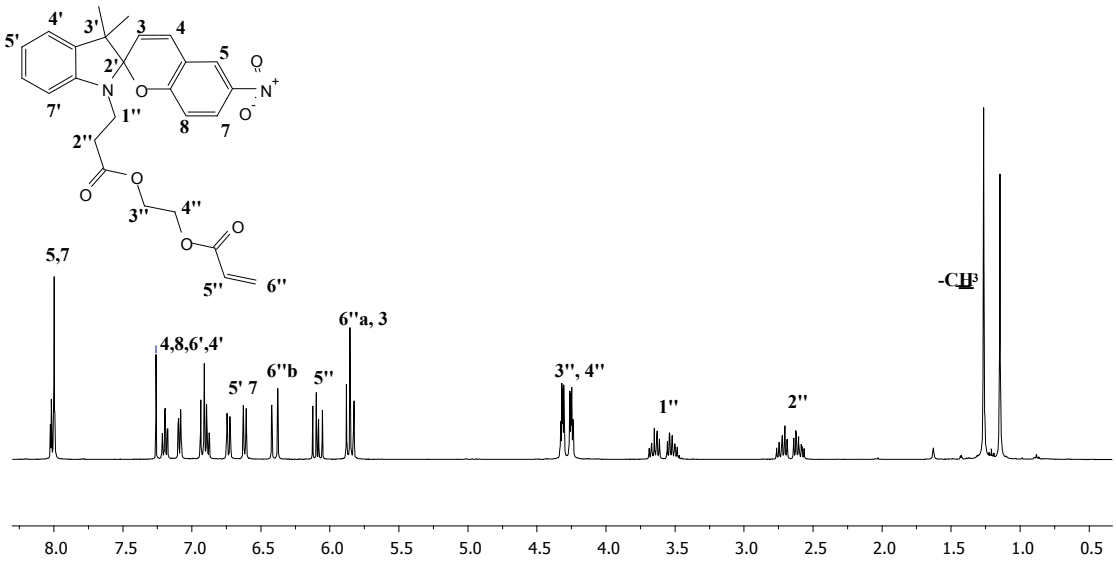

Figure 5-5: ^{1}H NMR spectroscopy of SpEA

5.2.1.5 Copolymerization of Sty and SpEA

SpEA and Sty were copolymerized in a 1:9 ratio (SpEA:Sty) using TPMA as a ligand. The polymerization was run for 24 hours at 100 ^{o}C using the same conditions used for PStyEA. After 24 hours, the solution was not viscous and crude ^{1}H NMR spectroscopy showed possible dimer formation, but mainly monomer of both Sty and SpEA. The same reaction was catalyzed using PMDETA and Me_6Tren as ligands with $CuBr_2$, but gave similar results. There have been no reported papers on the ARGET ATRP copolymerization of Sty and EA, let alone the copolymerization of SpEA and Sty.

The strange behaviour observed in the copolymerization of Sty and EA/SpEA might be explained by considering multiple equilibria that are in place at the same time. Firstly, two different end-groups exist during propagation, either styrene or an acrylate. These endgroups can both interchange with each other via cross-propagation. Secondly, each chain end has their own reduction reaction that generates the right Cu^{I}/Cu^{II} ratio in the system. It is likely that each chain ends need a different ratio of Cu^{I}/Cu^{II} and that this is where the problem with lack of

polymerization or poor control begins to arise. Due to these complications, it was decided that conventional ATRP might solve this predicament.

5.2.2 Conventional ATRP model system

ARGET ATRP was meant to overcome the drawbacks of conventional ATRP that include high concentration of copper and its later removal. However, the ARGET study proved more complicated than originally envisioned and as a result, the study shifted towards conventional ATRP as a means to copolymerize Sty and SpEA. It was decided that *tert*-butyl acrylate (tBA) would better simulate the bulkiness of SpEA and it replaced EA for the model copolymerization study for ATRP. No preliminary homopolymerizations were run for Sty or tBA respectively, because literature confirmed that controlled polymerization was viable for both monomers using either PMDETA or Me_6Tren.[12,13]

5.2.2.1 Model ATRP copolymerization studies of Sty and tBA

Model studies for Sty and tBa were attempted using three ligands, PMDETA, Me_6Tren and TPMA. Benzyl chloride (BnCl) was used as the initiator because it would better mimic the PSMI-Cl-F surface-based initiator. CuCl was used as the copper source because it was better to have a chloride-counter ion while working with a chloride-based initiator. Anisole was used in a one-to-one ratio (solvent:monomer) and polymerizations were run at 100 ^{o}C for 24 hours as illustrated in scheme 5-6.

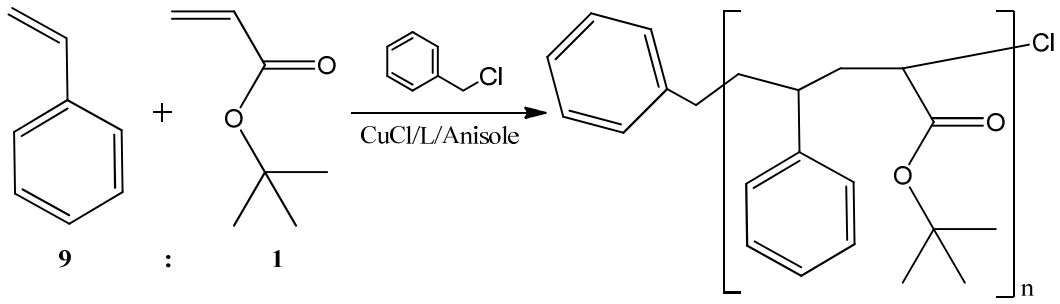

Scheme 5-6: ATRP of Sty and tBA

In order to deoxygenate the system, clean CuCl was added to a degassed 20 mL pear-shaped Schlenk flask. The rest of the reaction mixture was degassed thoroughly by means of three freeze-pump-thaw cycles followed by the introduction of argon. This solution was then injected into the CuCl containing Schlenk flask, using a degassed syringe, to initiate the polymerization. The results are summed up in table 5-4.

Table 5-4: ATRP conditions and results for the copolymerization of Sty and tBa.

Ligand	Sty/tBA/BnCl/CuCl/L	Conv.[a](%)	$M_{n,theo}$[b]	$M_{n,SEC}$	Đ
PMDETA	90/10/1/1/1.5	85	9147	27149	1.19
Me_6Tren	90/10/1/1/1.5	93	9949	13583	1.16
TPMA	90/10/1/1/1.5	89	9525	14550	1.34

[a] Monomer conversion calculated from ^{1}H NMR. [b] $M_{n,theo} = DP \times MW_{monomer} \times conv. + MW_{initiator}$

The SEC chromatograms were monomodal for all three polymers, but the expected theoretical molar masses was quite far apart from the SEC-measured molar masses. This is most likely due to poor initiation efficiency of BnCl. This would result in higher monomer content, for less propagating radicals, leading to an increase in molar mass. Nonetheless, Me_6Tren gave the best comparison with the expected molar mass.

The same conditions that were used for the copolymerization of Sty and tBA were used to copolymerize Sty and SpEA. Although these conditions worked in the model study, no poly(Sty-co-SpEA) was formed. ^{1}H NMR spectroscopy revealed that dimers or trimers had possibly been formed but otherwise nothing. This was similar to the result obtained using ARGET ATRP for the respective polymerization. Further, in depth examination of the literature revealed that spiropyran monomers were generally (meth)acrylate-based and were most often copolymerized with other (meth)acrylates. This discovery resulted in a change of direction and it was decided that a non-polar acrylate should replace the role of Sty. n-Butyl acrylate (nBA) was thus chosen to fulfil this position.

5.2.2.2 ATRP copolymerization of nBA and SpEA

Once again, polymerization of nBA and SpEA was attempted using PMDETA, Me_6Tren and TPMA. Polymerizations were run at 60 ^{o}C for 24 hours in 50% anisole solutions. It was found that the copolymerization only resulted in polymer while using Me_6Tren as the ligand. The previous study using tBA and Sty, led to the hypothesis that an increase in temperature may increase the initiator efficiency of BnCl, leading to more control over molar mass. This was investigated by performing the copolymerization at 60 ^{o}C and 90 ^{o}C and is summed up in table 5-5.

Table 5-5: ATRP conditions and results for the copolymerization of nBA and SpEA

Temp.	nBA/SpEA/BnCl/CuCl/Me_6Tren	Conv.[a](%)	$M_{n,theo}$[b]	$M_{n,SEC}$	Đ
60 ^{o}C	90/10/1/1/1.5	65	10555	23321	1.75

90 °C	90/10/1/1/1.5	70	11396	13122	1.69

[a] Monomer conversion calculated from ^{1}H NMR. [b] $M_{n,theo} = DP \times MW_{monomer} \times conv. + MW_{initiator}$

It is clear that molar mass is better controlled at higher temperature, although dispersity is not greatly affected. The increase in accuracy for targeted molar mass is probably due to higher initiator rate. The SEC chromatograms show some tailing in the lower molar mass region for the polymerization run at 60 °C while better control is achieved at 90 °C, as illustrated in figure 5-6. At lower temperature, polymer chains are continually being initiated throughout the polymerization, yielding a larger proportion of polymer chains with lower molar masses.

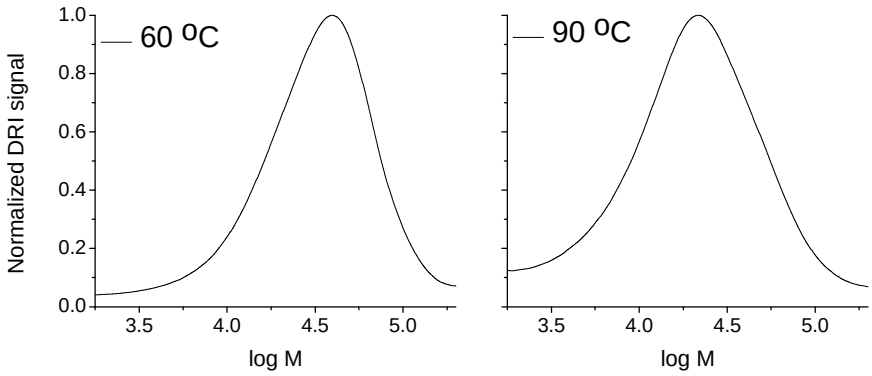

Figure 5-6: SEC chromatograms of poly(nBA-co-SpEA) run at 60 and 90 °C respectively

^{1}H NMR spectroscopy confirms that the ratio of SpEA to nBA is one-to-ten and the polymer is structurally sound, as illustrated in figure 5-7. Peak "5/7" (2 protons) was integrated against peak "a" (2 protons) and they confirmed a one-to-ten ratio. This confirmed that a predominantly hydrophobic copolymer of poly(nBA-co-SpEA) had been polymerized. The large dispersity was probably due to different reactivity rates for SpEA and nBA respectively. These optimized conditions were then used to perform SI-ATRP from the PSMI-Cl-F nanofibrous mat.

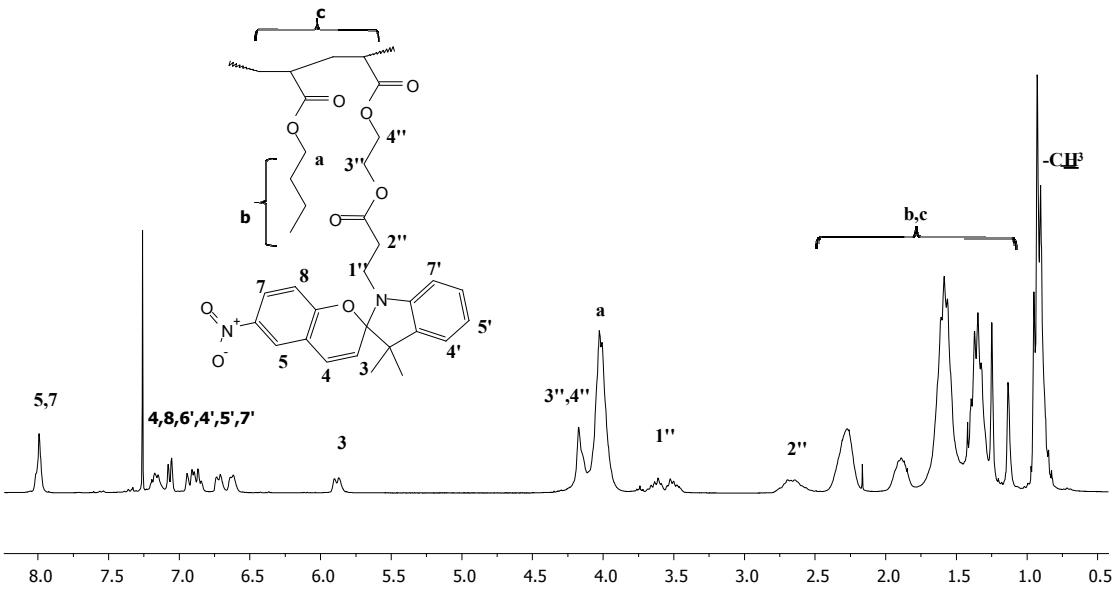

Figure 5-7: ^{1}H NMR spectroscopy of poly(nBA-co-SpEA)

5.2.3 Polarity changes from poly(nBA-co-SpEA)

Prior to growing nBA and SpEA from the PSMI-Cl-F nanofibrous surface, it was important to prove that a polarity change occurred when poly(nBA-co-SpEA), present in its spiropyran form, was converted to its merocyanine form. A small model study was undertaken to confirm that poly(nBA-co-SpEA) would be suitable for reversible adhesion studies. Poly(nBA-co-SpEA) (50 mg) was dissolved in THF (5 mL, 0.76 mM) and 1 mL portions were added to two separate vials. A non-polar miscible solvent, pentane, and a polar miscible solvent, methanol, was added each vial respectively, until poly(nBA-co-SpEA) precipitated out of solution (solution became milky). It was found that 0.8 mL pentane could be added prior to the polymer precipitated out of solution (0.42 mM). On the other hand, 0.2 mL of methanol could be added in order that the polymer just precipitated out of solution (6.3 mM). The non-polar limit, polar limit and standard were irradiated with UV light as illustrated in figure 5-8.

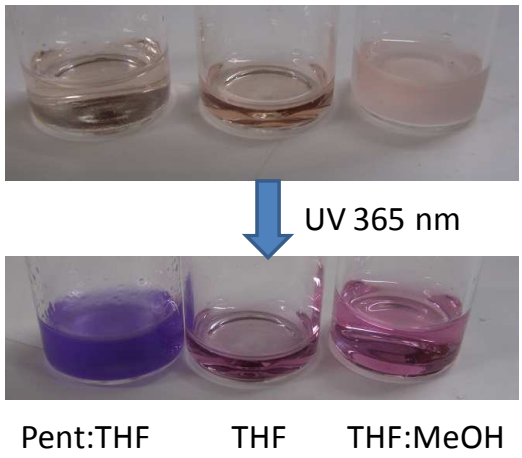

Figure 5-8: Poly(nBA-co-SpEA) polarity study

All solutions changed from a light-pink shade (spiropyran state) to a purple/pink shade (merocyanine state). The range of colours exhibited was due to different solvent systems. The pentane:THF non-polar solution became milky illustrating that the change in polarity caused by the ring-opening isomerisation, caused the copolymer to become too polar for this solvent system, causing it to precipitate out of solution. On the other hand, the methanol:THF polar solution became clear, illustrating that the ring-opening isomerisation, caused the copolymer to increase in polarity, allowing it to solubilize. This model experiment proved that poly(nBA-co-SpEA) could reversibly change its polarity, suggesting its promise as a surface modifier on the nanofibrous mat, inducing reversible adhesion to a water droplet.

5.2.4 SI-ATRP from the PSMI-Cl-F nanofibrous mat

The 90 ^{o}C copolymerization of nBA and SpEA was repeated in the custom-built reactor described in chapter 4. A 1 cm^2 piece of PSMI-Cl-F was present in the surface-compartment of the reactor. In this polymerization, BnCl acted as a sacrificial initiator to confirm the molar mass and dispersities of the tethered copolymer chains grown from the surface. Similar results were obtained by SEC and ^{1}H NMR spectroscopy as previously described. This evidence suggested that SI-ATRP had taken place and further characterization was performed to confirm this result. Prior to characterization, the surface was thoroughly cleaned using soxhlet extraction with THF, to remove sacrificial polymer and was then stirred in a solution of ethylenediaminetetraacetic acid (EDTA) in order to remove excess copper. The EDTA forms a water soluble complex with copper and washes remaining copper from the surface.

5.2.4.1Visual evidence that SI-ATRP had taken place

Initially, a visual test was used to determine whether PSMI-Cl-F-graft-poly(nBA-co-SpEA) (PSMI-F-G) has been formed. This was done by irradiating the surface with UV light for 30 seconds as

illustrated in figure 5-9. The cream-coloured surface changed to pink/purple after 30 seconds under UV irradiation; it returned to the cream colour after storing the surface in the dark for 5 minutes. This result confirmed the incorporation of the spiropyran moiety.

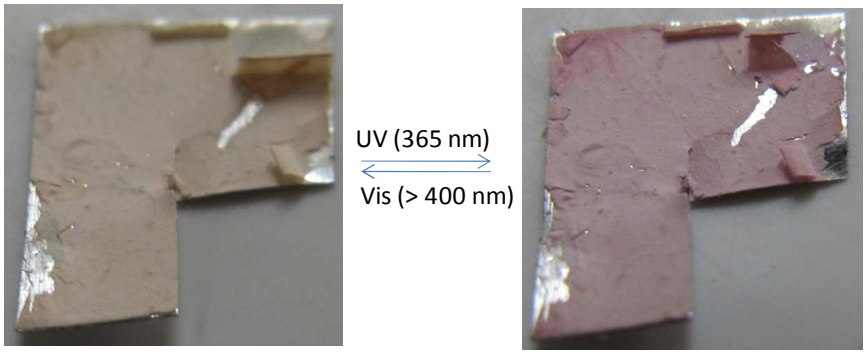

Figure 5-9: Visual test to check for successful SI-ATRP.

5.2.4.2 SEM and EDX characterization of PSMI-F-G

It has previously been shown that SI-ATRP from nanofibres increases their diameter.[14] SEM images of the PSMI-F-G were taken before and after SI-ATRP to confirm whether this was observed here. Figure 5-10 illustrates a PSMI-Cl-F virgin nanofibrous mat (A) versus a PSMI-F-G grafted nanofibrous mat (B). First, it is important to notice that nanofibrous structure has been maintained. Secondly, average fibre diameter shows that an increase of roughly 70 nm has occurred due to the SI-ATRP process.

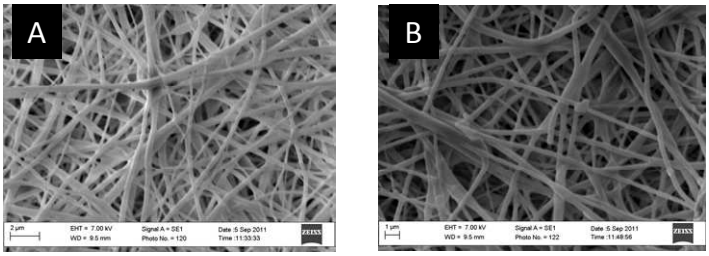

Figure 5-10: SEM images of a A) PSMI-Cl-F mat 420 ± 71 nm B) PSMI-Cl-G mat 491 ± 100 nm

Further, EDX was used to determine the qualitative elemental composition between the PSMI-Cl-F and PSMI-Cl-G nanofibrous mats. Table 5-6 sums up the results. It is interesting to note the large increase in the chlorine between the two surfaces. The only way to explain this phenomenon would be to speculate that the chlorine endgroups present on the grafted SI-ATRP-made polymer are more visible than when they were present on the PSMI-Cl backbone. The slight increase in oxygen is due to the increased total oxygen content as a result of the oxygen present in the nBA ester bonds. The decrease in nitrogen observed, is largely due to the relative increase of other elements.

Table 5-6: EDX data of PSMI-Cl-F mat versus PSMI-Cl-G mat

	C (%)	N (%)	O (%)	F (%)	Cl (%)
PSMI-Cl-F	71.40	11.40	16.59	0.72	0.09
PSMI-F-G	65.87	7.68	18.87	0.69	6.89

5.2.4.3 ATR-FTIR analysis of PSMI-F-G

ATR-FTIR was used to confirm the presence of the grafted poly(nBA-co-SpEA); however, as observed in figure 5-11, it was difficult to observe the presence of the grafted poly(nBA-co-SpEA). One of the reasons the grafted polymer was not visible, is due to the fact that ATR-FTIR observes deeper than the superficial surface. Another reason may be that the PSMI-Cl-F surface only contained around 1% of initiating benzyl chloride units and thus a fairly low concentration of tethered copolymer.

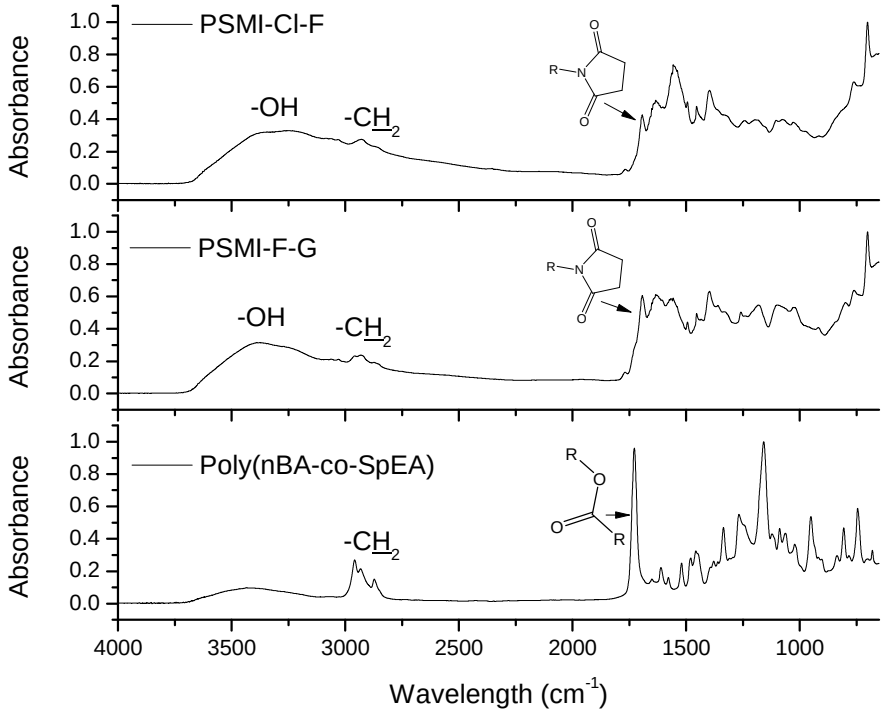

Figure 5-11: ATR-FTIR spectra comparing the PSMI-Cl-F mat to the PSMI-F-G mat

The carbonyl peak due to the ester bond in nBA at 1727 cm^{-1} is masked by the carbonyl imide peak present at both 1764 and 1700 cm^{-1} in the PSMI-F-G surface. Again, it was possible to see hydroxyl groups present from under the superficial nanofibrous surface. A slight increase in the $–CH_2$ stretch at 2923 cm^{-1}can be observed and this is due to the butyl chains present in nBA.

5.2.4.4 Static contact angle analysis of the PSMI-F-G surface

Static contact angle (SCA) measurements were performed on the PSMI-F-G mat both before and after irradiation with UV light. In visible light, the PSMI-F-G nanofibrous surface had a SCA of

78.1 ± 2 ^{o}. This is lower than the SCA of the PSMI-Cl-F mat (93.4 ± 3 ^{o}). This is most likely due to some poly(nBA-co-SpEA) chains blocking the fluorine groups present on the nanofibrous surface. After the PSMI-F-G surface had been irradiated with UV light for 5 minutes, the SCA angle measurement was 78.4 ± 2 ^{o}. This meant that the ring-opened merocyanine, present in poly(nBA-co-SpEA), had no effect on the SCA of the surface. This meant that the SCA was mainly as a result of the fluorine groups in combination with the butyl groups present on the surface. It was clear that the ring-opening isomerisation had taken place due to the purple/pink colour change present on the surface. This result suggested that the polar ring-opened merocyanine units merely adhere to the water droplet, holding it on the surface, but do not affect the water droplets SCA.

5.2.4.5 Reversibly “sticky” surface

The final objective of this study was to investigate the reversibly “sticky” nature of the PSMI-F-G nanofibrous surface. A water droplet was placed on the surface in visible light and the surface was tilted. Unfortunately, the droplet did not roll off as envisioned but adhered to the surface. Irradiating the PSMI-F-G surface with UV light had no affect on the adhesion of the droplet and the SCA of the water droplet remained the same as previously described.

5.3 Conclusion

ARGET ATRP allowed controlled homopolymerizations of both EA and Sty, however copolymerization of the combination provided far less control. ARGET ATRP copolymerization of Sty and SpEA was unsuccessful and was related to the fact that multiple equilibria were present in the system.

Copolymerization of tBA and Sty was well controlled with SEC-determined molar masses being slightly larger than expected. This was due to the poor initiator efficiency of BnCl. Copolymerization of Sty and SpEA did not produce polymer and this was ascribed to the unfavourable copolymerization reaction parameters between monomers. nBA and SpEA were successfully copolymerized using Me_6Tren as a ligand. SI-ATRP was performed from the PSMI-Cl-F nanofibrous mat and was extensively characterized. The surface had reversible photochromic properties, visibly observed by a colour change. The surface, however, did not show reversible adhesion, even though the concept appeared sound through the polarity model study on poly(nBA-co-SpEA).

5.4 Experimental

5.4.1 Materials

The following chemicals were utilized in this part of the project: Styrene (Sigma Aldrich, 99%), ethyl acrylate (Fluka, 99%), *tert*-butyl acrylate (Aldrich, 98%) and n-butyl acrylate (Aldrich, 99%) were washed three times with aqueous 0.3 M KOH solution to remove the inhibitor after which they were subsequently distilled under reduced pressure and stored on molecular sieves (4 Å pore size). 2-Hydroxyethyl acrylate (Acros, 97%) was dissolved in water (25% by volume) and washed 10 times with hexane to remove diacrylates. The aqueous solution was salted (200 g NaCl/L) and then the monomer was extracted from the aqueous phase (4 times), removing acrylic acid, using diethyl ether. $MgSO_4$ was used to remove traces of water before the ether was removed on a rotary evaporator. The purified monomer was distilled under vacuum, immediately before further use. Tetrahydrofuran (Aldrich, 98%) was distilled over lithium with benzophenone as an indicator. Pentane, diethyl ether, methanol, diethyl ether, dichloromethane (KIMIX, CP-grade, 99.5%), anisole (Sigma-Aldrich, 99%) and acetonitrile (Sigma-Aldrich, 99.8%) were used without further purification. Copper (II) bromide (Sigma-Aldrich, 99%), Copper (I) chloride (Sigma-Aldrich, ≥ 99%), benzyl chloride (Aldrich, 99%), tin(II) 2-ethylhexanoate (Aldrich, 95%), N,N,N′,N″,N″-pentamethyldiethylenetriamine (Aldrich, 99%), tris[2-(dimethylamino)ethyl]amine (Aldrich), 2-(chloromethyl)pyridine hydrochloride (Aldrich, 98%), 2-picolylamine (Aldrich, 99%), sodium hydroxide (Sigma Aldrich, 98%), potassium carbonate (Sigma-Aldrich, ≥ 99%), N,N-diisopropylcarbodimide (Fluka, 99%), 1-hydroxybenzotrizole hydrate (Aldrich, 95%), ethylenediaminetetraacetic acid (Sigma Aldrich, 99.4%) and chloroform-D1 (Merck, 99.8%) were used without further purification.

5.4.2 Experimental procedures

5.4.2.1 Preparation of tris(2-pyridylmethyl)amine (TPMA)

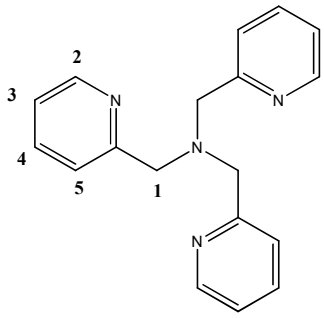

2-(Chloromethyl)pyridine hydrochloride (3.0 g, 18 mmol), 2-picolylamine (0.97 g, 9.0 mmol) and potassium carbonate (7.57 g, 55 mmol) were dissolved in acetonitrile (20 mL) and stirred at room temperature for 48 hours. The solution was filtered and the acetonitrile was removed under vacuum.

The residue was dissolved into dichloromethane and washed with water 3 times. The dichloromethane was dried over magnesium sulphate and then removed under vacuum. The brown residue was extracted into boiling diethyl ether three times. TPMA was then crystallized out of solution by cooling to 0 °C. (1.65 g, 62%) ^{1}H NMR (400 MHz, $CDCl_3$) δ 8.49 (dd, *J* = 4.8, 0.6 Hz, 3H, H-2), 7.59 (ddd, *J* = 24.8, 15.4, 4.8 Hz, 6H, H-2,4), 7.10 (ddd, *J* = 7.1, 4.9, 1.1 Hz, 3H, H-3), 3.85 (s, 6H, H-1).

5.4.2.2 Preparation of 2-[(3-(3′,3′-dimethyl-6-nitrospiro[chromene-2,2′-indolin]-1′-yl)propanoyl)oxy]ethyl acrylate (SpEA)

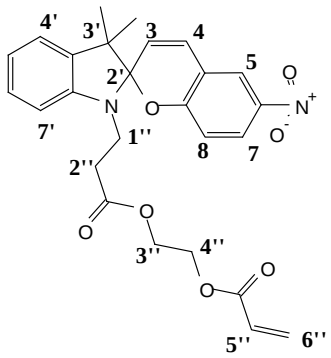

SpAcid (7.00 g, 18.4 mmol), N,N-diisopropylcarbodimide (2.78 g, 22.1 mmol), 1-hydroxybenzotrizole hydrate (1.41g, 10.4 mmol) were dissolved in tetrahydrofuran (70 mL) in an ambered 3-neck flask. The solution was cooled to 0 °C and allowed to stir for 1 hour after which 2-hydroxyethyl acrylate (2.14 g, 18.4 mmol) in tetrahydrofuran (5 mL) was added dropwise over a 1 hour. The solution was kept on ice for a further hour after which it was warmed to room temperature and left stirring for 24 hours. The product was purified by flash column chromatography (diethyl ether : pentane 1 : 1) yielding off-yellow crystals (5.28 g, 60%). ^{1}H NMR (400 MHz, $CDCl_3$) δ 8.03 – 7.97 (m, 2H, H-5,7), 7.20 (m, *J* = 7.7, 1.3 Hz, 1H, H-4), 7.09 (dd, *J* = 7.3, 0.8 Hz, 1H, H-8), 6.97 – 6.85 (m, 2H, H-6′,4′), 6.73 (dd, *J* = 9.2, 0.7 Hz, 1H, 5′), 6.62 (d, *J* = 7.7 Hz, 1H, H-7), 6.40 (dd, *J* = 17.3, 1.4 Hz, 1H, H-6″b), 6.09 (dd, *J* = 17.3, 10.4 Hz, 1H, H-5″), 5.91 – 5.80 (m, 2H, H-3,6″a), 4.37 – 4.19 (m, 4H, H-3″,4″), 3.72 – 3.43 (m, 1H, H-1″), 2.78 – 2.50 (m, 1H, H-2″), 1.34 – 1.06 (m, 6H, -C$\underline{H}_3$).

5.4.2.3 General ARGET ATRP polymerization procedure

Stock solutions (0.2 M) were made up for PMDETA, Me_6Tren and TPMA together with copper (II) bromide in dimethyl sulphoxide. Table 5-7 sums up the stock solutions.

Table 5-7: Ligand stock solution summary

	PMDETA	Me6Tren	TPMA
Ligand (0.5000 mmol)	106.5 mg	115.2 mg	145.2 mg
$CuBr_2$ (0.05000 mmol)	11.80 mg	11.80 mg	11.80 mg
DMSO (mL)	2.5 mL	2.5 mL	2.5 mL

The following procedure was typical for an ARGET ATRP run: A dry 20 mL pear-shaped Schlenk flask was charged with ethyl acrylate (1.00 g, 10.0 mmol), $CuBr_2$/Me_6Tren stock solution (50 µL, 0.00050 mmol $CuBr_2$, 0.00500 mmol Me_6Tren), EBiB (14.7µL, 0.100 mmol), anisole (1 g) and a stirrer bar. The flask was thoroughly degassed via three freeze-pump-thaw cycles, backfilled with argon, sealed and immersed in a preheated and thermostatted oil bath at 60 ^{o}C. $Sn(EH)_2$ (1.6 µL, 0.00500 mmol) was injected to initiate the polymerization. The polymerization was allowed to run for 24 hours after which the reaction was stopped by removing the flask from the oil bath and exposing it to air. The reaction mixture was diluted with THF and the polymer was isolated by precipitation in diethyl ether. The polymer was then dried in a vacuum oven at 60 ^{o}C. ^{1}H-NMR spectroscopy was performed on the raw sample to determine conversion. Theoretical molar masses ($M_{n,theo}$) were determined using equation 5-1. When two monomers were present, the proportional average of their respective molar masses was used. Molar mass (M_n) and dispersity were determined using SEC.

$$M_{n,theo} = DP \times MW_{monomer} \times conversion \times MW_{initiator} \quad 5\text{-}1$$

5.4.2.4 General ATRP polymerization procedure

The following procedure was typical for an ATRP run: A dry 20 mL degassed pear-shaped Schlenk flask was charged with CuCl (5.5 mg, 0.056 mmol). n-Butylacrylate (0.64 g, 5.0 mmol), SpEA (0.27 g, 0.050 mmol), Me_6Tren (19 mg, 0.082 mmol), BnCl (6.4 µL, 0.056 mmol), anisole (1 g) and a stirrer bar were added into a separate Schlenk flask. The flask was thoroughly degassed via three freeze-pump-thaw cycles and backfilled with argon. The degassed solution was injected, by means of a degassed syringe, into the sealed CuCl-containing Schlenk flask and immersed in a preheated and thermostatted oil bath at 90 ^{o}C. The polymerization was allowed to run for 24 hours after which the reaction was stopped by removing the flask from the oil bath and exposing it to air. The reaction mixture was diluted with THF and purified through a neutral aluminium oxide column to remove copper, after which it was precipitated in hexane. The polymer was characterized in the same manner as described for ARGET ATRP.

5.4.2.5 General SI-ATRP polymerization procedure

A typical polymerization was carried out as described for ATRP polymerization except for a few changes. The CuCl and PSMI-Cl-F surface were added to the degassed custom built reactor described in chapter 4. The degassed other components were then added to the custom reactor after their freeze-pump-thaw cycles. After 24 hours, the sacrificial polymer was worked up, as described above but the grafted-surface, PSMI-F-G, was subjected to Soxhlet extraction with THF to remove residual polymer from the surface. Then it was stirred in a solution of EDTA (0.1 M) to remove residual copper left on the surface. The surface was then analysed as described in the body of this chapter.

5.4.3 Characterization

5.4.3.1 NMR Spectroscopy

^{1}H NMR spectra were obtained in $CDCl_3$ with a Varian VXR-Unity (400MHz) spectrometer. Chemical shifts were reported in parts per million (ppm) and tetramethylsilane (TMS) was used as internal reference.

5.4.3.2 SEC

Molar mass and dispersity were obtained using SEC. The SEC instrument comprised a Waters Alliance apparatus fitted with two PLGel 5 µm Mixed-C SDV columns and one PLGel 3 µm Guard Column, a Waters 1515 HPLC pump, a Waters 171+ autosampler, a Waters 2414 refractive index detector and a Waters 2487 dual wavelength UV detector. The flow rate was set at 1 mL/min, and the injection volume was 100 µL. THF (HPLC grade) was used for the solvent, with 0.0125% (w/v) 2,6-di-*tert*-butyl-4-methylphenol (BHT). The calculated molar masses were relative to a calibration curve for poly(styrene) standards (molar mass range of 8.50×10^2 to 3.5×10^5 g/mol) of low dispersity from Polymer Laboratories. Data acquisition and processing were performed using Millemium software.

5.4.3.3 ATR-FTIR

Infrared spectra were recorder using a Thermo-Nicoletter iS10 FTIR spectrometer with a ZnSe ATR and LC-transform attachment. No sample preparation was necessary and samples could either be in the liquid or solid state. Omnic software was used for data acquisition and processing.

5.4.3.4 SEM and EDX

Sections of nanofibrous mats were cut out and fixed to SEM stubs. The samples were sputter-coated with gold for 2.5 minutes. Images were obtained using a Leo® 1430VP scanning electron microscope equipped with an Oxford Instruments® 133KeV detector using Oxford INCA software.

Elemental analysis was possible with an energy dispersive x-ray spectrometer attachment. The average fibre diameters were obtained using Carl Zeiss AxioVision LE software. Three images were taken at various places on each sample and approximately 100 measurements were taken on each image.

5.4.3.5 Static contact angle

The hydrophobicity of surfaces was measured using static contact angle. Magnification was achieved using a Zeiss microscope unit. A 1µL drop of distilled water was placed onto the sample mat and the magnified image was captured using a Nikon SMZ-2T (Japan). Static contact angles were measured using Carl Zeiss AxioVision LE software. Equation 5-2 was used to determine the static contact angle.

$$\theta = 2 \times tan^{-1}\left(\frac{H}{R}\right) \qquad 5\text{-}2$$

The average of 10 droplets was used in order to determine the static contact angle.

5.5 References

(1) Senaratne, W.; Andruzzi, L.; Ober, C. K. *Biomacromolecules* **2005**, *6*, 2427-2448.

(2) Xu, F. J.; Neoh, K. G.; Kang, E. T. *Prog. Polym. Sci.* **2009**, *34*, 719-761.

(3) Zhao, B.; Brittain, W. J. *Prog. Polym. Sci.* **2000**, *25*, 677-710.

(4) Zhao, C.; Li, L.; Zheng, J. *Langmuir* **2010**, *26*, 17375-17382.

(5) Matyjaszewski, K.; Dong, H.; Jakubowski, W.; Pietrasik, J.; Kusumo, A. *Langmuir* **2007**, *23*, 4528-4531.

(6) Pietrasik, J.; Dong, H.; Matyjaszewski, K. *Macromolecules* **2006**, *39*, 6384-6390.

(7) Samanta, S.; Locklin, J. *Langmuir* **2008**, *24*, 9558-9565.

(8) Achilleos, D. S.; Vamvakaki, M. *Macromolecules* **2010**, *43*, 7073-7081.

(9) Matyjaszewski, K.; Jakubowski, W.; Min, K.; Tang, W.; Huang, J.; Braunecker, W. A.; Tsarevsky, N. V. *Proc. Natl. Acad. Sci.* **2006**, *103*, 15309-15314.

(10) Min, K.; Matyjaszewski, K. *Macromolecules* **2007**. 40, 1789-1791.

(11) Chan, N.; Cunningham, M. F.; Hutchinson, R. A. *Macromol. Chem. Phys.* **2008**, *209*, 1797-1805.

(12) Braunecker, W. A.; Matyjaszewski, K. *J. Mol. Catal. A: Chem.* **2006**, *254*, 155-164.

(13) Ayres, N. *Polym. Rev.* **2011**, *51*, 138-162.

(14) Yoshikawa, C.; Zhang, K.; Zawadzak, E.; Kobayashi, H. *Sci. Tech. Adv. Mater.* **2011**, *12*, 015003.

Chapter 6: Conclusions and outlook

6.1 Conclusions

The development of the PSMI-F-G surface was triggered by the initial synthesis of SpAcid and attempted synthesis of the amine-functionalized spiropyran (SpAmine). The original intention was to directly modify the surface using SpAmine, but the unanticipated unsuccessful synthesis of SpAmine, led to an alternative strategy.

PSMA-Cl was synthesized using FRP, electrospun onto a non-solvent, crosslinked using OH-DA and ring-closed at high temperature to produce the PSMI-Cl nanofibrous mat, which contained surface hydroxyl moieties and benzyl chloride initiating groups. The hydrophobicity of the surface was increased through the fluorination of the surface hydroxyl-functionalities to produce the PSMI-Cl-F nanofibrous surface with a SCA of 94 ^{o}.

Initially, a model study was performed using ARGET ATRP, in order to develop reaction conditions, so that Sty and SpEA could be copolymerized. It was found that the copolymerization of these two monomers was not possible using ARGET ATRP and it was proposed that the complication possibly arose due to multiple equilibria present in the system. The study shifted towards ATRP and it was found that acrylates copolymerized better with other acrylates, rather than with styrene. With this in mind, nBA was chosed to represent the hydrophobic monomer, instead of styrene. Poly(nBA-co-SpEA) was successfully polymerized using ATRP and was found to induce a reversible polarity change through irradiation with UV and visible light respectively. SpEA and nBA were successfully grafted from the PSMI-Cl-F nanofibrous mat using SI-ATRP to obtain the PSMI-F-G nanofibrous surface.

In conclusion, a crosslinked hydrophobic nanofibrous mat (PSMI-F-G), containing surface-initiated poly(nBA-co-SpEA) chains, was prepared. The surface exhibited a reversible colour change, brought about by the ring-opening and –closing isomerisation of the spiropyran units incorporated in the surface-initiated copolymer. The surface however, did not show reversible adhesion towards a water droplet that would result in the formation of a reversibly “sticky” surface. Instead, a water droplet (contact angle ~ 78 ^{o}) remained attached to the tilted surface in both isomeric states.

6.2 Recommendations

6.2.1 Creating a reversibly "sticky" surface

One of the possible reasons why a reversibly "sticky" surface was not achieved was due to the inadequacy of the PSMI-F-G nanofibrous surface hydrophobicity. In literature, fluorinated surfaces are generally superhydrophobic and have SCA's greater than 150 ^{o}.[1] The surface produced in this study only had a SCA of 78 ^{o}, which allowed the water droplet to have a greater adhesion to the surface. Increasing the hydrophobicity of the surface may decrease the adhesion between the droplet and the surface, allowing the water droplet to roll off, in the hydrophobic state. This could be achieved by ensuring that no free hydroxyl groups remain on the surface after fluorination, to ensure that the hydrophobicity is not jeopardized by the polar hydroxyl groups. One method to accomplish this would involve protecting the amine groups of OH-DA and coupling it to PFOC as illustrated in scheme 6-1. PSMA-Cl could then be crosslinked with the newly synthesized fluorinated diamine to ensure that no free hydroxyl moiety would be available to increase the hydrophilicity of the surface.

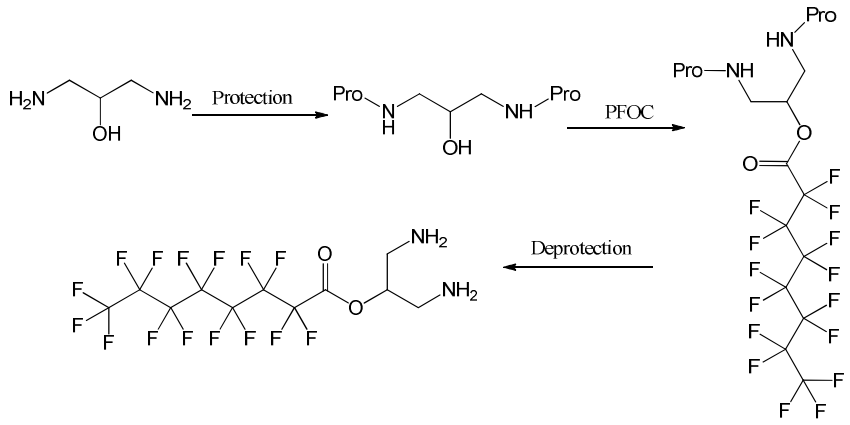

Scheme 6-1: Proposed synthesis of a fluorinated diamine

6.2.2 Investigation of the SpAcid salt effect

In chapter 3, various different metal salts of SpAcid were investigated. Unfortunately, a multi-beam UV spectrometer, which was not available, was needed to explore the effects that the various metal ions played in the UV and visible absorption spectrums of the salts. Visibly, different colours were observed from the salts in solution and it would be interesting to quantify these observed results. It is expected that there would be a shift in the merocyanine absorbtion of each salt.

6.2.3 Investigation into ARGET ATRP copolymerization

In chapter 4, ARGET ATRP of styrene and ethyl acrylate was investigated. It was found that homopolymerization of both ethyl acrylate and styrene resulted in well-controlled polymers with low dispersities. Copolymerization, however, yielded high dispersity polymers with poor control, for a range of ligands. SEC also showed multimodal curves illustrating the lack of control. We suggested that this behaviour could be due to multiple equilibria due to different endgroups during propagation. It would be interesting to investigate this, both experimentally and theoretically, through modelling software such as Predici™.

During the ATRP studies, it was found that SpEA copolymerized better with an acrylate monomer, such as nBA. It would be interesting to investigate whether nBA and SpEA could be copolymerized under ARGET ATRP conditions, as a “greener” alternative to ATRP.

6.3 References

(1) Yoshimitsu, Z.; Nakajima, A.; Watanabe, T.; Hashimoto, K. *Langmuir* **2002**, *18*, 5818-5822.